X63 14867

CODE-2

TECHNICAL MEMORANDUM

X-829

AERODYNAMIC CHARACTERISTICS OF 0.016-SCALE MODELS

OF TWO- AND THREE-STAGE SATURN LAUNCH VEHICLES

WITH CONICAL AND WINGED SPACECRAFT AT

MACH NUMBERS FROM 1.57 TO 4.65

By James R. Morgan, Roger H. Fournier,
and Dorothy T. Howell

Langley Research Center
Langley Station, Hampton, Va.

CLASSIFICATION CHANGED

UNCLASSIFIED

TO ----

By Authority of TD-22-198 Date 5/9/72

NATIONAL AERONAUTICS AND SPACE ADMINISTRATION

WASHINGTON   July 1963

NATIONAL AERONAUTICS AND SPACE ADMINISTRATION

TECHNICAL MEMORANDUM X-829

AERODYNAMIC CHARACTERISTICS OF 0.016-SCALE MODELS

OF TWO- AND THREE-STAGE SATURN LAUNCH VEHICLES

WITH CONICAL AND WINGED SPACECRAFT AT

MACH NUMBERS FROM 1.57 TO 4.65*

By James R. Morgan, Roger H. Fournier,
and Dorothy T. Howell

SUMMARY

An investigation was conducted in the Langley Unitary Plan wind tunnel to determine the aerodynamic characteristics of Saturn launch vehicles with conical and winged spacecraft, at Mach numbers from 1.57 to 4.65. All models had the same first and second stages and differed only in number of stages and space-craft configurations. The effects of fixed, cruciform, stabilizing surfaces located at the base of the second stage were determined for a two-stage version of the launch vehicle. Tests were made over an angle-of-attack range from about -6° to 6° and over an angle-of-sideslip range from approximately -4° to 6° at an angle of attack of approximately 0° at a constant Reynolds number of about 3.15×10^6 per foot.

The results of this investigation indicated that the stability level and normal-force characteristics of the two- and three-stage launch vehicles with conical payloads were the same throughout the Mach number range. Replacing the conical nose shape on the two-stage vehicle with a winged or lifting spacecraft increases the normal-force-curve slope about 10 percent and moves the center of pressure about 0.8 to 0.5 model diameter (first stage) ahead of that obtained with the conical nose shape.

Addition of the fixed stabilizing surfaces at the base of the first stage of the two-stage vehicle decreased the instability about 50 percent. Interdigitating the glider-configuration wings with the launch-vehicle control and stabilizing surfaces did not change the stability from that of the in-line configuration; however, the effectiveness of the control surfaces located at the base of the second stage was improved significantly.

---

*Title, Unclassified.

INTRODUCTION

The NASA has initiated wind-tunnel investigations to determine the static aerodynamic characteristics of several versions of Saturn launch vehicles. Aerodynamic characteristics at transonic speeds for a two-stage version of a Saturn launch vehicle with nose cones of two different fineness ratios are given in reference 1. Aerodynamic characteristics at supersonic speeds for a similar model with a proposed Apollo spacecraft are presented in reference 2. As part of this program tests have been conducted at supersonic speeds on a two-stage version of a proposed launch vehicle with a lifting or winged spacecraft and a conical spacecraft, and a three-stage version with a conical spacecraft, and the results are reported herein. The first two stages of all models are the same except for the geometry of the adapting conical frustum between stages one and two. The model of the two-stage launch vehicle with lifting spacecraft and the three-stage model are proposed flight vehicles; whereas the two-stage model with conical nose was tested for comparison purposes. The three-stage model has been designated as SA-1. All models have the same first stage which is of the Saturn C-1 launch-vehicle class. (The scale of the models tested was 0.016.) The effects on the two-stage configuration of fixed cruciform stabilizing surfaces located at the base of the first stage and of movable cruciform control surfaces at the base of the second stage for both control and stability were determined. This investigation was conducted in the Langley Unitary Plan wind tunnel at Mach numbers from 1.57 to 4.65 over an angle-of-attack range from about -6° to 6° and over an angle-of-sideslip range from about -4° to 6° at approximately 0° angle of attack.

SYMBOLS AND DESIGNATIONS

The data of this investigation are presented about the system of axes shown in figure 1. Moment coefficients are referred to a point located on each model center line at 9.176 inches from the base of the model. This point is representative of a typical full-scale center-of-gravity position at a Mach number of about 4.30 on configurations of the two- and three-stage vehicles.

Symbols

A   reference area (cross-sectional area of circle which would enclose first-stage tanks), 0.0929 sq ft

C_A axial-force coefficient, $\dfrac{\text{Axial force}}{qA}$

C_l rolling-moment coefficient, $\dfrac{\text{Rolling moment}}{qAd}$

C_m pitching-moment coefficient, $\dfrac{\text{Pitching moment}}{qAd}$

C_{m_α} slope of curve of pitching-moment coefficient as function of angle of attack at $\alpha = 0^\circ$, $\partial C_m/\partial \alpha$, per deg

C_{m_δ} slope of curve of pitching-moment coefficient as function of control deflection at $\delta = 0^\circ$, $\partial C_m/\partial \delta$, per deg

C_N normal-force coefficient, $\dfrac{\text{Normal force}}{qA}$

C_{N_α} slope of curve of normal-force coefficient as function of angle of attack at $\alpha = 0^\circ$, $\partial C_N/\partial \alpha$, per deg

C_{N_δ} slope of curve of normal-force coefficient as function of control deflection at $\delta = 0^\circ$, $\partial C_N/\partial \delta$, per deg

C_n yawing-moment coefficient, $\dfrac{\text{Yawing moment}}{qAd}$

C_Y side-force coefficient, $\dfrac{\text{Side force}}{qA}$

d reference diameter (diameter of a circle which would enclose first-stage tanks), 4.130 inches

M Mach number

p free-stream static pressure, lb/sq ft

p_t free-stream stagnation pressure, lb/sq ft

q free-stream dynamic pressure, $0.7pM^2$, lb/sq ft

R Reynolds number

X,Y,Z coordinate axes

$\dfrac{x_{cp}}{d}$ location of center of pressure, in reference diameters, from moment center (positive values are upstream of moment center)

α angle of attack of model center line, deg

β angle of sideslip of model center line, deg

δ control deflection (positive values trailing edge down), deg

Model-Component Designations

C   conical spacecraft

F   fixed stabilizing surfaces at base of first stage

G   winged spacecraft, at 0° incidence, with respect to launch-vehicle
           center-line wing-chord plane in line with control surfaces

G_2 winged spacecraft, at 2^O incidence with respect to launch-vehicle
           center-line wing-chord plane in line with control surfaces

G_3 winged spacecraft, at 2^O incidence with respect to launch-vehicle
           center-line wing-chord plane interdigitated 45° with control surfaces

S   two-stage version of Saturn launch vehicle with 24° flare at base of
           second stage

S_1 two-stage version of Saturn launch vehicle with 13° flare at base of
           second stage

S_2 three-stage version of Saturn launch vehicle with 24.3^O flare at base
           of second stage

V   movable control surfaces at base of second stage (1.88-sq-in. area
           in pitch plane and 2.04-sq-in. area in yaw plane per surface)

V_1 movable control surfaces of equal area (2.04 sq in. at base of second
           stage)

MODELS AND APPARATUS

The test models are designated herein as the Saturn-cone (fig. 2), the
Saturn-glider (fig. 3), and the three-stage Saturn-cone (fig. 4). All models
had the same first stage which consisted of eight tubular tanks distributed
around a center tank of larger diameter (fig. 2(a)). For the two-stage models
the first stage was attached to the second by a conical frustum having a half-
angle of either 13° or 24° (figs. 2(a) and 3(a)). The interstage connection
between the first and second stages of the three-stage model consisted of a
conical frustum having a half-angle of 24.3^O and a short length of cylinder
(fig. 4). The proportions of the various stages of the models relative to the
diameter of the first stage along with pertinent cone angles are listed in
table I. The diameter of the multitank first stage is defined as the diameter
of a circle which circumscribes the eight peripheral tanks.

One of the spacecraft shapes of the two-stage model consisted of an 18° cone
adapted to the second stage by a frustum of a cone having a half-cone angle of
13.25^O. The glider spacecraft was attached to the nose of the 18° cone as shown
in figure 3(a). The configuration with glider was investigated with the glider
incidence with respect to the launch-vehicle center line at 0° and also at 2^O.
Geometric characteristics of the glider model are shown in figure 3(c).

The two-stage model was stabilized by fixed surfaces at the base of the
first stage (fig. 2(a)). These surfaces have an aspect ratio of 1.24 per panel
(exposed area) and a taper ratio of 0.626. Control of the vehicle is achieved
by movable cruciform surfaces located at the base of the second stage. To

compensate for the presence of the glider wings the panel area of the movable surfaces in the horizontal plane is greater than that in the vertical plane (fig. 2(b)). The same fins were used when the glider was removed. The aspect ratio per panel (exposed area) of the surfaces in the horizontal plane is 1.702 with a taper ratio of 0.464 while the surfaces in the vertical plane have an aspect ratio of 1.471 and a taper ratio of 0.522. The movable surfaces in the horizontal plane were deflected a maximum of 20°, with trailing edge down being defined as a positive deflection. The control and stabilizing surfaces were investigated with their chord planes both in line with and interdigitated 45° with the chord plane of the glider wing. When these surfaces were interdigitated, control surfaces of equal area were used. The area chosen was that of the horizontal controls of the in-line configuration.

The three-stage Saturn-cone model CS_2 represents an early version of a development vehicle in the Saturn program that is designated SA-I. This configuration has no control or stabilizing surfaces (fig. 4). As previously mentioned, the first stage of this model is the same as the first stage of the two-stage configurations. The second and third stages consist of cylindrical sections attached to interstage conic adapters whose relative dimensions are presented in table I. The spacecraft consists of a blunted nose cone having a half-angle of 13.5° followed by a conical frustum having a half-angle of 12.5° (fig. 4). Photographs of the test models are presented in figure 5.

The tests were conducted in the Langley Unitary Plan wind tunnel, which is a variable-pressure continuous-flow type with two test sections 4 feet square and approximately 7 feet in length. An asymmetric sliding block nozzle provides the means of varying the Mach number continuously from 1.57 to 2.87 in the low Mach number test section and from 2.30 to 4.65 in the high Mach number test section.

Forces and moments acting on the model were measured by an internally mounted strain-gage balance. The model was sting supported and connected to the tunnel central-support system by a remotely operated adjustable angle coupling.

Pressure measurements at the base of the model were made with an electrical pickup.

TESTS

Tests were conducted over an angle-of-attack range from about -6° to 6° at an angle of sideslip of 0° to determine the longitudinal stability and control characteristics of the models investigated. The lateral characteristics were determined for an angle-of-sideslip range from about -4° to 6° at an angle of attack of approximately 0°. In the table that follows the types of test are listed for various model configurations. The symbol α is used to indicate tests for an angle-of-attack range, and the symbol β is used to indicate tests for an angle-of-sideslip range.

| Configuration | | | Type of test at Mach number of - | | | | | | |
Designation	Components	δ	1.57	1.80	2.16	2.29	2.98	3.96	4.65
Saturn-cone	CS_1VF	$0°$	α,β	α,β	α,β	α	α	α	α
	CS_1V	$0°$	α	α	α	----	----	----	----
	CS_1F	---	α	α	α	α	α	α	α
	CS_1	---	α	α	α	α	α	α	α
Saturn-glider	G_2S_1VF	$0°$	α,β	α,β	α,β	α,β	α,β	α,β	α,β
	G_2S_1V	$0°$	α	α	α	α	α	α	α
	G_2S_1F	---	α	α	α	α	α	α	α
	G_2S_1	---	α,β	α,β	α,β	α	α	α	α
	G_2SVF	$0°$	α,β	α,β	α,β	----	----	----	----
	G_2SF	---	α	α	α	----	----	----	----
	G_2S	---	α	α	α	----	----	----	----
	GS_1VF	$0°$	α	α	α	----	----	----	----
	$G_3S_1V_1F$	$0°$	α,β	α,β	α,β	α	α	α	α
	$G_3S_1V_1$	---	α,β	α,β	α,β	----	----	----	----
	G_3S_1F	---	α	α	α	----	----	----	----
Three-stage Saturn-cone	CS_2	---	----	----	----	α	α	α	α

Control characteristics were determined for the following model configurations (the entry δ in each column is to indicate that the control was deflected):

| Configuration | | Control test at Mach number of - | | | | | | |
Designation	Components	1.57	1.80	2.16	2.29	2.98	3.96	4.65
Saturn-cone	CS_1VF	δ	δ	δ	----	----	----	----
	CS_1V	δ	δ	δ	----	----	----	----
Saturn-glider	G_2S_1VF	δ	δ	δ	δ	δ	δ	δ
	G_2S_1V	δ	δ	δ	δ	δ	δ	δ
	G_2SVF	δ	δ	δ	----	----	----	----
	$G_3S_1V_1F$	δ	δ	δ	δ	δ	δ	δ
	$G_3S_1V_1$	δ	δ	δ	----	----	----	----

Note that δ indicates only that the controls were deflected and does not represent a specific angle range for each model configuration or Mach number. However, the control-deflection range was from $5°$ to $-20°$ in $5°$ increments. The specific values of control deflection investigated are presented in the figures for each model configuration and Mach number.

Test conditions are summarized in the following table:

M	p_t, lb/sq ft	q, lb/sq ft	R
1.57	1,670	709	3.15 × 10⁶
1.80	1,814	716	
2.16	2,117	688	
2.29	2,419	721	
2.98	3,542	618	
3.96	5,904	450	
4.65	8,770	381	

Transition was fixed on all stabilizing and control surfaces by means of a 1/16-inch-wide strip of roughness particles of 0.009-inch diameter. On the Saturn-glider model a 1/16-inch-wide strip of roughness particles of 0.009-inch diameter was attached to the glider nose. Transition was also fixed on the cylindrical portion of the third stage of the three-stage Saturn model by means of a suspended ring consisting of 0.018-inch-diameter wire supported at three points to give a total height of 0.09 inch from the surface of the cylinder and located 1/4-inch downstream of the 12.5° half-cone angle frustum-cylinder junction (fig. 4).

CORRECTIONS AND ACCURACIES

All angles of attack have been adjusted for flow angularity and structural deflection of the sting-balance combination under load. Angles of sideslip have also been corrected for structural deflection.

Axial-force coefficients have been adjusted to correspond to free-stream static pressure acting at the base of the model.

The maximum deviation of the local Mach number in the region of the tunnel occupied by the model is ±0.015. The estimated accuracies of the angles of attack and sideslip and the coefficients, based on balance calibrations and repeatability of the data, are within the following limits:

α, deg . . . . ±0.1
β, deg . . . . ±0.1
C_N . . . . ±0.042
C_A . . . . ±0.008
C_m . . . . ±0.034
C_l . . . . ±0.007
C_n . . . . ±0.034
C_Y . . . . ±0.042

PRESENTATION OF RESULTS

The results of this investigation are presented in the following figures:

DISCUSSION OF RESULTS

Conical Spacecraft Vehicles

The basic configuration (without movable or fixed surfaces) of both the two-stage and the three-stage Saturn models are unstable throughout the Mach number range tested. (See figs. 7(d), 9(a), 19, and 21.) The pitching-moment-curve slopes and normal-force-curve slopes show little significant difference for these two models, although the geometry of the upper stages is considerably different. It should be recalled that a common location of the center of moments with respect to the base of the first stage has been selected for data presentation of all models. Thus, all pitching-moment results directly reflect the aerodynamic effects of changes in upper-stage geometry. A comparison of the center-of-pressure locations for the two-stage Saturn-cone model and the three-stage Saturn-cone model (transition fixed) shows that the combined differences in pitching-moment and normal-force characteristics result in at most a difference of about 0.25 model diameter in center-of-pressure location for the two configurations throughout the Mach number range (figs. 19 and 21). The largest difference occurs at $M = 4.65$. It appears that the relatively large cone angle of th

two-stage Saturn-cone model is, in general, producing the same longitudinal stability characteristics as the third stage plus spacecraft of the three-stage Saturn-cone model.

The effect of fixing transition by the suspended ring technique on the three-stage Saturn-cone model is stabilizing as shown by the center-of-pressure location (fig. 21). The three-stage model with fixed transition was chosen for comparison with the two-stage Saturn-cone model having free transition because shadowgraph monitoring showed that the flow remained attached to the nose region of both configurations as would be expected in flight. However, shadowgraph monitoring also showed that the three-stage model with free transition experienced extensive separation at the junction of the first and second stages.

As a means of establishing a basis of comparison for the lifting spacecraft, a buildup of stabilizing fins and control surfaces was made on the Saturn-cone model (CS_1) and the results are summarized in figure 19. Addition of the fixed stabilizing surfaces F at the base of the first stage of the two-stage vehicle decreases the instability about 50 percent. The results show that the complete configuration CS_1FV is unstable and has a center-of-pressure location that averages approximately 0.6 body diameter ahead of the moment center through the Mach number range. Both sets of lifting surfaces (stabilizing fins and control surfaces) show the usual reduction in lift-curve slope with increasing Mach number. For the stabilizing fins, this condition results in a reduction in configuration stability; whereas for the control fins, this condition results in a reduction in the destabilizing effect of the controls.

Lifting Spacecraft Vehicles

Comparing the center-of-pressure locations of the two-stage Saturn-cone model (fig. 19) with those obtained with the Saturn-glider model (fig. 20) shows that the glider causes a forward movement of the center of pressure of 0.8 body diameter at the lower Mach numbers to 0.5 body diameter at the highest Mach number and also increases the normal-force-curve slope about 10 percent. The complete glider configuration (G_2S_1VF) has essentially the same variation of center-of-pressure position with Mach number as the conical configuration and the additional instability of the complete combination is approximately the same as that contributed by the glider $(\Delta x_{cp}/d$ equal to from 0.8 to 0.5$)$. Consequently, the interference of the glider on the stability of the combined fin-control surfaces and body is not appreciable.

Some results obtained over a limited Mach number range with a 24° frustum of a cone S in place of the 13° conic section S_1 are presented in figures 8(h) to 8(j). Shadowgraph monitoring of the flow in the area of this adapter indicated regions of flow separation extending well behind and forward of the juncture of the 24° conic section and the cylindrical second stage. The separation area was considerably more limited with the 13° conic section. Although the stability parameters are not presented for the results with the 24° conical section, they have shown, when compared with those obtained with the 13° conical section, little or no effect of either the change in angle of the conic section or the difference in the areas of separation with the 24° adapter.

The results obtained with the stabilizing control surfaces interdigitated with the glider-wing chord plane are shown in figure 20(b). Compared with the in-line arrangement (fig. 20(a)), it is apparent that except at the lowest Mach numbers, interdigitation had no effect on the location of the center of pressure. In order that equal area fins would be available for the interdigitated arrangements, the area of the vertical fins of the in-line configuration was increased to equal that of the horizontal fins.

Control Characteristics

The control characteristics for the Saturn-cone $\left(CS_1VF\right)$ and Saturn-glider $\left(G_2S_1VF \text{ and } G_3S_1V_1F, \text{ in-line and interdigitated}\right)$ models are shown in figures 19 and 20. The control effectiveness, which also reflects the stabilizing influence that can be produced by programed deflection of the movable surfaces, was identical for the Saturn-cone model $\left(CS_1VF\right)$ and the in-line Saturn-glider model $\left(G_2S_1VF\right)$; however, the normal force generated per unit control deflection is reduced by the presence of the glider. For this configuration interference effects between the glider wing and the movable surfaces appear to introduce an appreciably adverse effect. The significance of normal forces, which to a great extent are unpredictable because of interference, is that launch trajectories must frequently be corrected by applying to the vehicle lateral accelerations which are directly proportional to control normal forces. In addition, of course vehicle attitude corrections that are proportional to vehicle stability are made. Consequently, the results shown, although they suggest no effect of interference on control deflection stability, can introduce guidance problems resulting from the effect of interference on the normal forces generated by control deflection of the in-line glider arrangement.

Interdigitation of the movable and fixed surfaces with the glider wing-chord plane on the Saturn-glider model increased the control effectiveness and normal force (fig. 21). The increase in control effectiveness $\left(C_{m_\delta}\right)$ is approximately equal to the 41-percent increase in control area resulting from interdigitation. It should be noted in this respect that although a similar effective geometric increase in stabilizing area occurs, a compensating reduction in the effective tail angle of attack also occurs. Consequently, interdigitation would not be expected to alter appreciably the stability over that of the in-line configuration. The results discussed in previous sections show, in fact, that no change in stability occurred as a result of interdigitation.

The control load per unit control deflection shows two effects. One is that the increase in C_{N_δ} due to interdigitation is somewhat greater than 41 percent, particularly at the lower Mach numbers and the other is that the glider of the in-line configuration caused a significant decrease in C_{N_δ} compared to the conic spacecraft. The decrease in C_{N_δ} due to the winged spacecraft suggests that the larger than 41-percent increase coming from interdigitation is a result of the fins and control surfaces moving into a less unfavorable downwash region behind the glider wings.

Lateral Stability Characteristics

The results show that the Saturn-cone model with fixed and movable surfaces in place (fig. 17) is directionally unstable and has negative C_{l_β}. Within the Mach number range from 1.57 to 2.16, change in Mach number had little effect on either C_{n_β} or C_{l_β}. It should be noted that rolling-moment coefficients are not equal to zero at angles of sideslip of $0°$ as would be expected. This condition, which occurs for all configurations having either the movable or the fixed surfaces, is probably due to some angular misalinement of the surfaces.

Change in spacecraft shape from the cone CS_1VF (fig. 17) to the glider G_2S_1VF with wings and Saturn fins alined (fig. 18(a)) shows no appreciable effect on the directional stability of the vehicle in spite of the added side area ahead of the moment center contributed by the glider. However, the glider does result in a significant increase in $-C_{l_\beta}$ at Mach numbers comparable to those of the cone CS_1VF. Furthermore, a substantial reduction in the negative values of C_{l_β} occurs with increase in Mach numbers beyond about $M = 2.29$. At a Mach number of 4.65, C_{l_β} is approximately equal to zero. The largest values of C_{l_β} occur at Mach numbers of 1.57 to 1.80 where the largest dynamic pressures also exist (fig. 18). This condition can lead to a structural problem on the stabilizing surfaces of such a vehicle, particularly when the surfaces are also required to carry a load for vehicle trim that is additive to the load due to rolling moment.

Interdigitation of the glider wings with the fins of the Saturn model (compare fig. 18(b), $G_3S_1V_1F$, with fig. 18(a), G_2S_1VF) results in added instability of the configuration at $M = 1.57$ but has little or no effect on C_{n_β} at the higher Mach numbers (1.80 and 2.16). It will be remembered that interdigitation by a $45°$ setting of the vehicle stabilizing surfaces results in a 41-percent increase in exposed surface area when four fins of equal area are involved. However, the vertical fins of the in-line configuration were about 8.5 percent smaller in area than the horizontal fins. The interdigitated fins were all of the same area and this area was made equal to that of larger-area fins (horizontal) of the in-line configuration. The net increase in vertical fin area coming from interdigitation was then 49.5 percent. A decrease in the inherent directional instability of the configuration comparable to a 49.5-percent increase in stabilizing area could then be expected. Since no improvement in directional stability occurred as a result of interdigitation, it appears then that adverse interference effects are considerable with such an arrangement of glider and vehicle stabilizing surfaces.

CONCLUSIONS

An investigation was conducted to determine the aerodynamic characteristics of Saturn launch vehicles in combination with conical and winged spacecraft, at Mach numbers from 1.57 to 4.65. The following results are indicated:

1. The stability level and normal-force characteristics of the two- and three-stage Saturn-cone vehicles were for the most part comparable throughout the Mach number range even though the overall lengths and nose shapes were considerably different.

2. Addition of the fixed stabilizing surfaces at the base of the first stage of the two-stage launch vehicle decreased the instability about 50 percent.

3. Replacing the conical spacecraft on the two-stage vehicle with a winged or lifting spacecraft increased the normal-force-curve slope about 10 percent and moved the center of pressure about 0.8 to 0.5 model diameter (first stage) ahead of that for the conical spacecraft configuration.

4. Interdigitating the glider wings with the launch-vehicle control and stabilizing surfaces did not change the stability of the Saturn-glider configuration from that of the in-line configuration; however, the effectiveness of the control surfaces located at the base of the second stage was improved significantly by this change.

Langley Research Center,
    National Aeronautics and Space Administration,
        Langley Station, Hampton, Va., April 19, 1963.
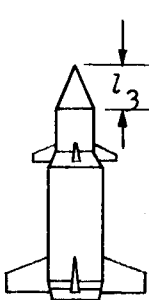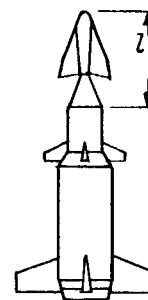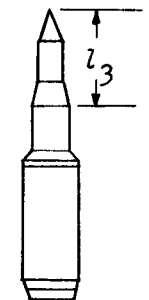
<div align="center">REFERENCES</div>

1. Pearson, Albin O.: Wind-Tunnel Investigation at Mach Numbers From 0.30 to 1.20 of the Static Aerodynamic Characteristics of a Two-Stage Saturn Launch Vehicle. NASA TM X-601, 1961.

2. Morgan, James R., and Fournier, R. H.: Static Longitudinal Aerodynamic Characteristics of a Model of a Two-Stage Version of a Saturn Launch Vehicle with a Proposed Apollo Payload at Mach Numbers From 1.57 to 2.87. NASA TM X-602, 1961.

TABLE I

GENERAL PHYSICAL CHARACTERISTICS OF THE VEHICLE SYSTEMS INVESTIGATED
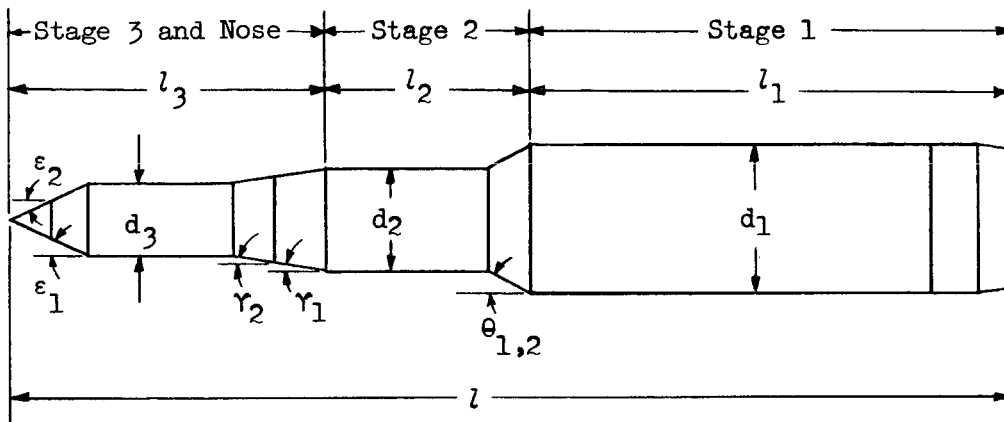
Item	Configuration		
	Saturn-cone	Saturn-glider	3-stage Saturn
l/d_1	7.69	6.59	7.54
l_1/d_1	3.46	3.46	3.46
l_2/d_1	1.66	1.66	1.66
l_3/d_1	2.57	1.47	2.42
d_2/d_1	0.856	0.856	0.856
d_3/d_1	-----	-----	.467
θ_1, deg	13	13	24.5
θ_2, deg	24	-----	-----
γ_1, deg	13.25	13.25	15
γ_2, deg	18	18	-----
ϵ_1, deg	-----	-----	12.5
ϵ_2, deg	-----	-----	13.5

Figure 1.- System of axes. Arrows indicate positive values.

View A-A
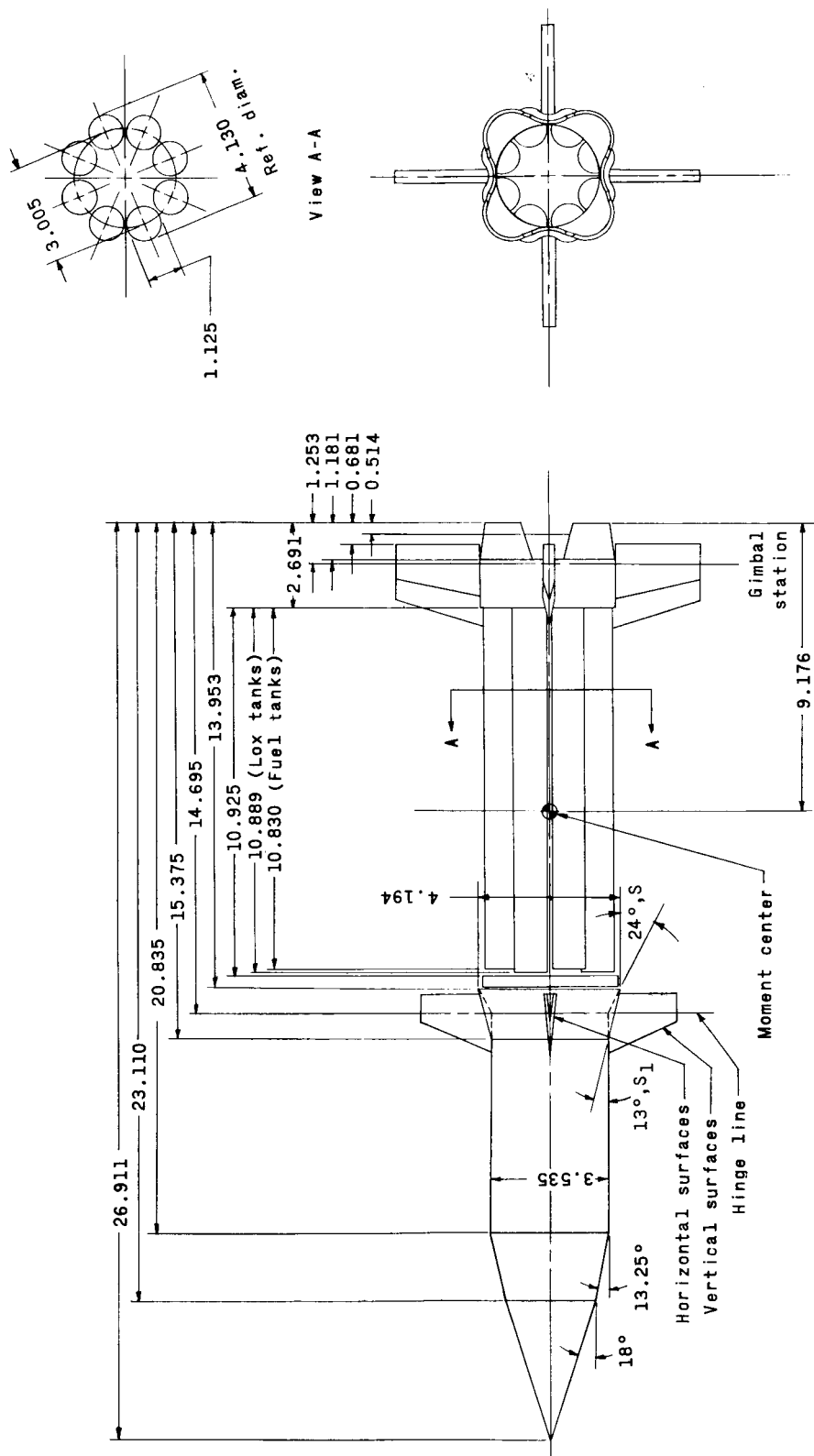
(a) Saturn-cone model, CS₁VF and CSVF.

Figure 2.- Drawing of Saturn-cone model. All dimensions are in inches unless otherwise specified.

16
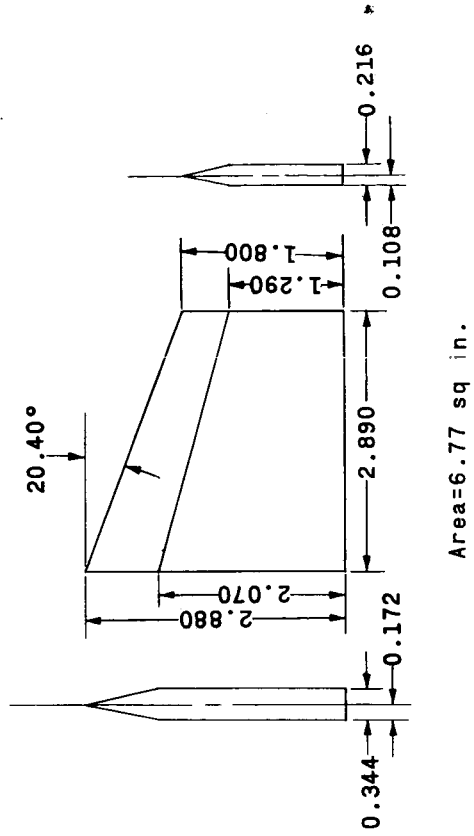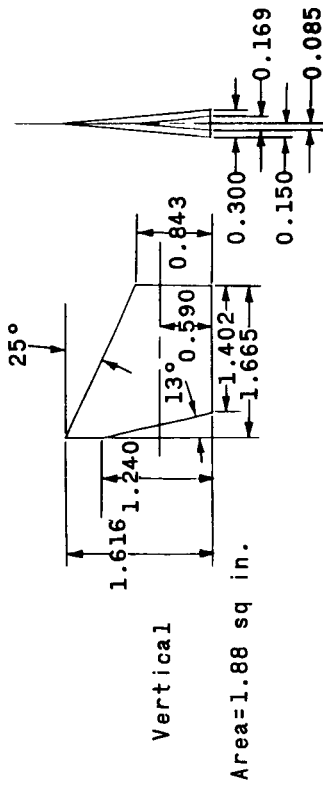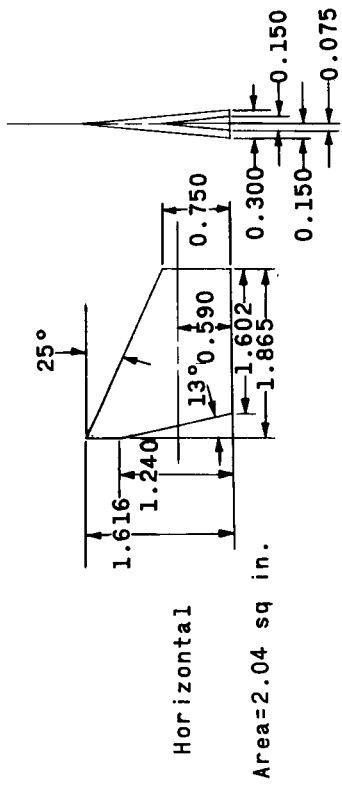
Stabilizing surfaces
First stage

Area=6.77 sq in.

20.40°

1.800
1.290
0.108
0.216
2.890
2.070
2.880
0.172
0.344

Control surfaces
Second stage

Horizontal

Area=2.04 sq in.

25°
13°
1.616
1.240
0.590
1.602
1.865
0.750
0.300
0.150
0.150
0.075

Vertical

Area=1.88 sq in.

25°
13°
1.616
1.240
0.590
1.402
1.665
0.843
0.300
0.150
0.169
0.085

(b) Control and stabilizing surfaces.

Figure 2.- Concluded.
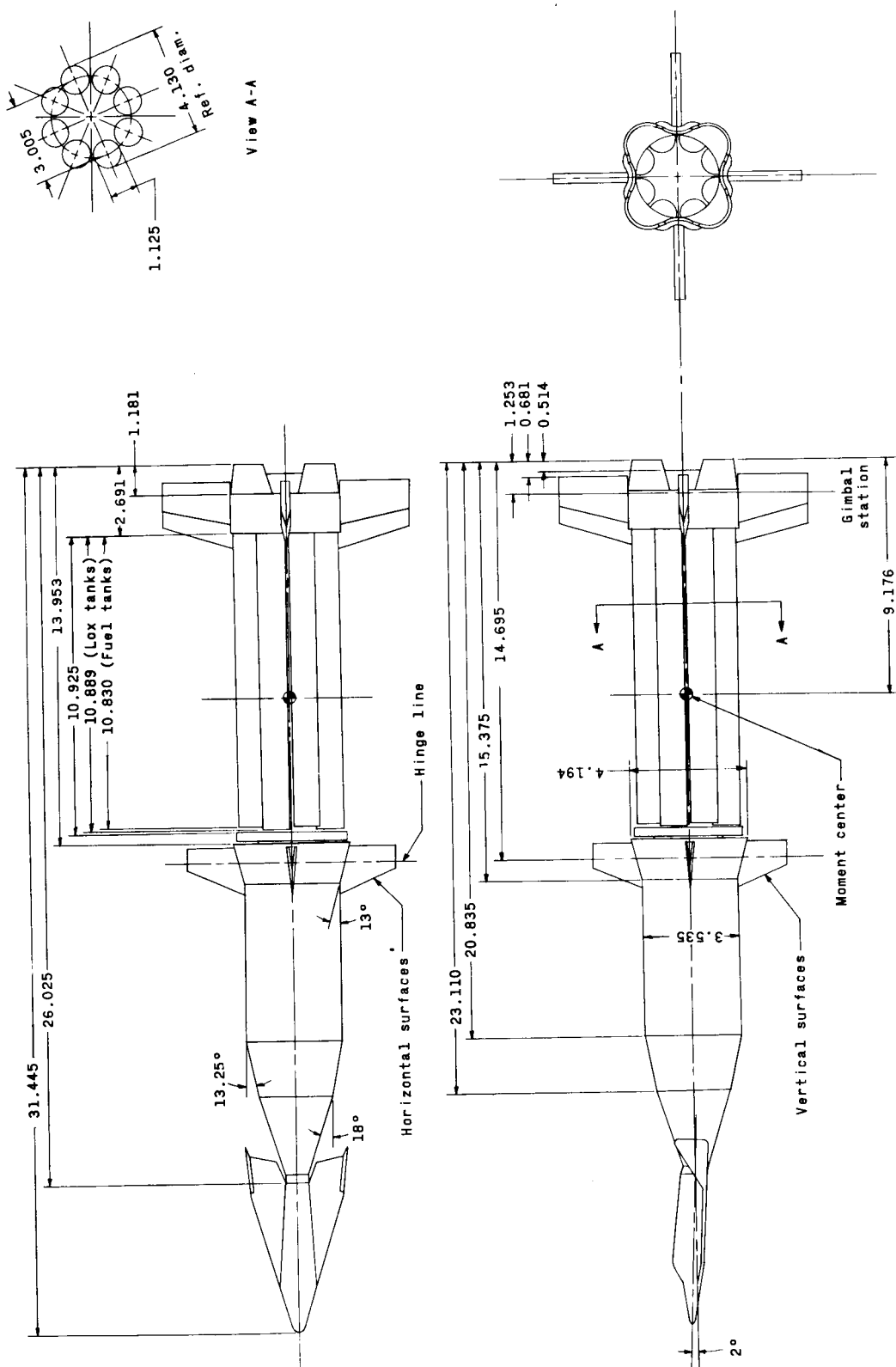
(a) Saturn-glider model. All dimensions are in inches unless otherwise specified.

Figure 3.- Drawing of Saturn-glider model.

18
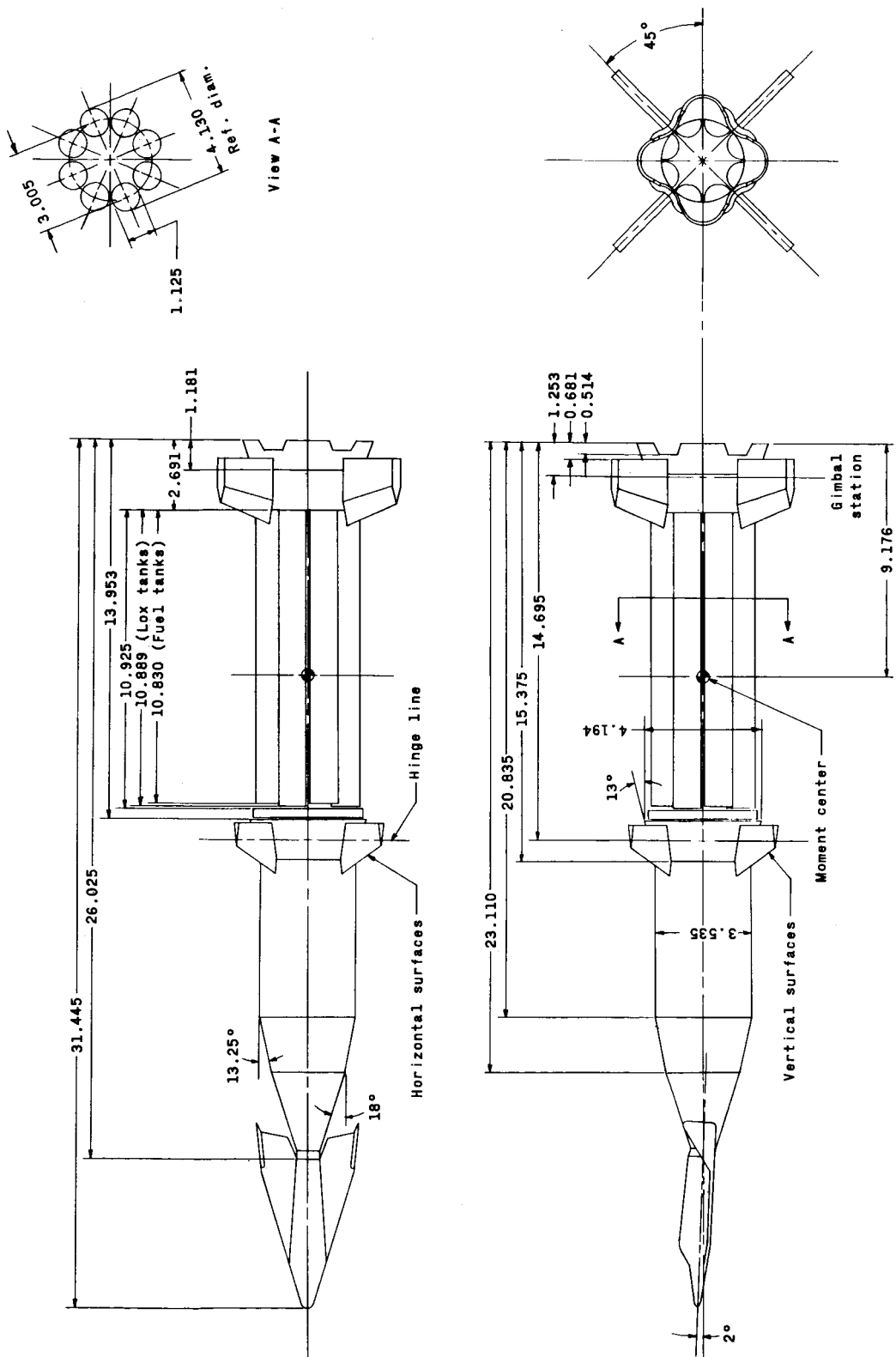
(b) Saturn-glider model; control and stabilizing surfaces interdigitated with glider wing, $G_3S_1V_1F$.

Figure 3.- Continued.
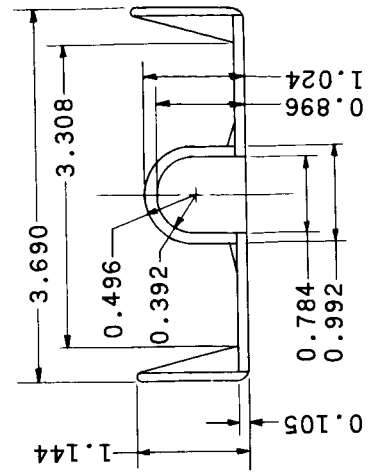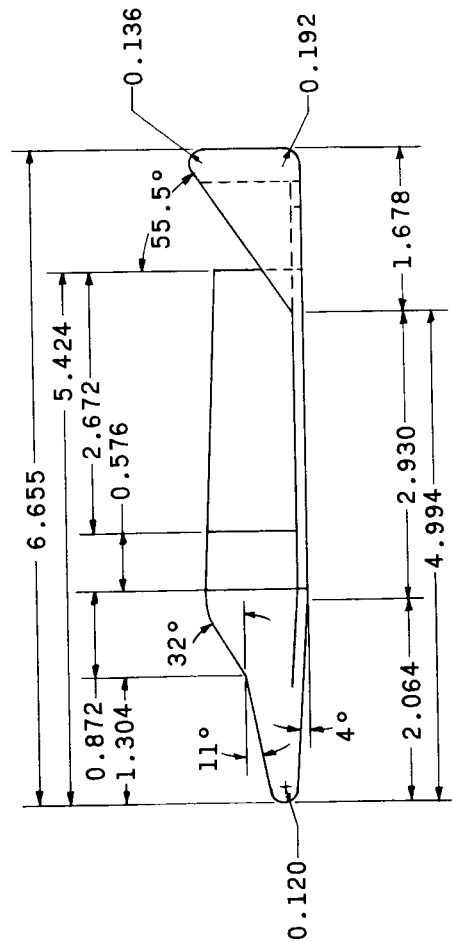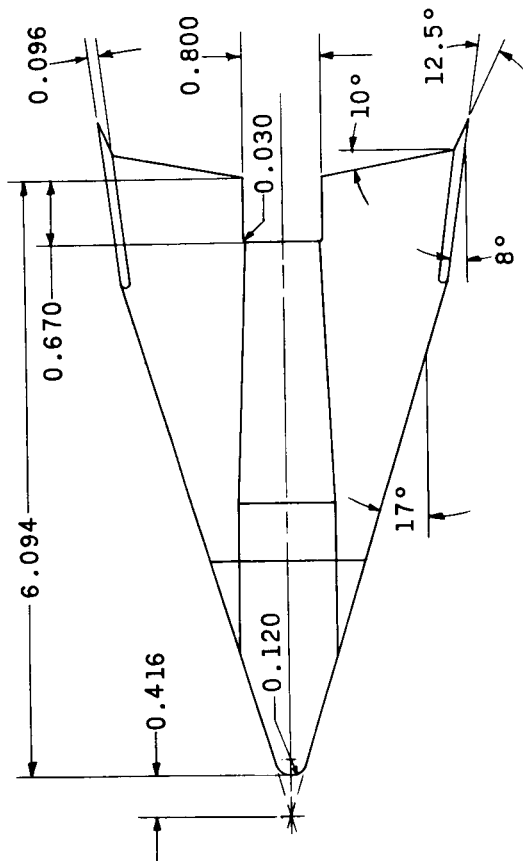
(c) Glider details.

Figure 3.- Concluded.
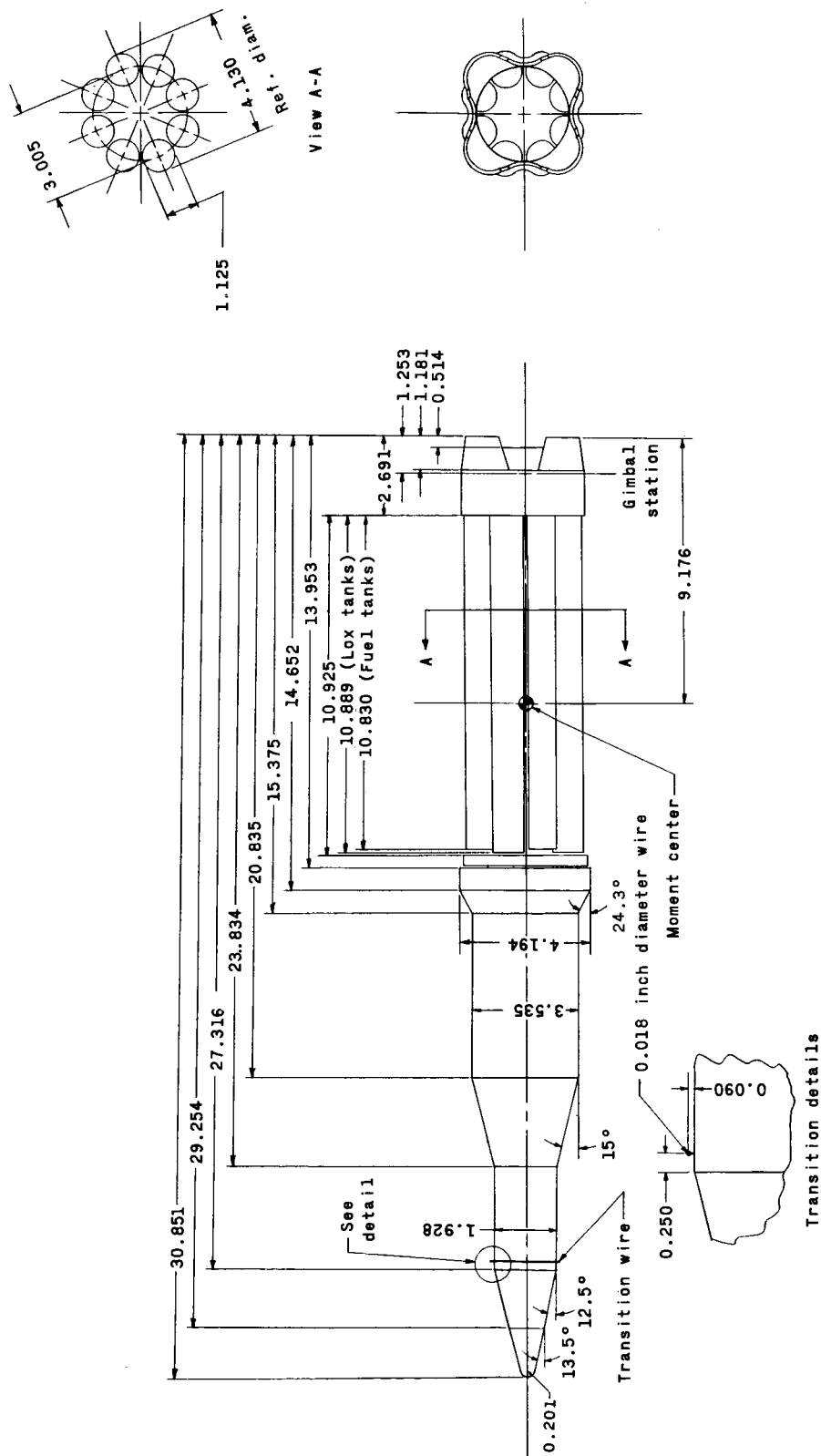
Figure 4.- Three-stage Saturn-cone model CS₂. All dimensions are in inches unless otherwise specified.

21
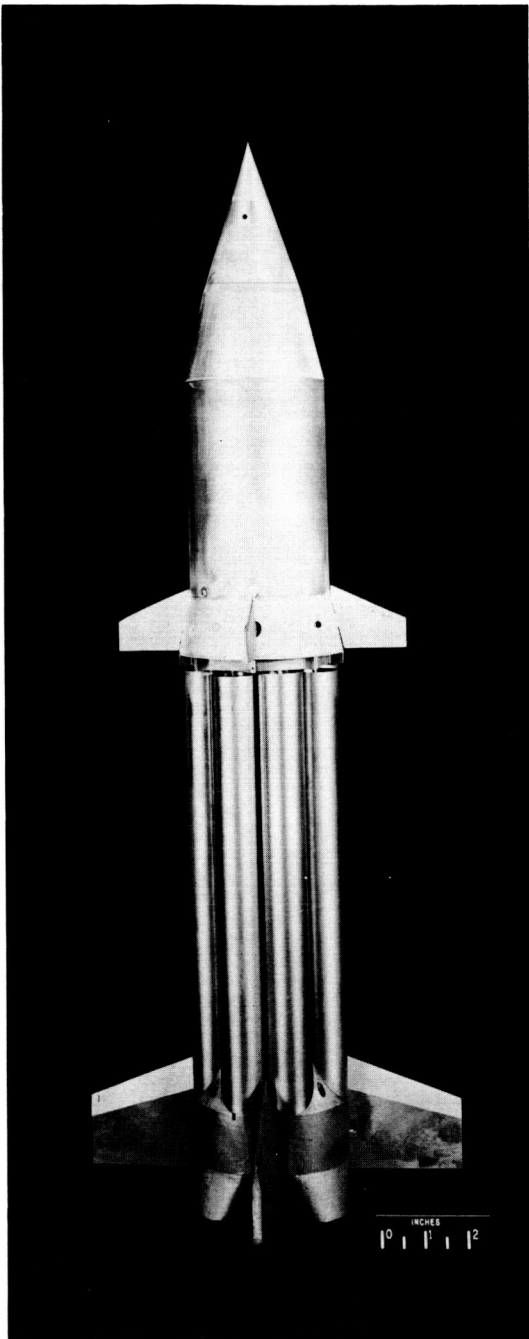
L-62-390

Saturn-cone model
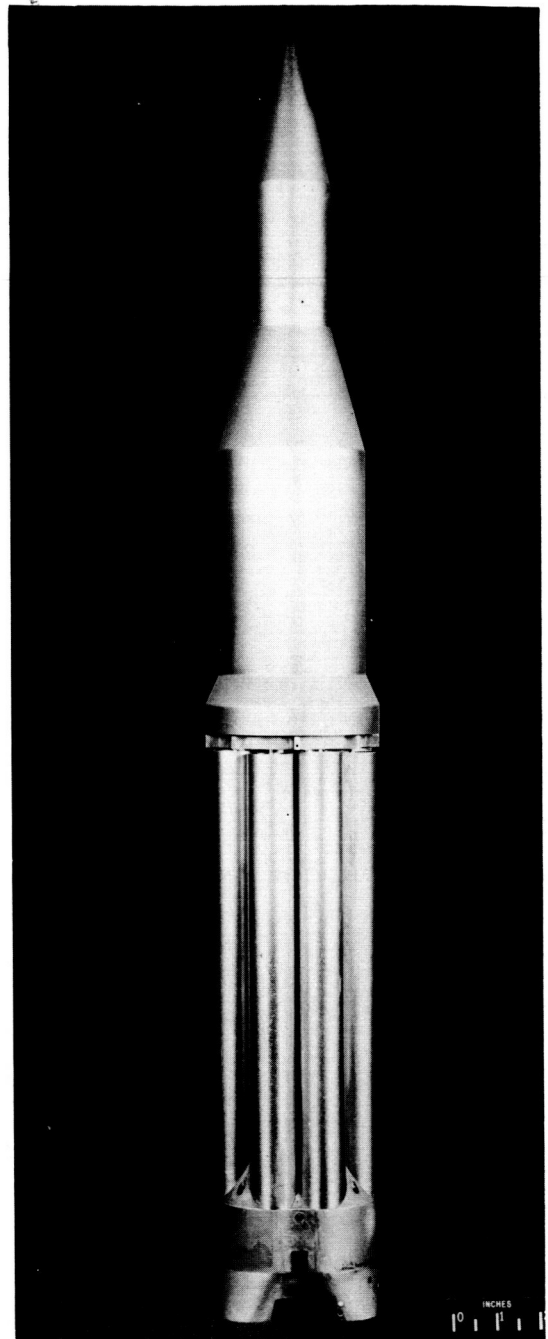
L-62-392

Three-stage Saturn-cone model

(a) Conical spacecraft vehicles.

Figure 5.- Photographs of models tested.
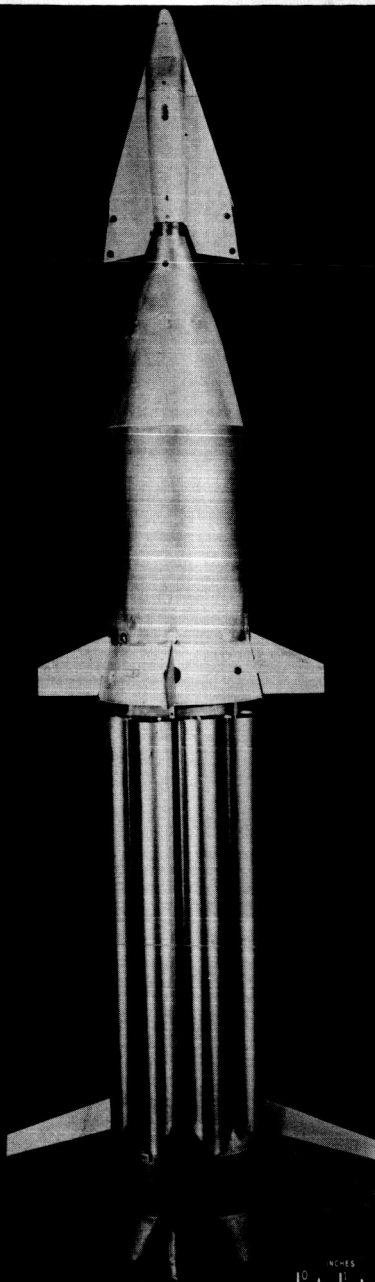
L-62-391   L-62-389
Saturn-glider in-line model   Saturn-glider interdigitated model
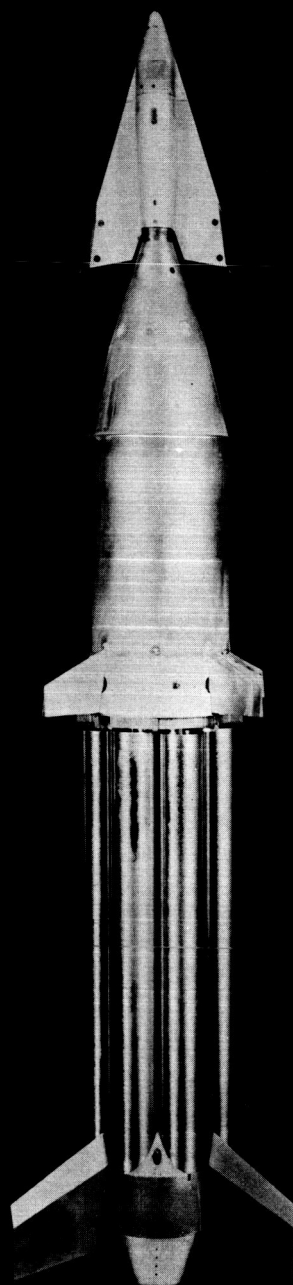
(b) Winged spacecraft vehicles.

Figure 5.- Concluded.

α = 4.5°

α = 0.1°

M = 1.57

α = -4.3°

α = 4.2°

α = 0°

M = 2.98

α = -4.4°
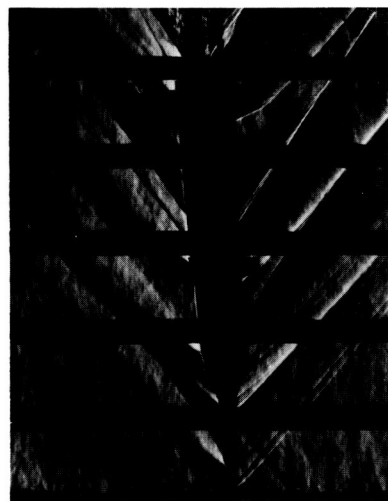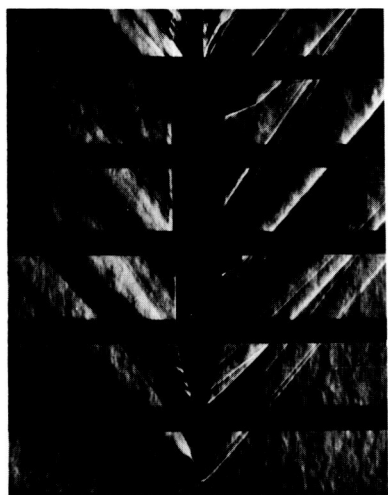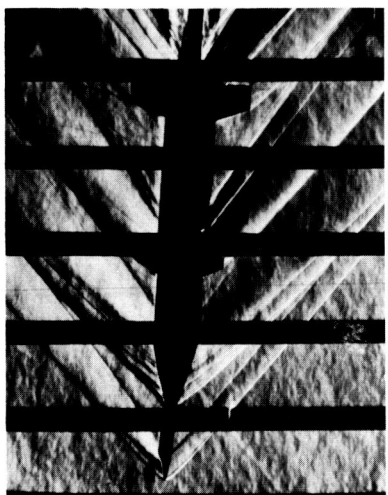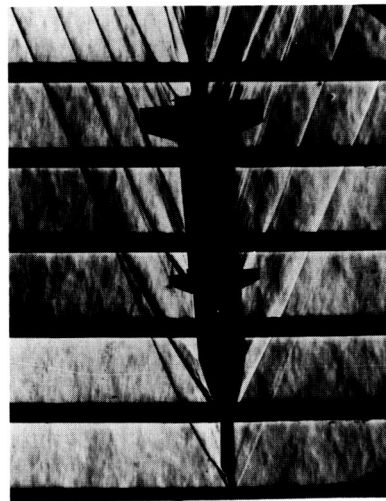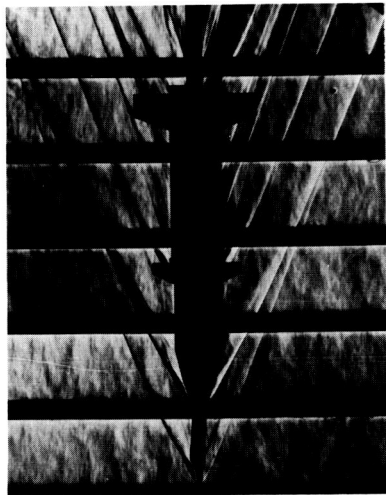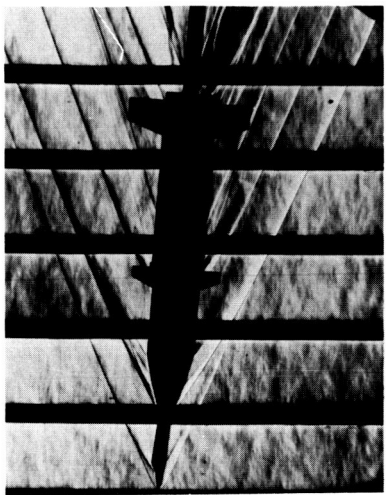
Figure 6.- Typical schlieren photographs for Saturn-glider model G_2S_1VF.

L-63-3112

α = 4.1°

α = 3.6°

α = 0°

M = 3.96

α = 0°

M = 4.65

α = -4.2°

α = -3.7°
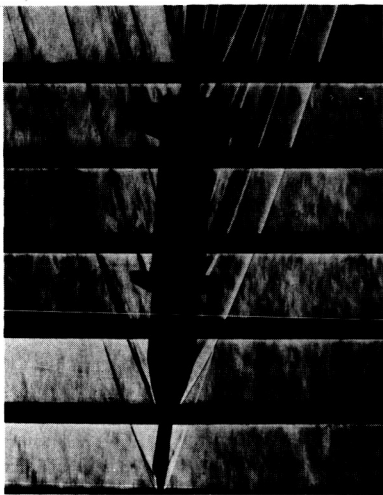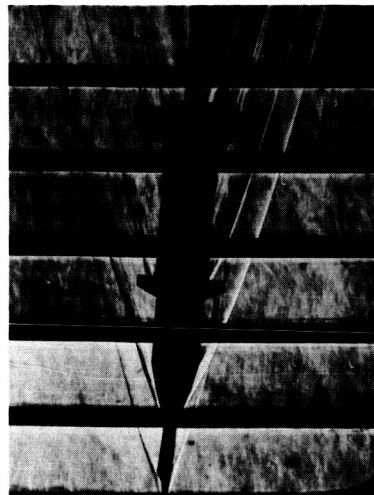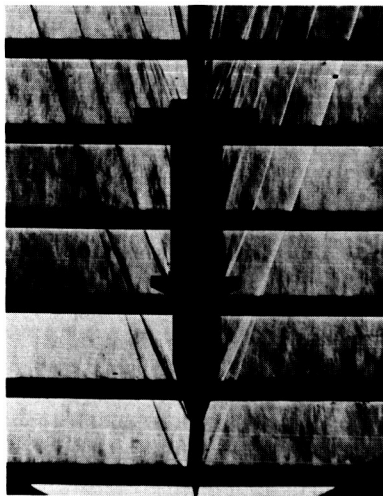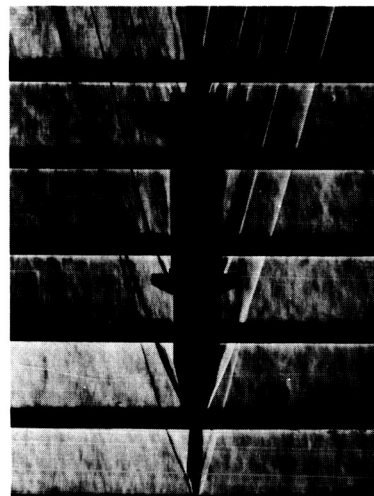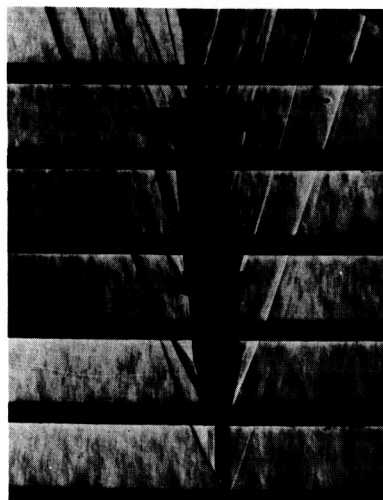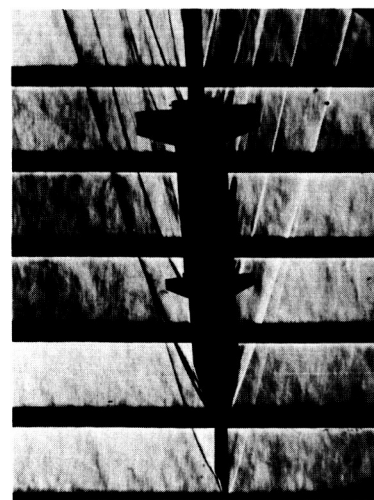
L-63-3113

Figure 6.- Concluded.

25
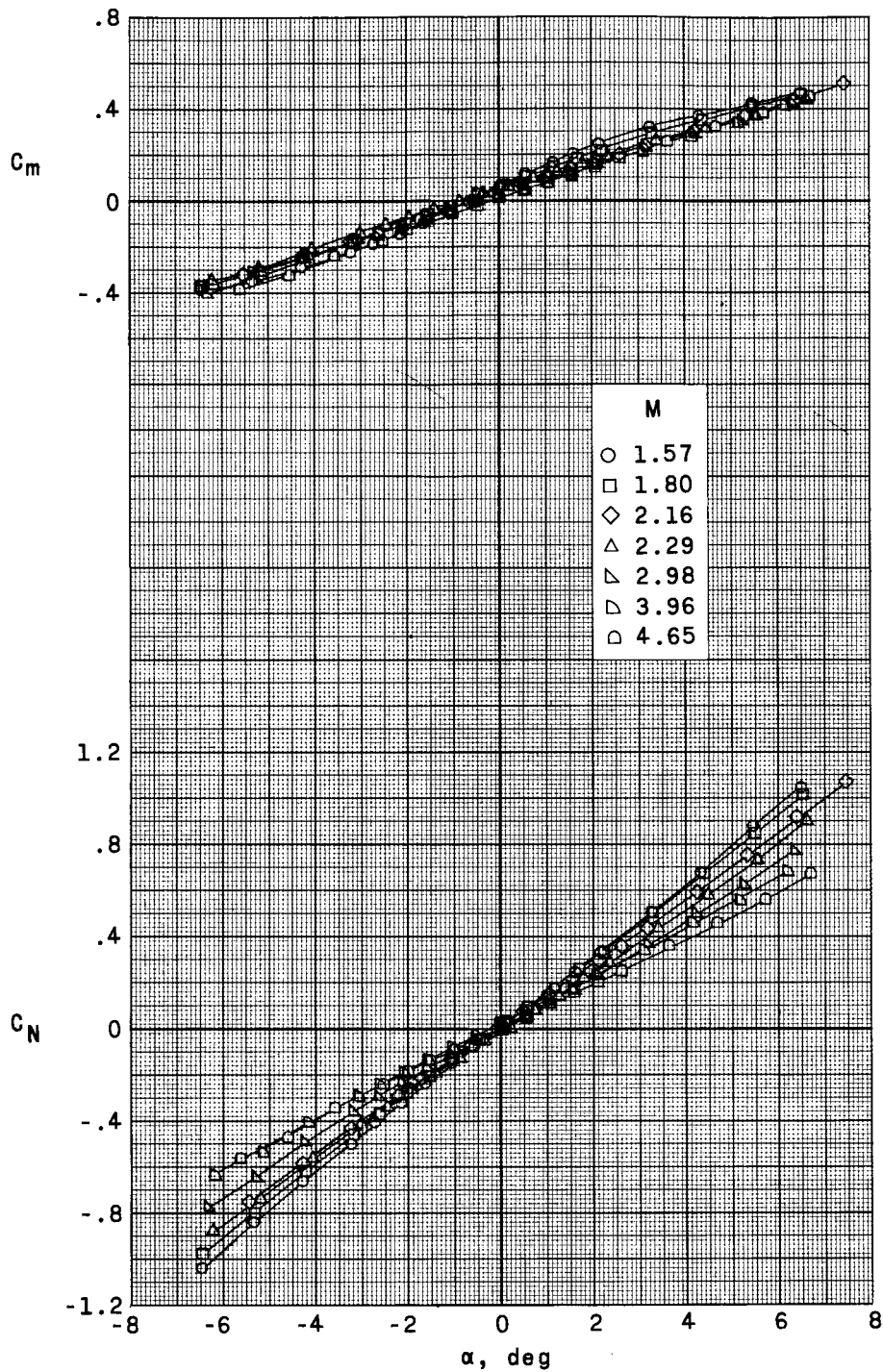
(a) Model CS$_1$VF.

Figure 7.- Longitudinal aerodynamic characteristics in pitch for the Saturn-cone model.
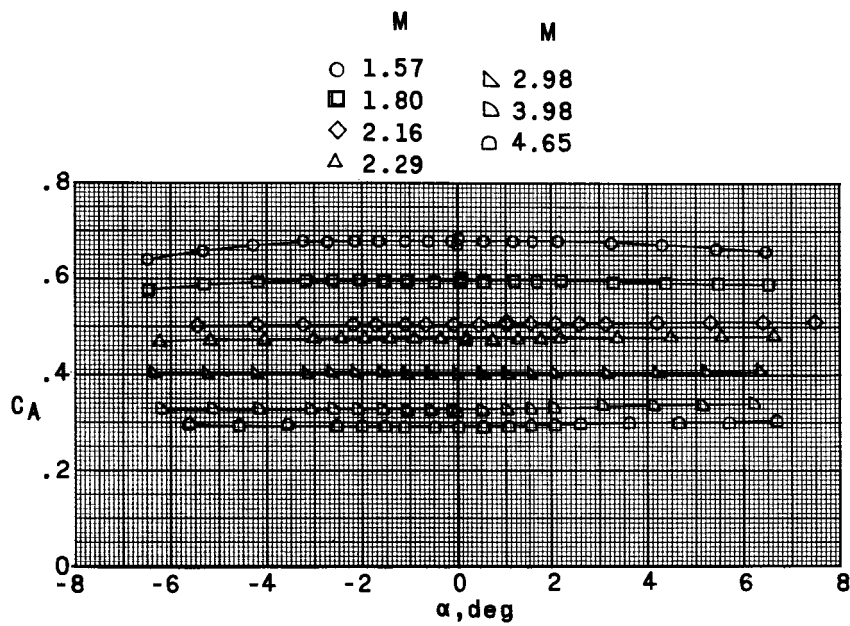
(a) Model CS₁VF. Concluded.

Figure 7.- Continued.
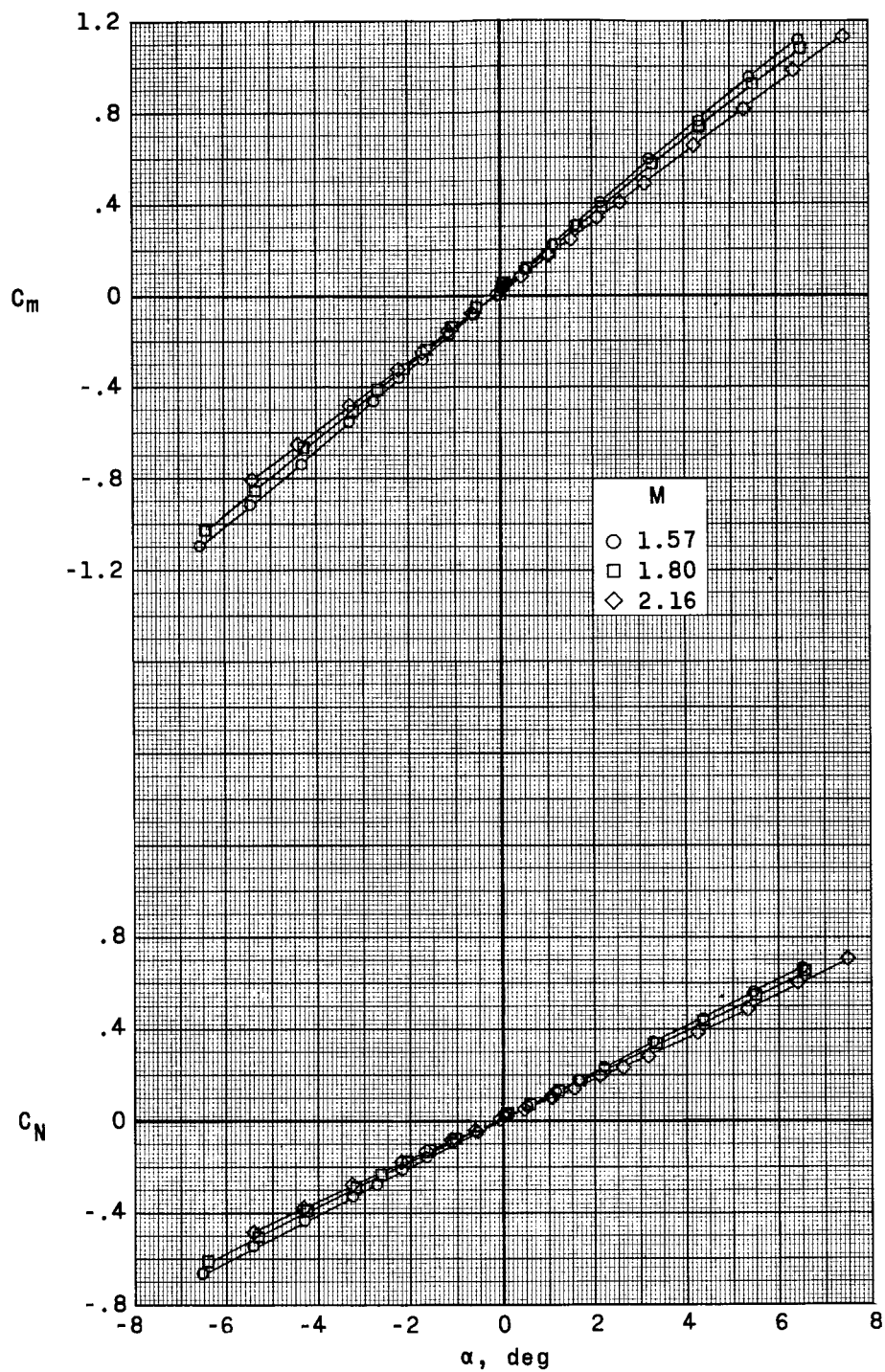
(b) Model CS_1V.

Figure 7.- Continued.

M
○ 1.57
□ 1.80
◇ 2.16
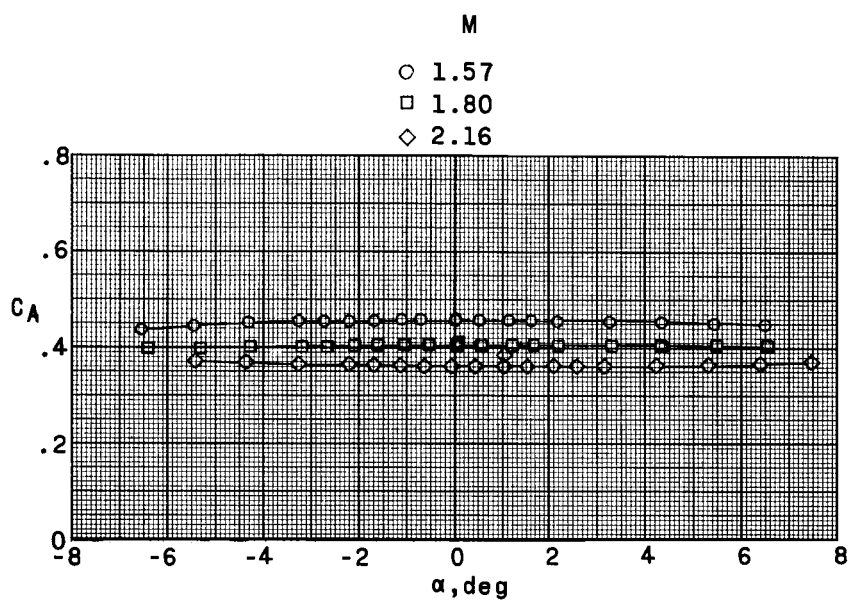
(b) Model CS_1V. Concluded.

Figure 7.- Continued.
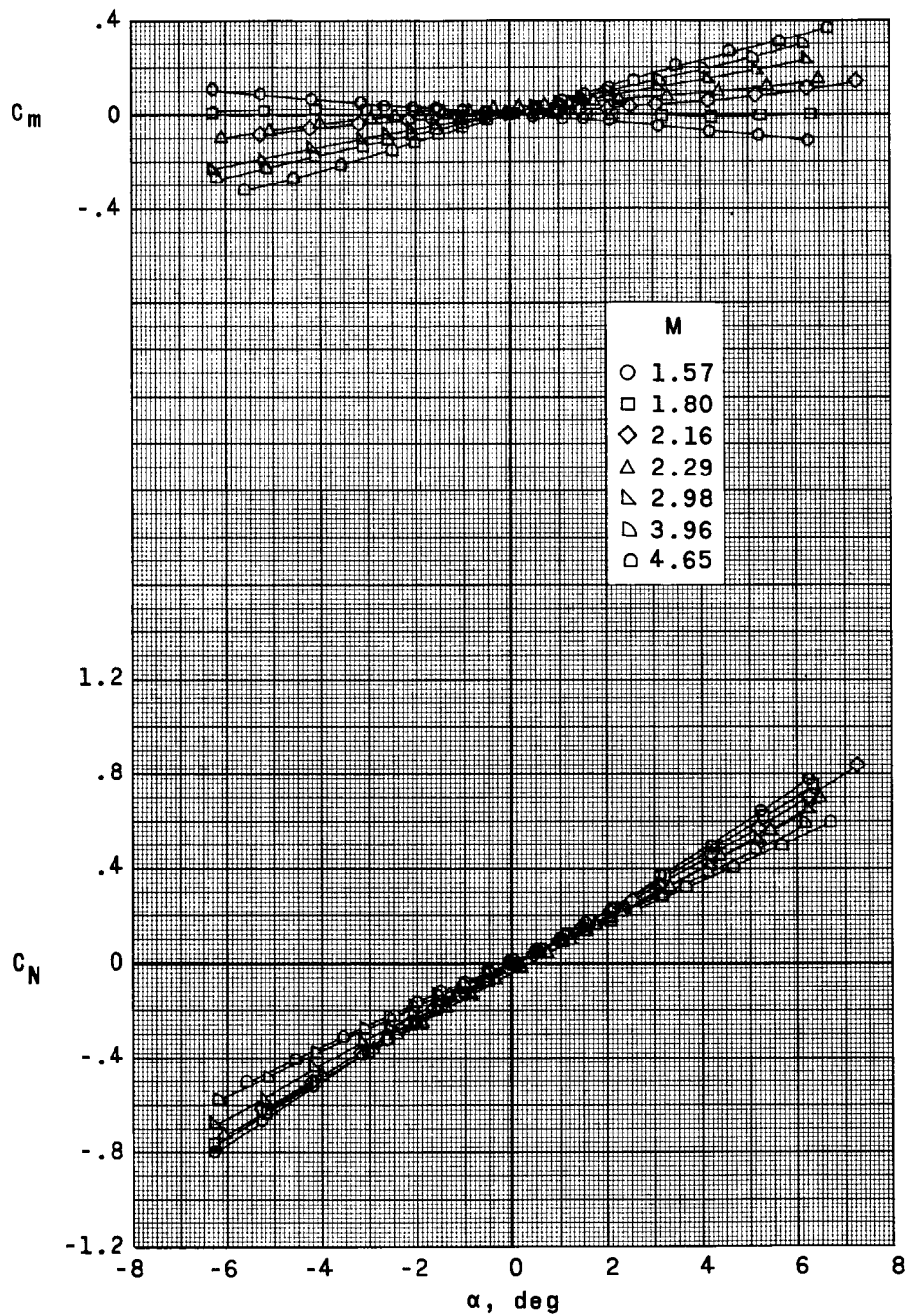
(c) Model CS_1F.

Figure 7.- Continued.

M

○ 1.57
□ 1.80
◇ 2.16
△ 2.29

M

◁ 2.98
▷ 3.98
◻ 4.65
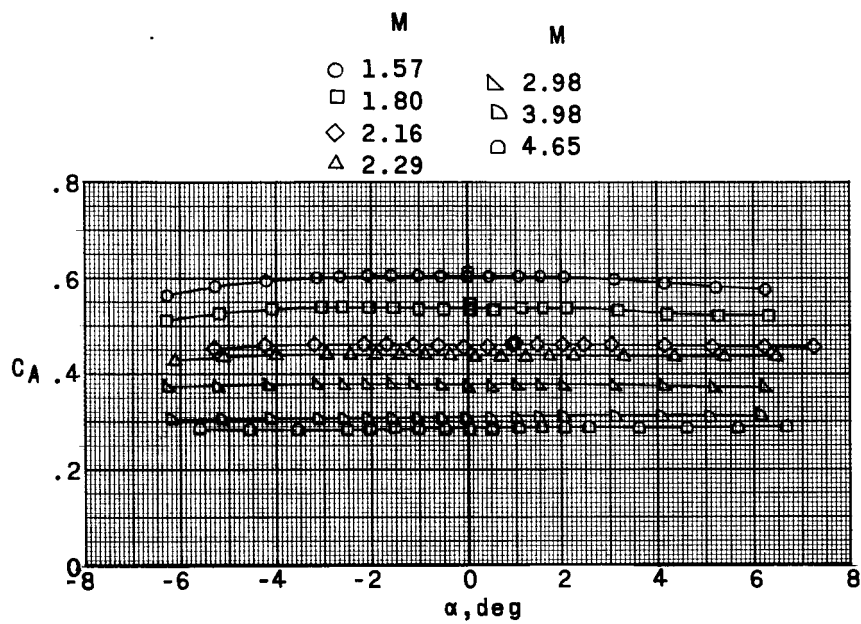
(c) Model CS_1F. Concluded.

Figure 7.- Continued.
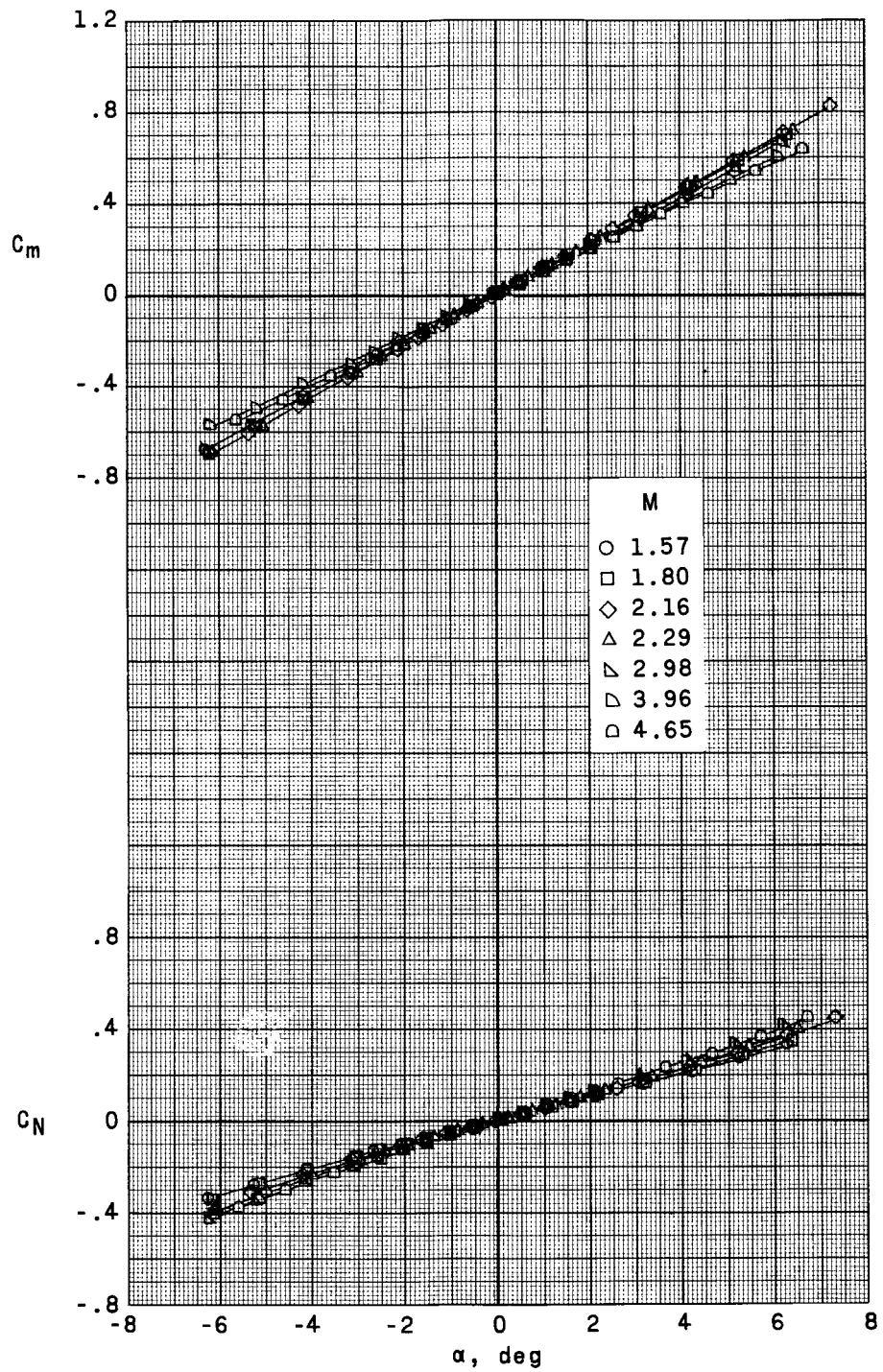
(d) Model CS_1.

Figure 7.- Continued.
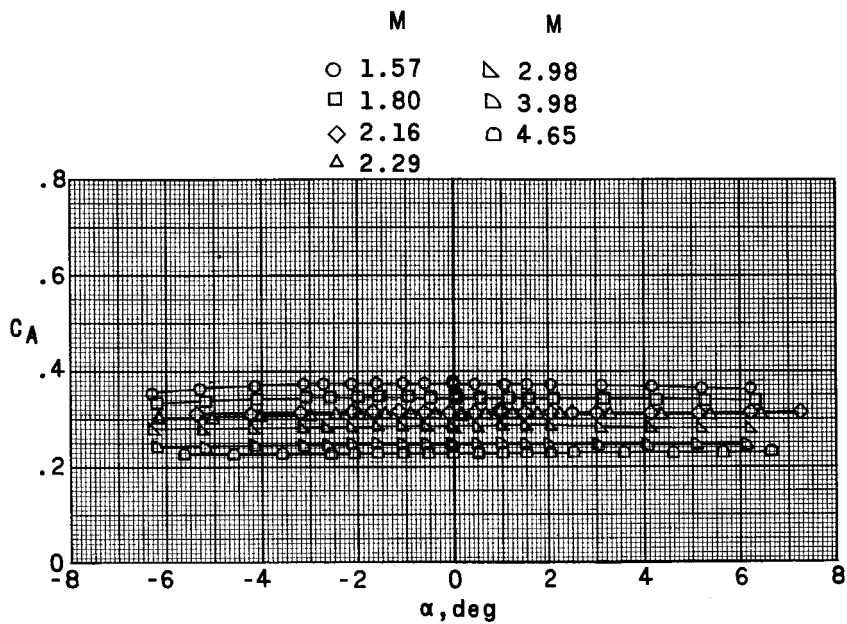
(d) Model CS_1. Concluded.

Figure 7.- Concluded.
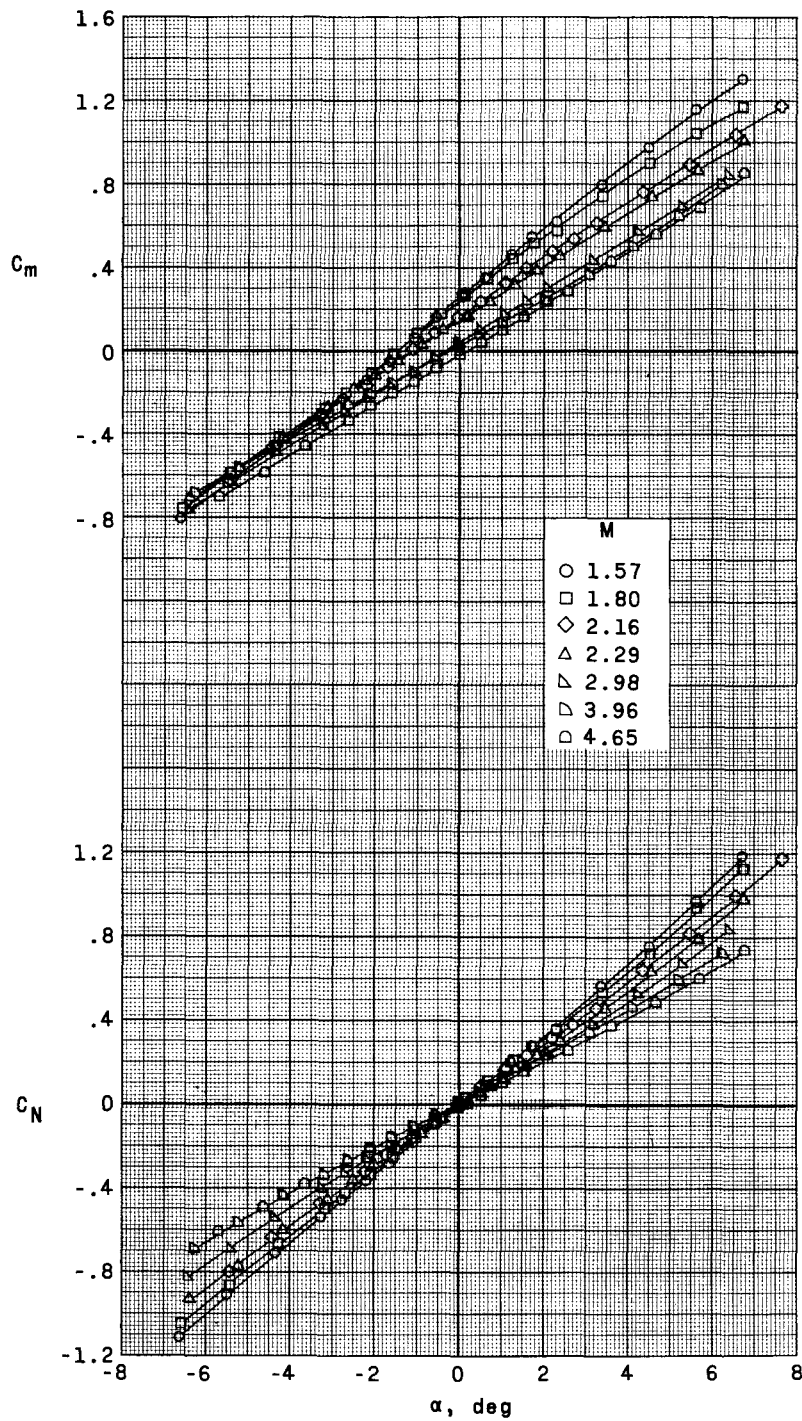
(a) Model G_2S_1VF.

Figure 8.- Longitudinal aerodynamic characteristics in pitch for the Saturn-glider model.
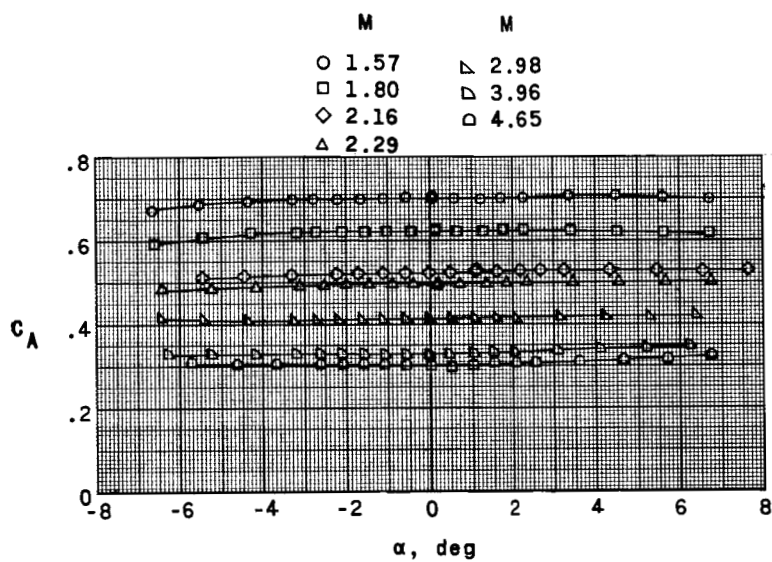
(a) Model G_2S_1VF. Concluded.

Figure 8.- Continued.
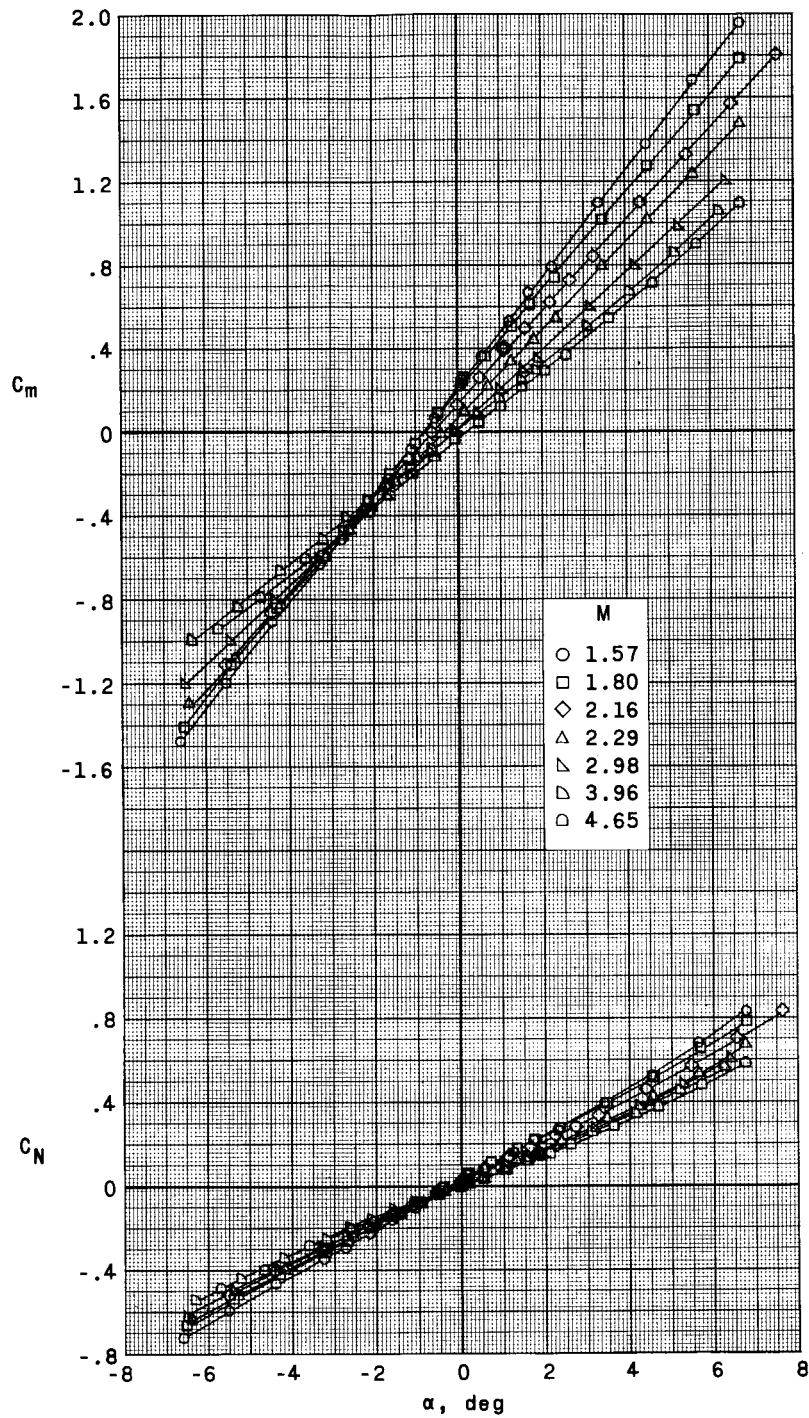
(b) Model G_2S_1V.

Figure 8.- Continued.

	M		M
○	1.57	◁	2.98
◻	1.80	◺	3.98
◇	2.16	◹	4.65
△	2.29		
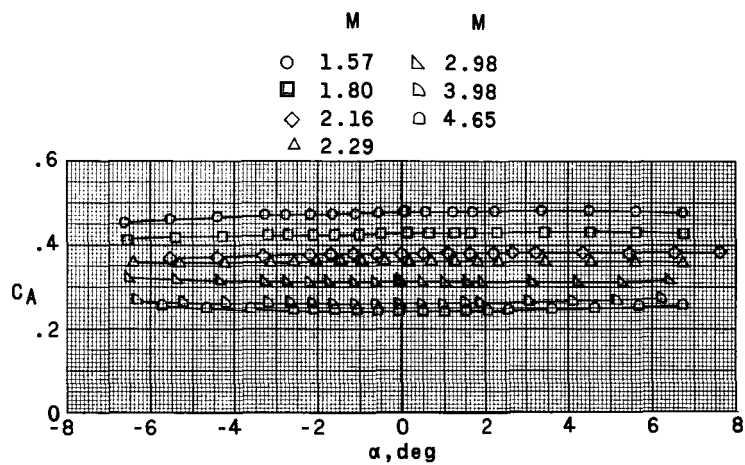
(b) Model G_2S_1V. Concluded.

Figure 8.- Continued.
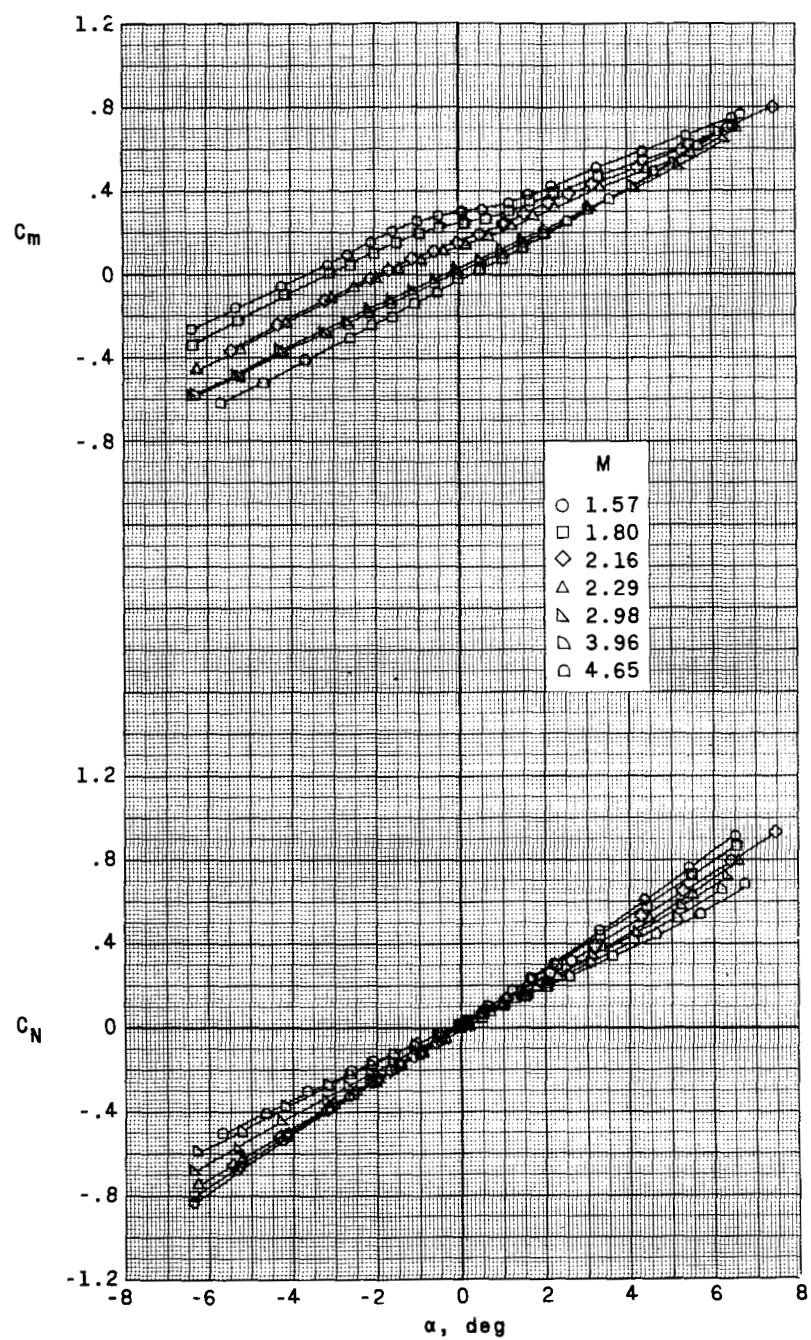
(c) Model G_2S_1F.

Figure 8.- Continued.
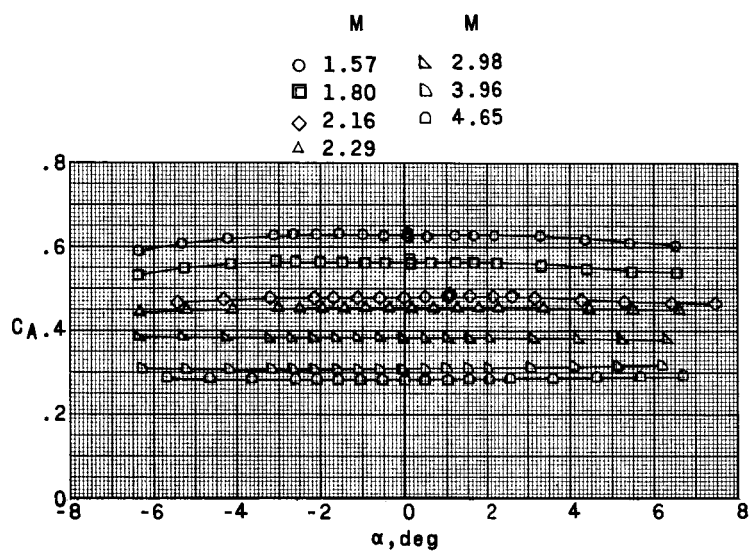
(c) Model G_2S_1F. Concluded.

Figure 8.- Continued.
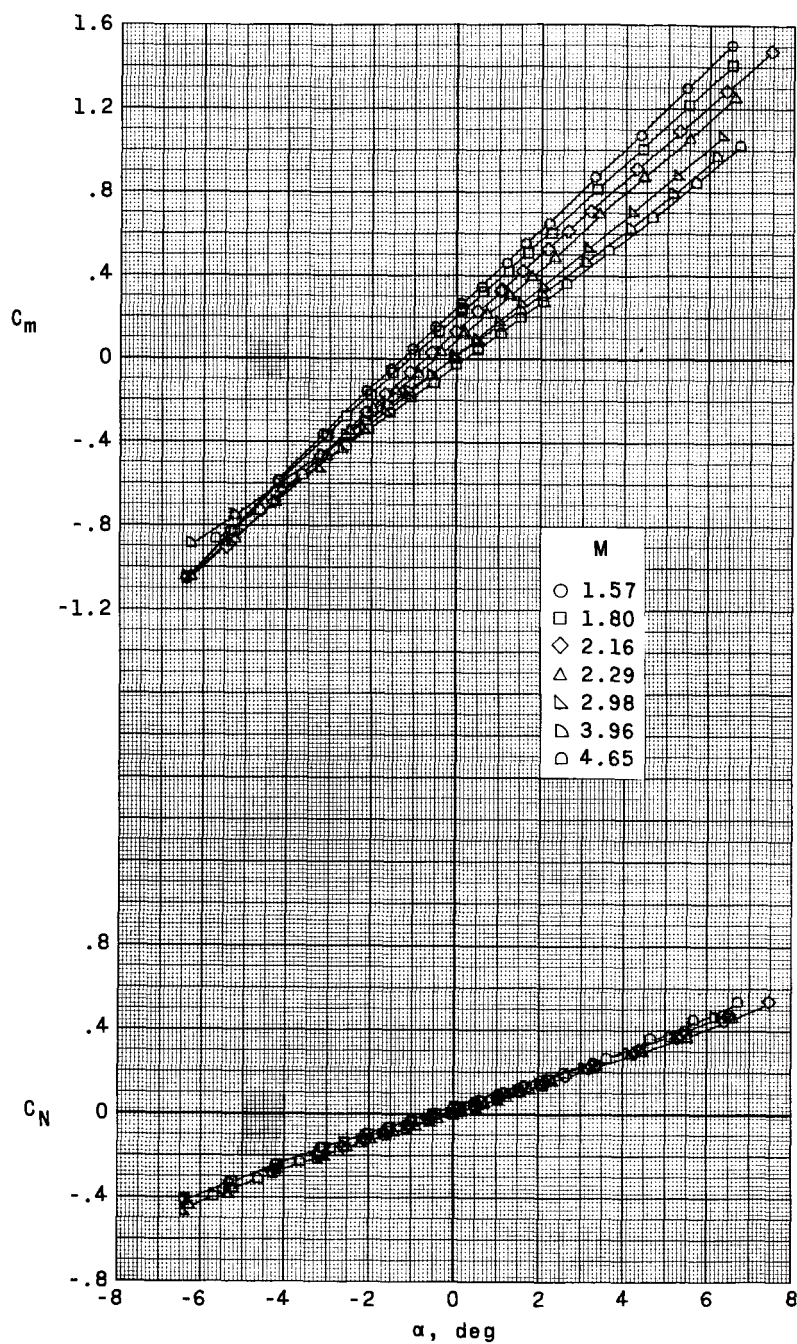
(d) Model G_2S_1.

Figure 8.- Continued.
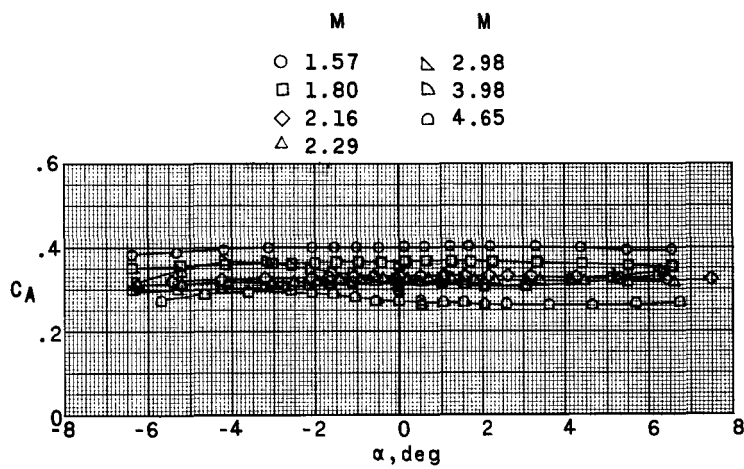
(d) Model G_2S_1. Concluded.

Figure 8.- Continued.
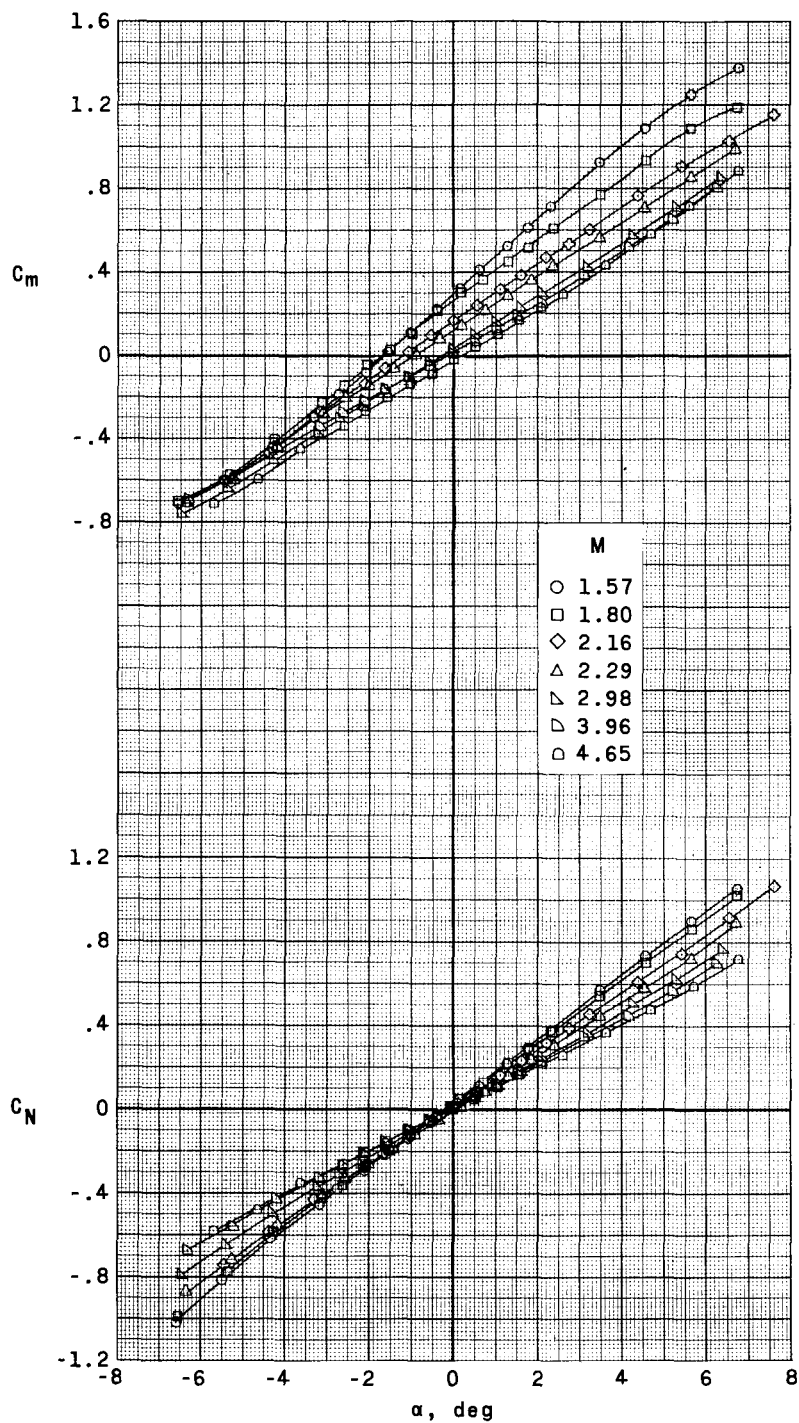
(e) Model $G_3S_1V_1F$.

Figure 8.- Continued.
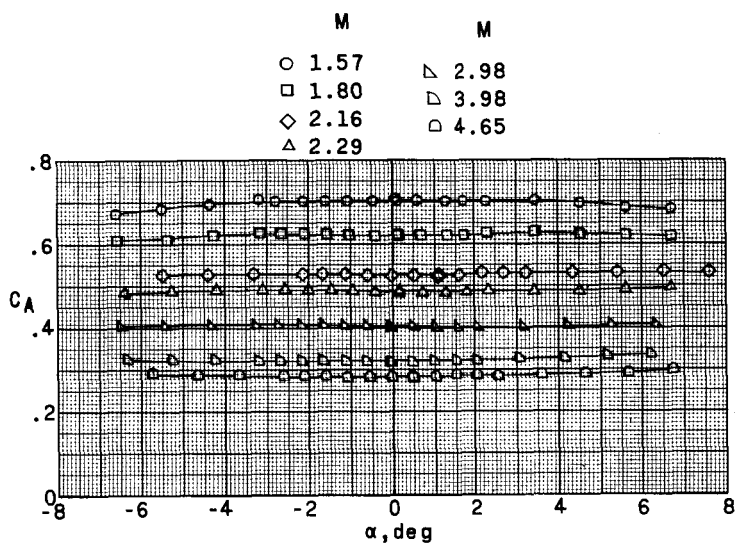
(e) Model $G_3S_1V_1F$. Concluded.

Figure 8.- Continued.
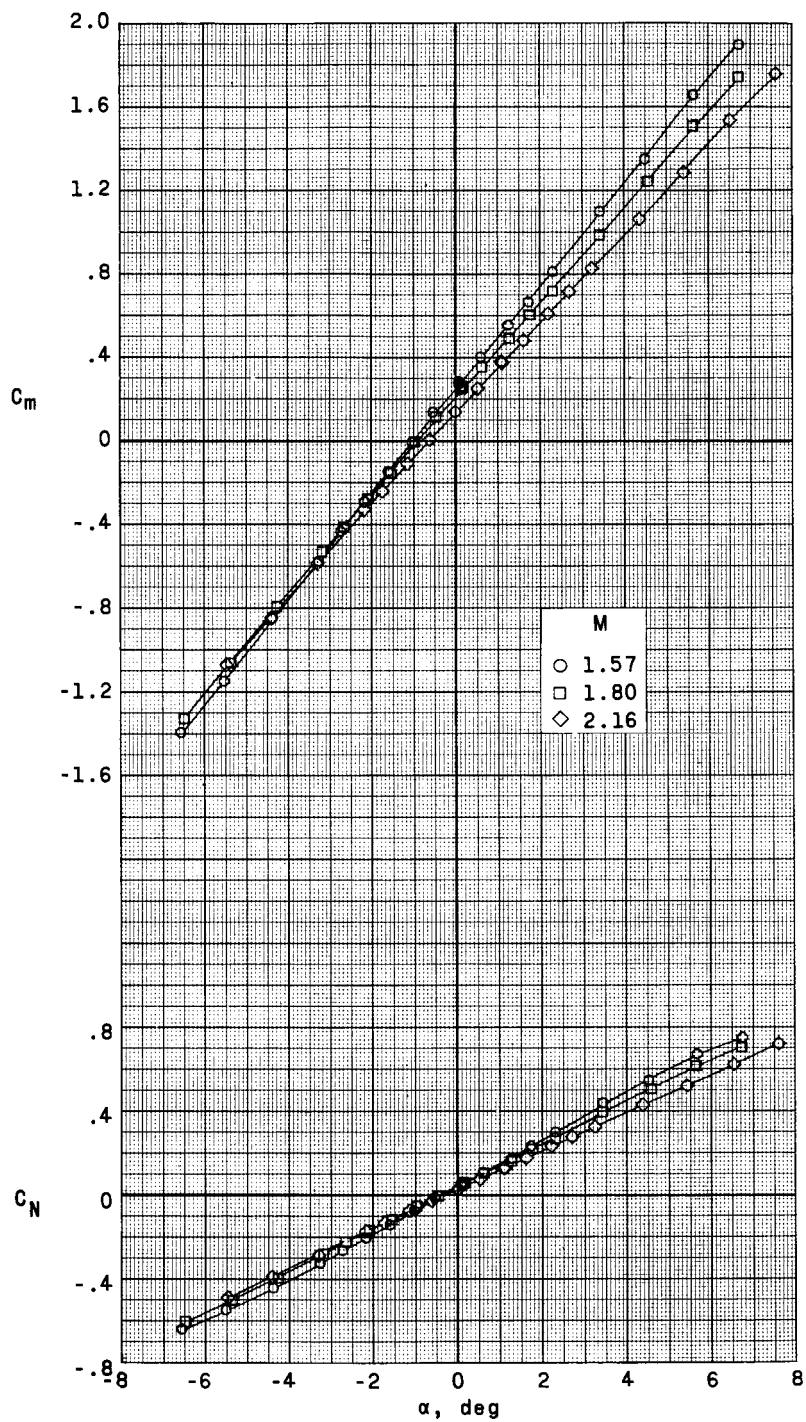
(f) Model $G_3S_1V_1$.

Figure 8.- Continued.
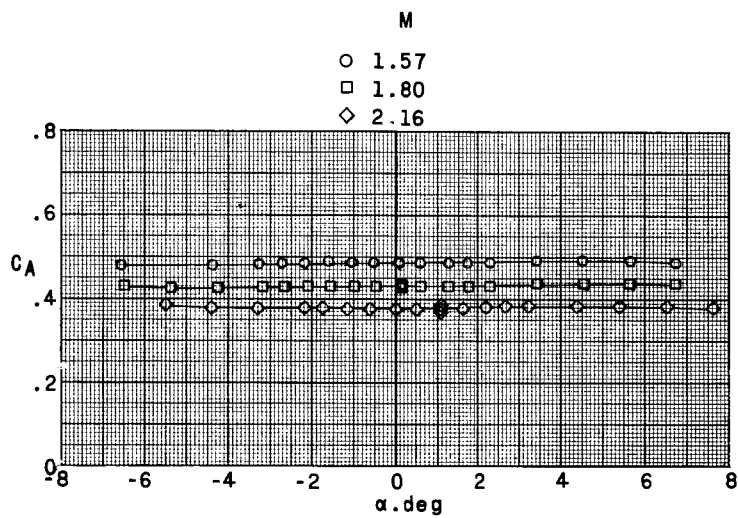
(f) Model $G_3S_1V_1$. Concluded.

Figure 8.- Continued.
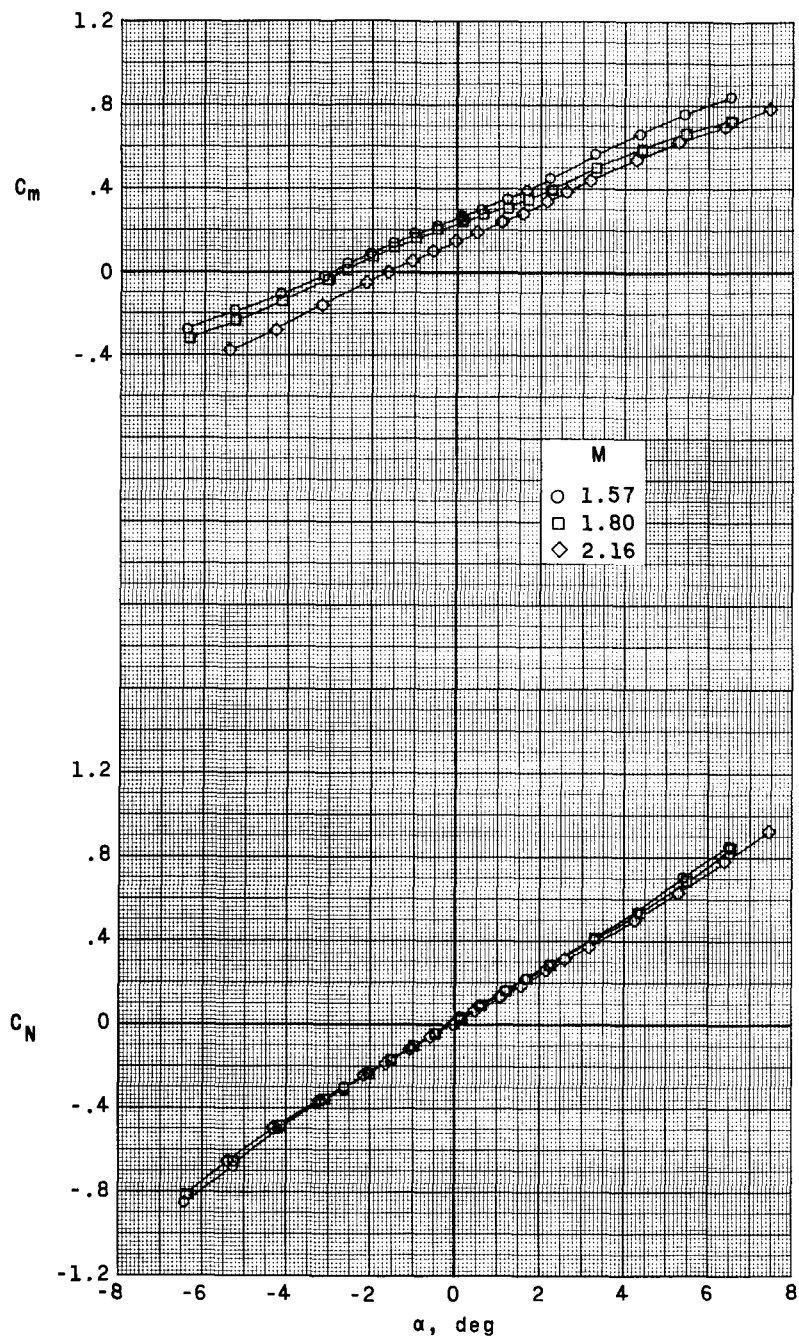
(g) Model G_3S_1F.

Figure 8.- Continued.

(g) Model G_3S_1F.   Concluded.
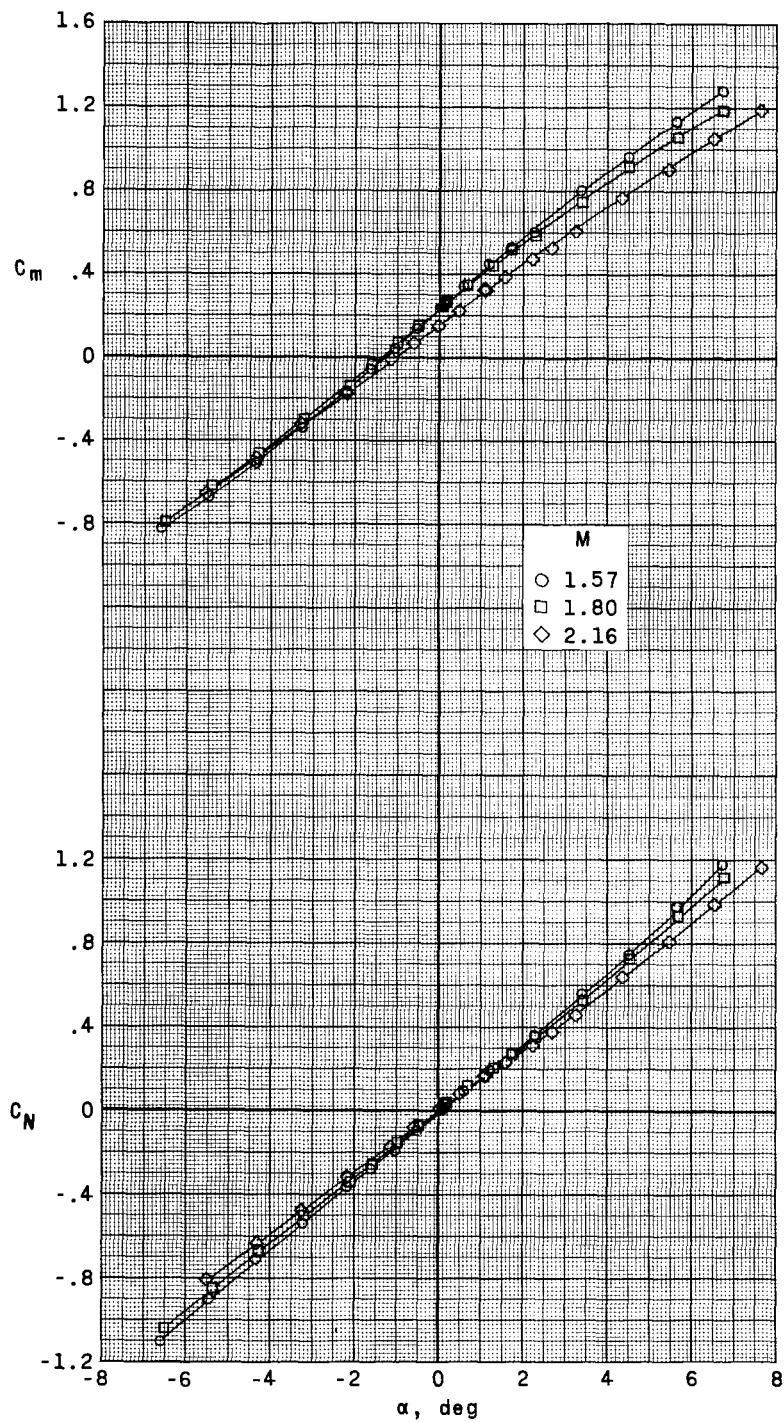
Figure 8.- Continued.

(h) Model G$_2$SVF.

Figure 8.- Continued.
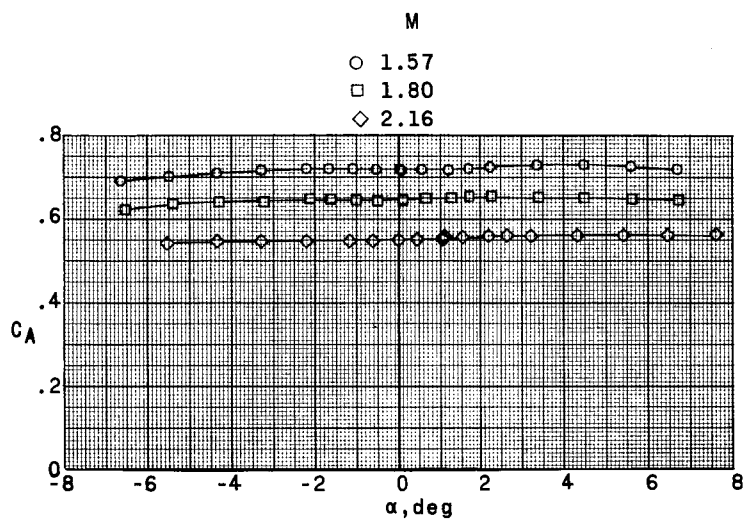
(h) Model G$_2$SVF.   Concluded.

Figure 8.- Continued.
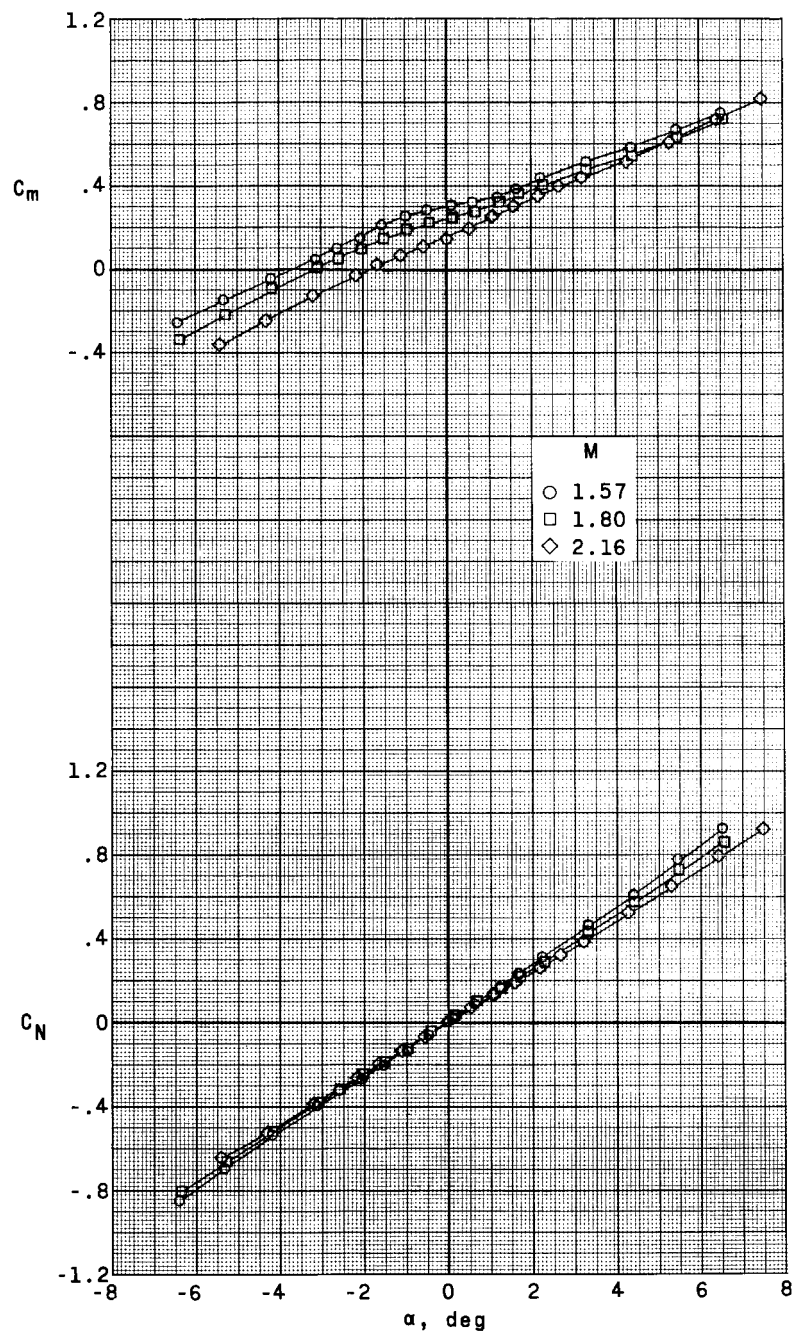
(i) Model G_2SF.

Figure 8.- Continued.

M
○ 1.57
□ 1.80
◇ 2.16
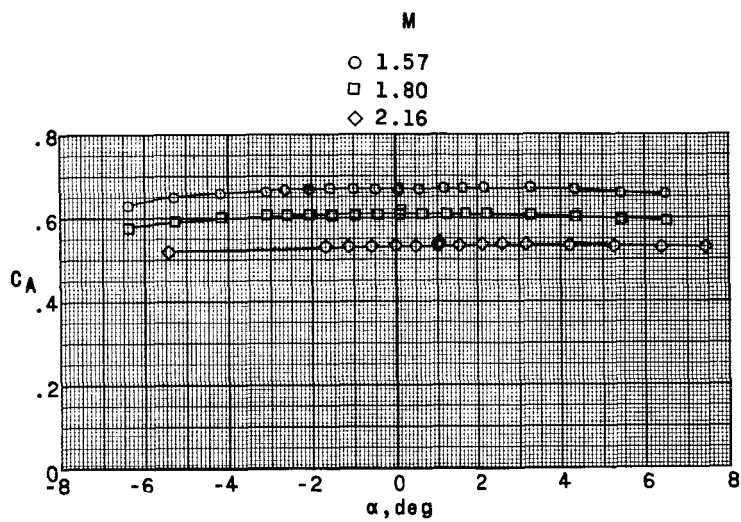
(i) Model G$_2$SF. Concluded.

Figure 8.- Continued.
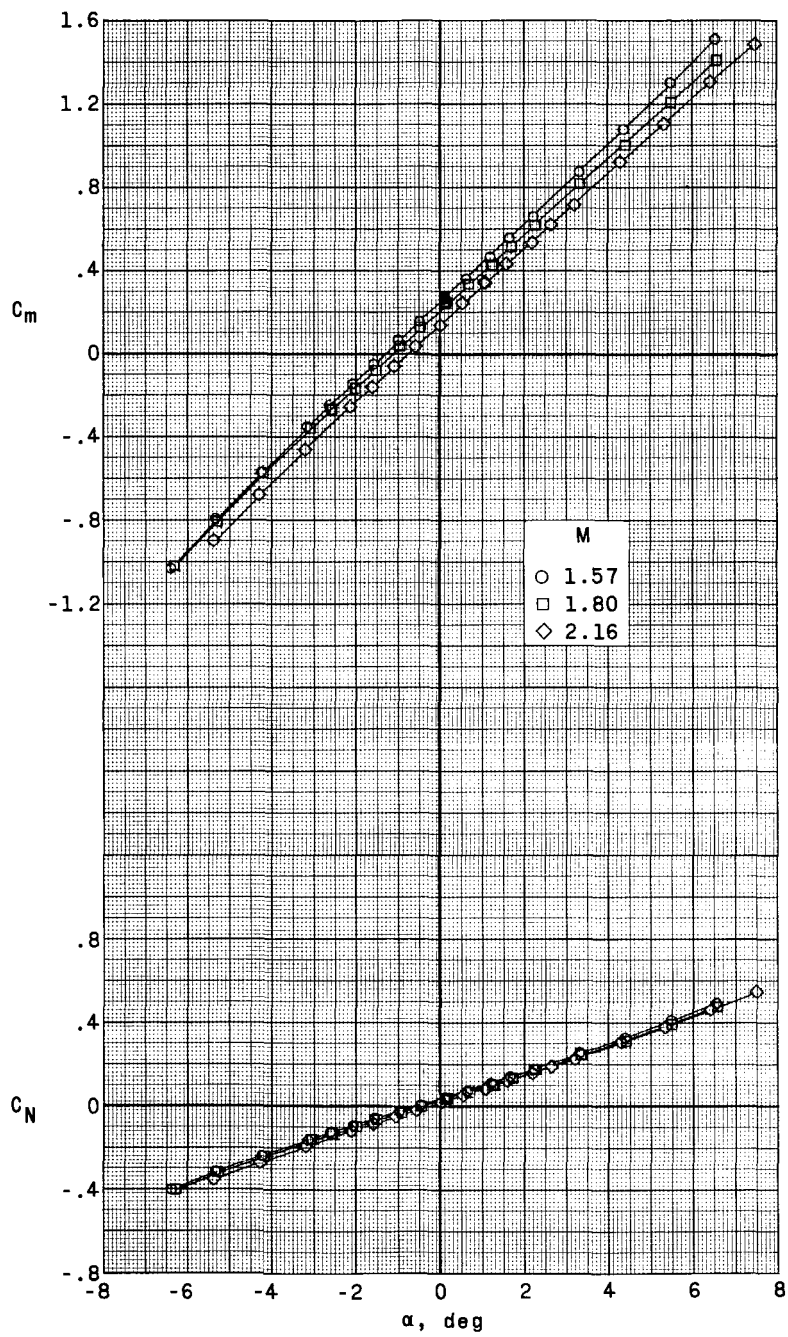
(j) Model G_2S.

Figure 8.- Continued.
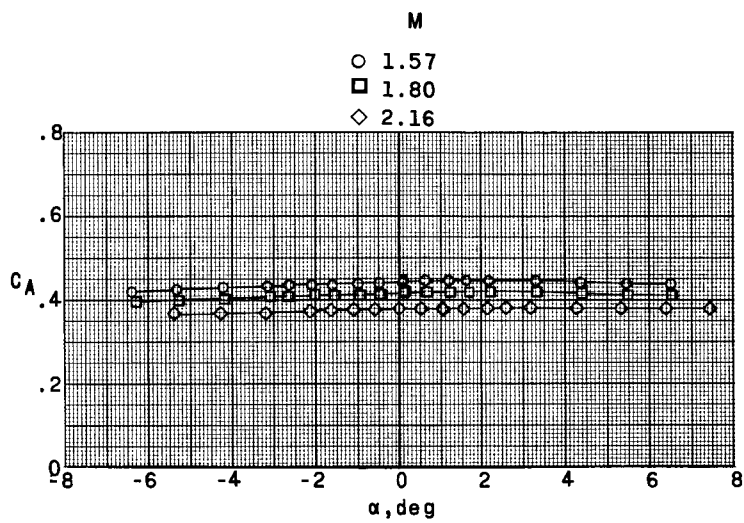
(j) Model G_2S.   Concluded.

Figure 8.- Continued.
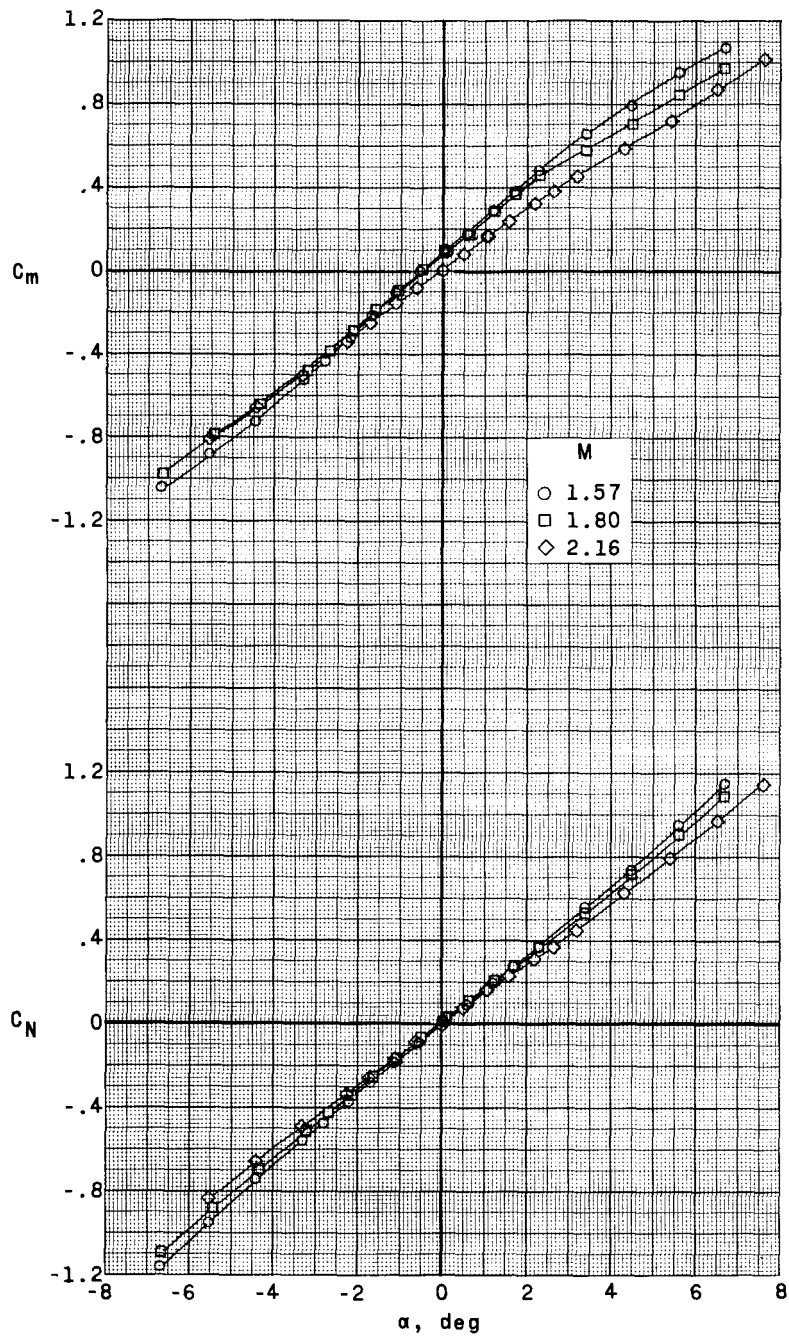
(k) Model GS_1VF.

Figure 8.- Continued.
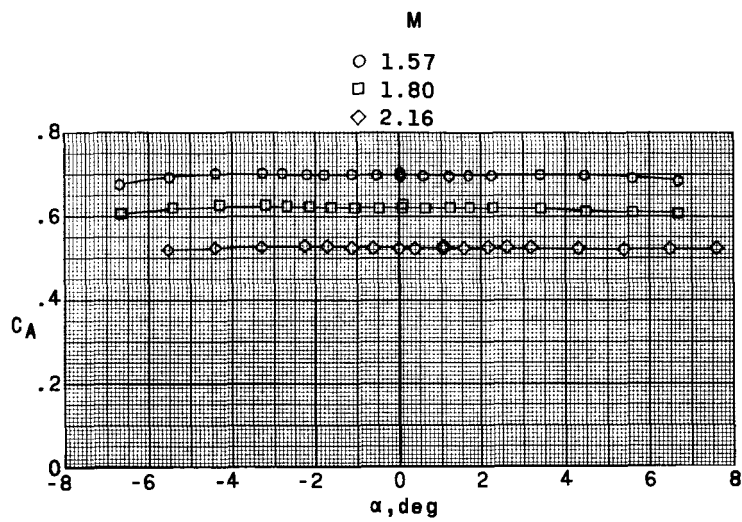
(k) Model GS$_1$VF. Concluded.

Figure 8.- Concluded.
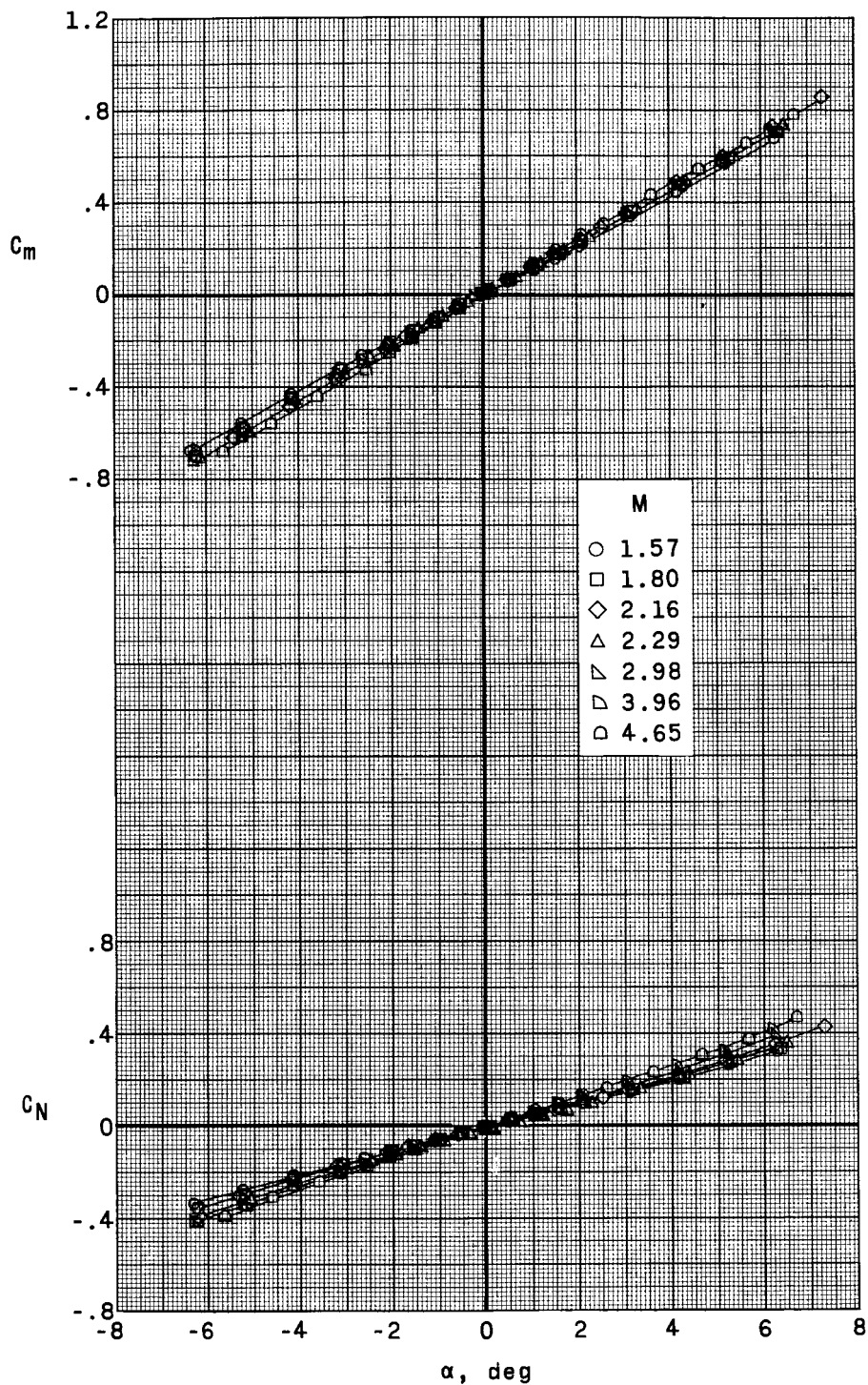
(a) Model CS$_2$, transition fixed.

Figure 9.- Longitudinal aerodynamic characteristics in pitch for the three-stage Saturn-cone model.
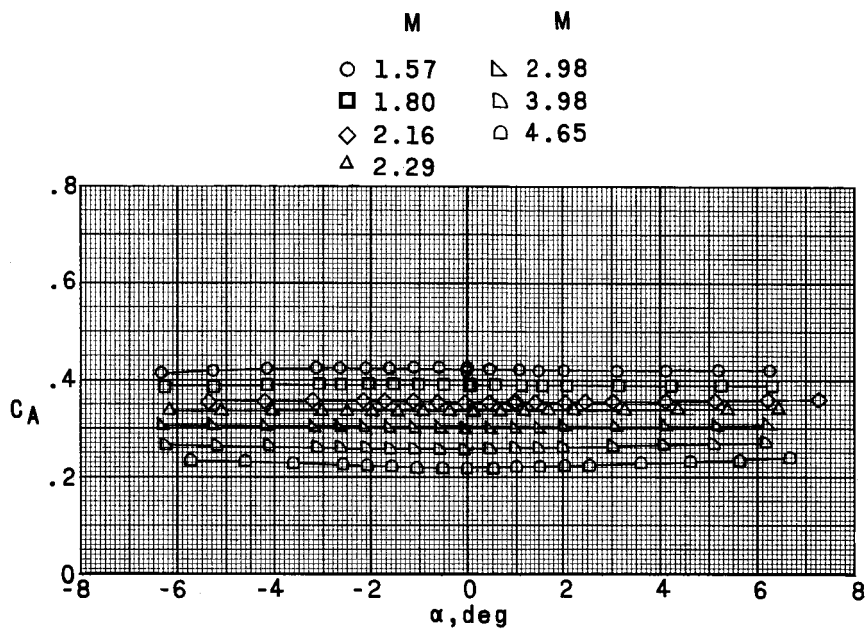
(a) Model CS$_2$, transition fixed. Concluded.

Figure 9.- Continued.
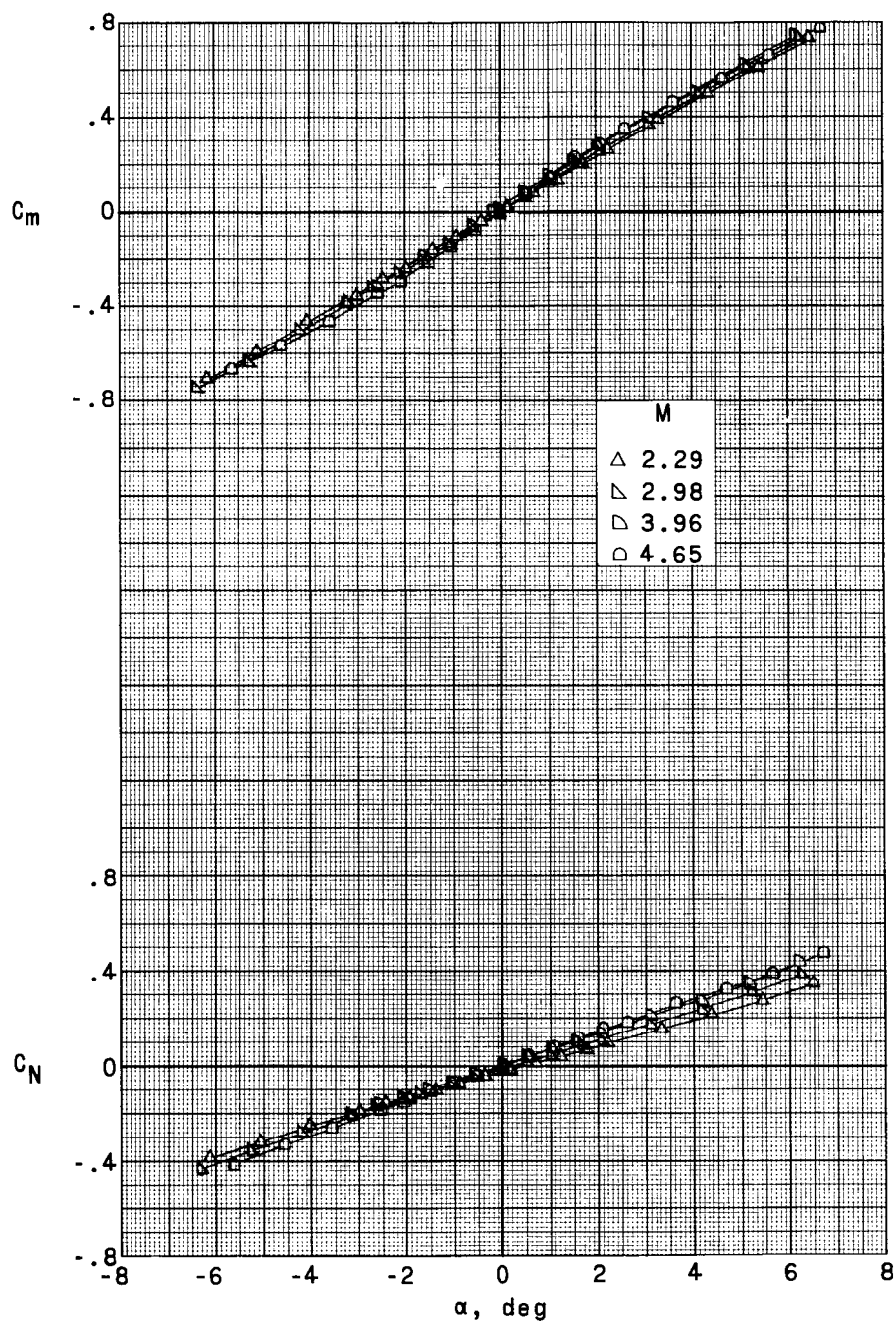
(b) Model CS$_2$, transition free.

Figure 9.- Continued.
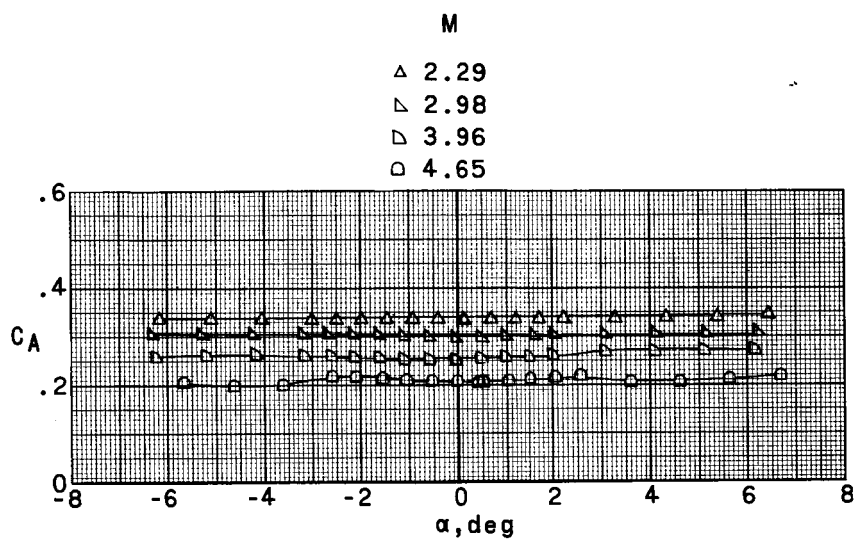
(b) Model CS$_2$, transition free. Concluded.
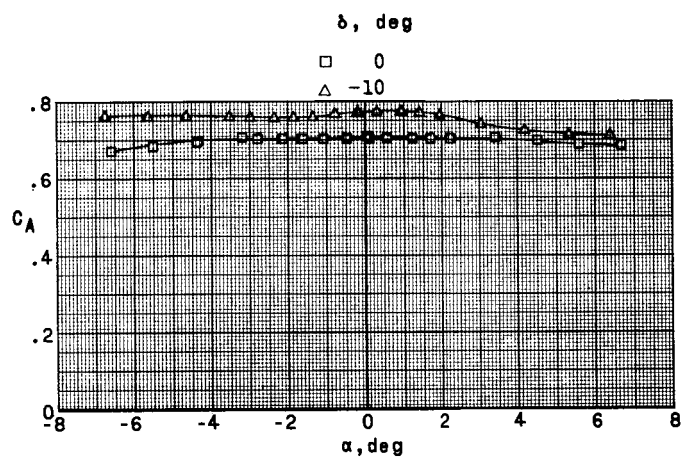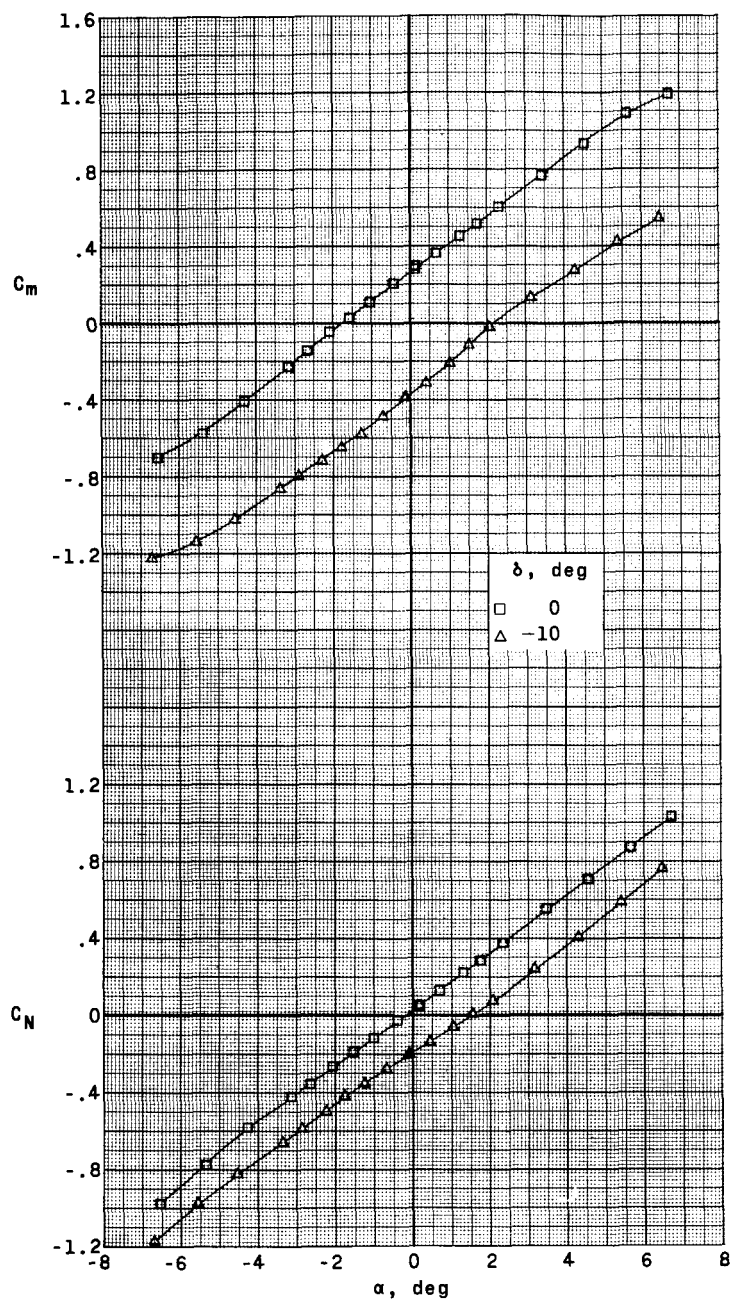
Figure 9.- Concluded.
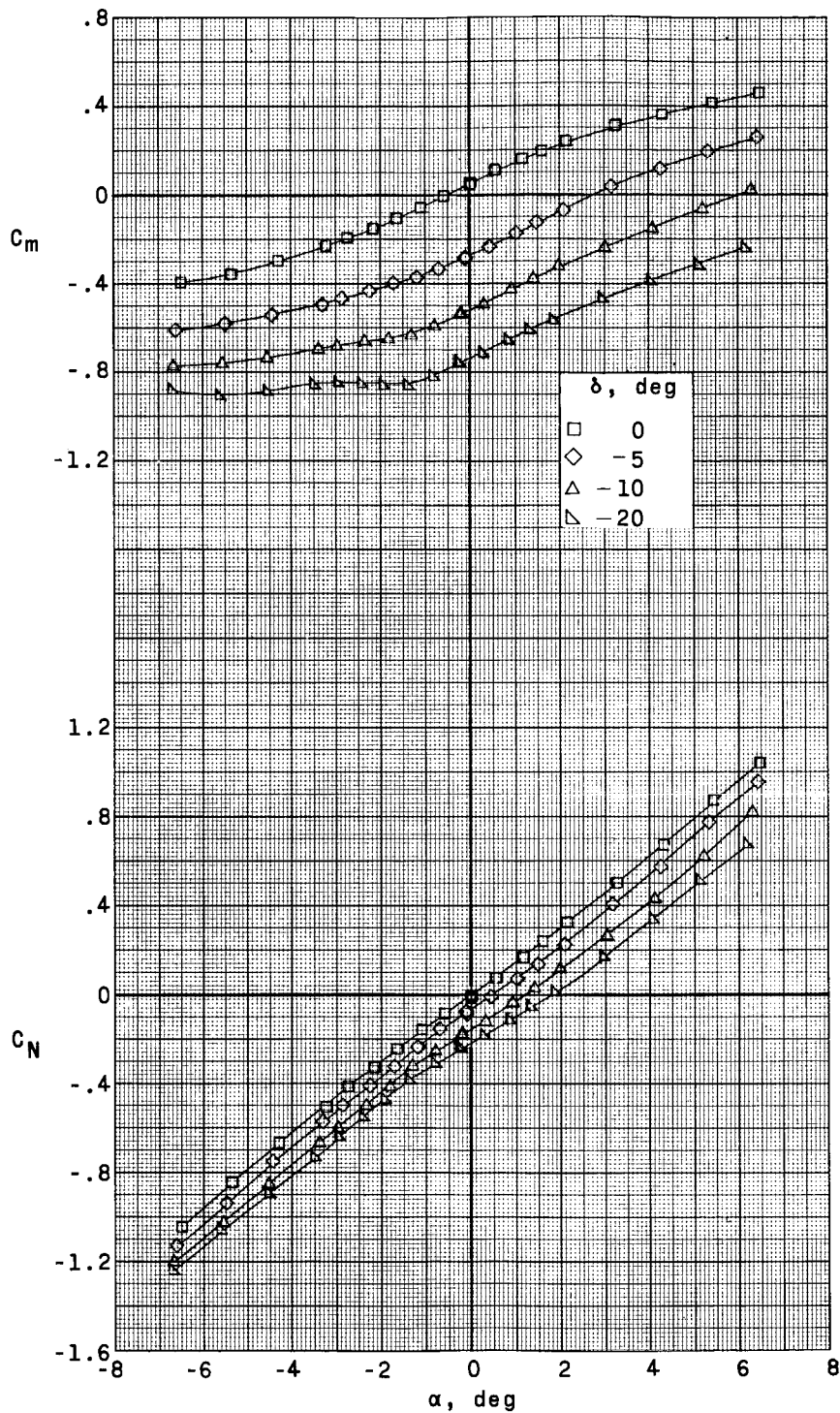
(a) M = 1.57.

Figure 10.- Effects of control deflection of the longitudinal aerodynamic characteristics of the Saturn-cone model with stabilizing fins CS_1VF.

δ, deg

□ 0
◇ -5
△ -10
△ -20
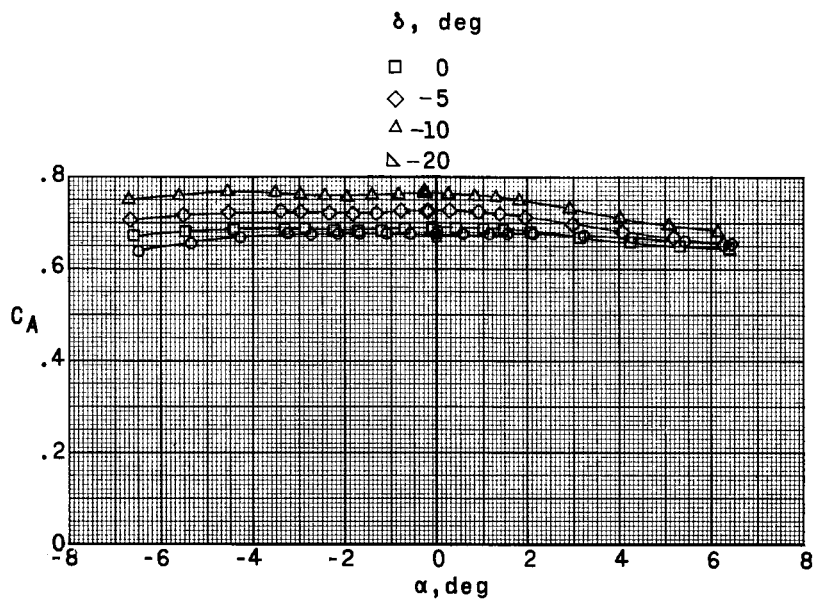

(a) M = 1.57. Concluded.

Figure 10.- Continued.
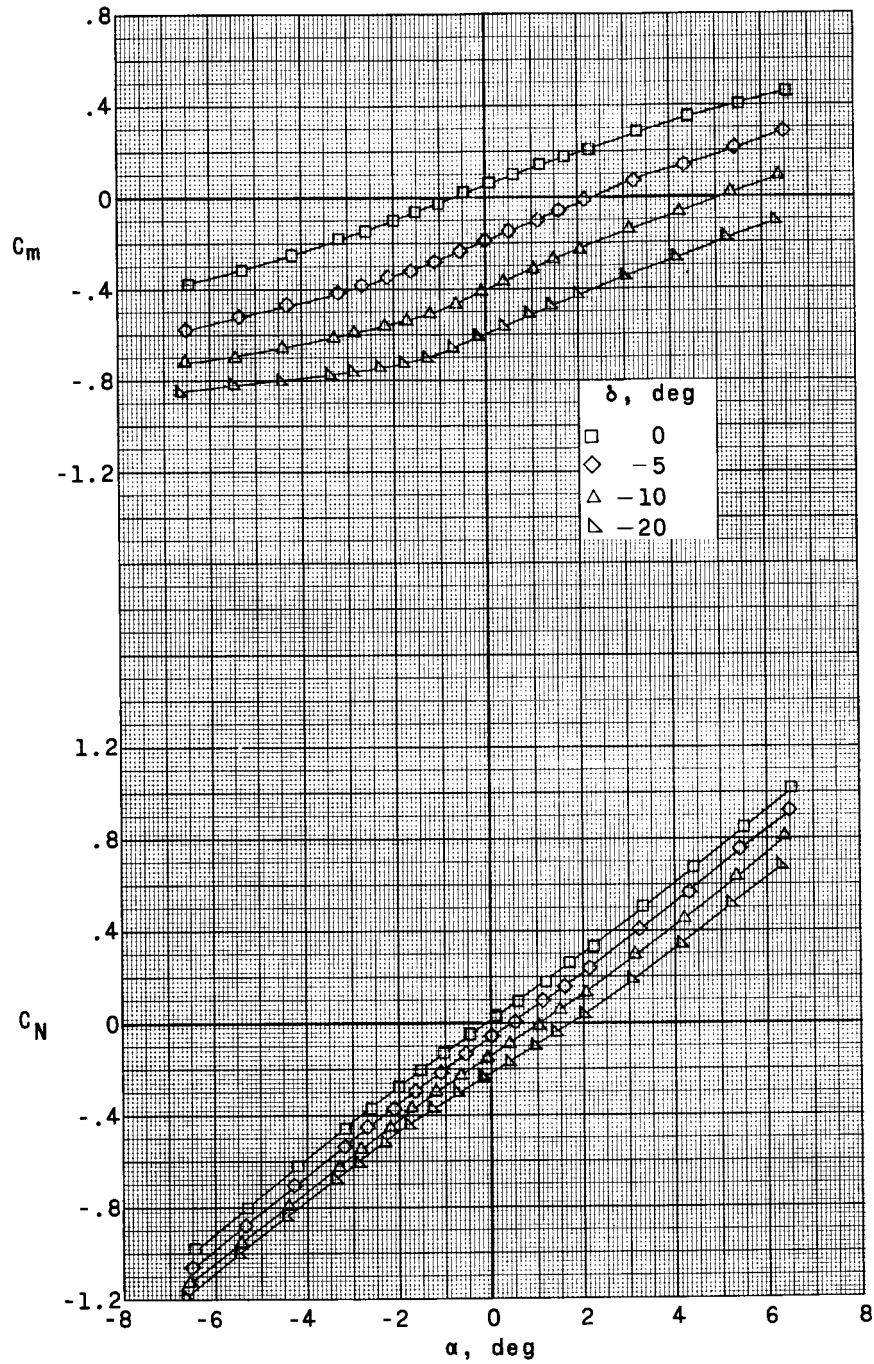
(b) M = 1.80.

Figure 10.- Continued.
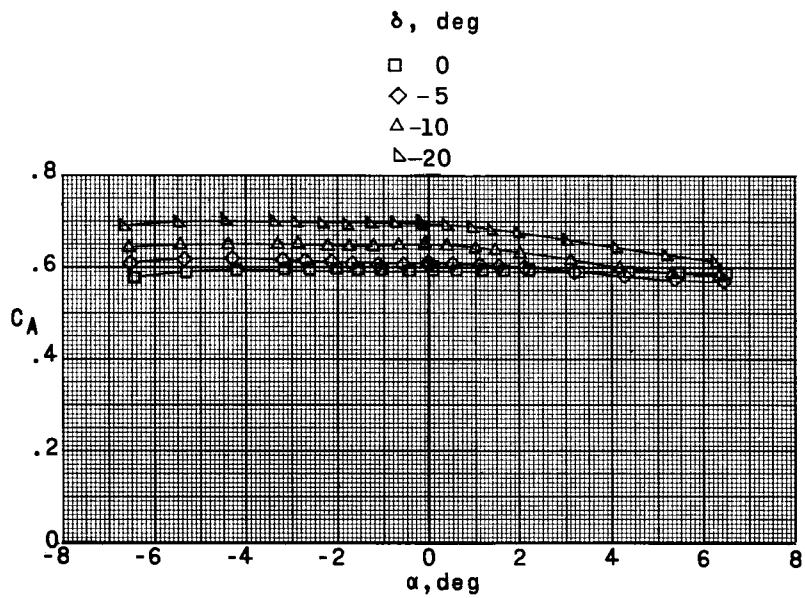
(b) M = 1.80. Concluded.

Figure 10.- Continued.
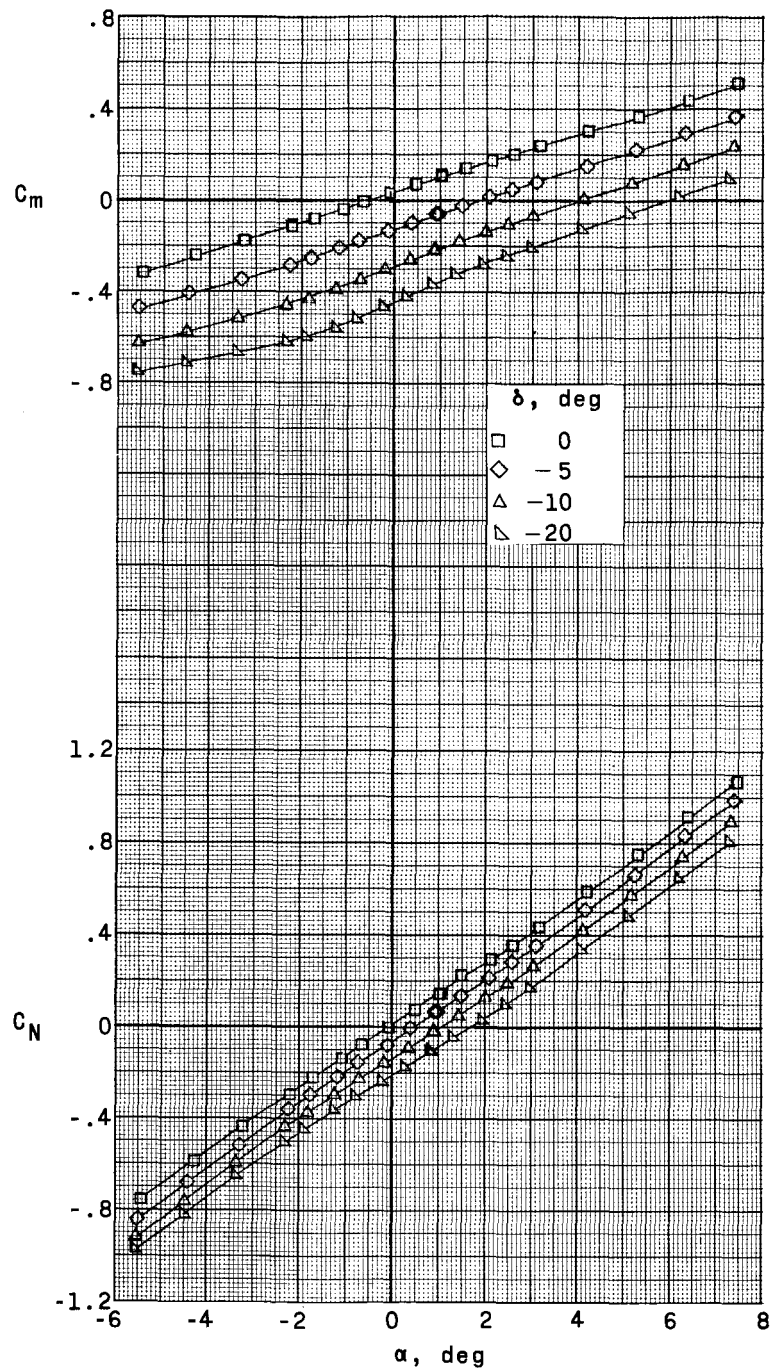
(c) M = 2.16.

Figure 10.- Continued.
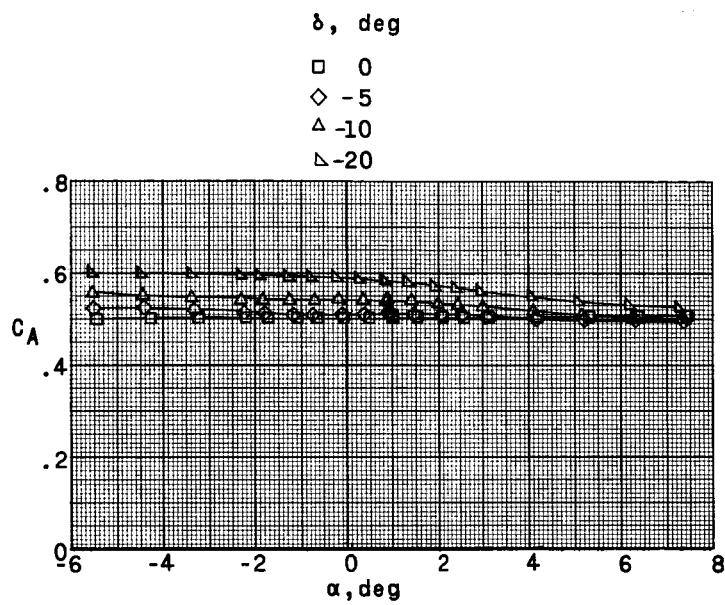
(c) M = 2.16. Concluded.

Figure 10.- Concluded.
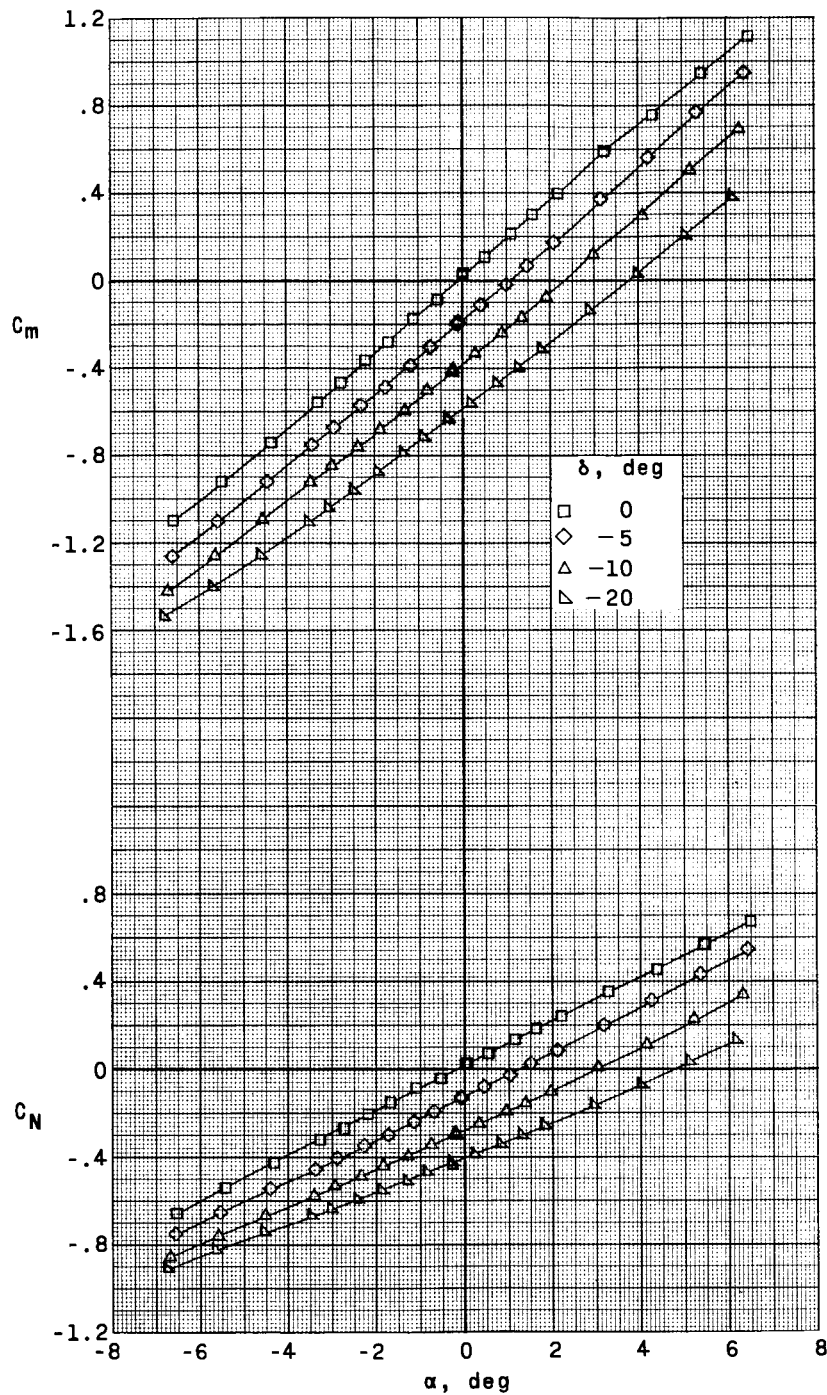
(a) M = 1.57.

Figure 11.- Effects of control deflection of the longitudinal aerodynamic characteristics of the Saturn-cone model without stabilizing fins CS_1V.
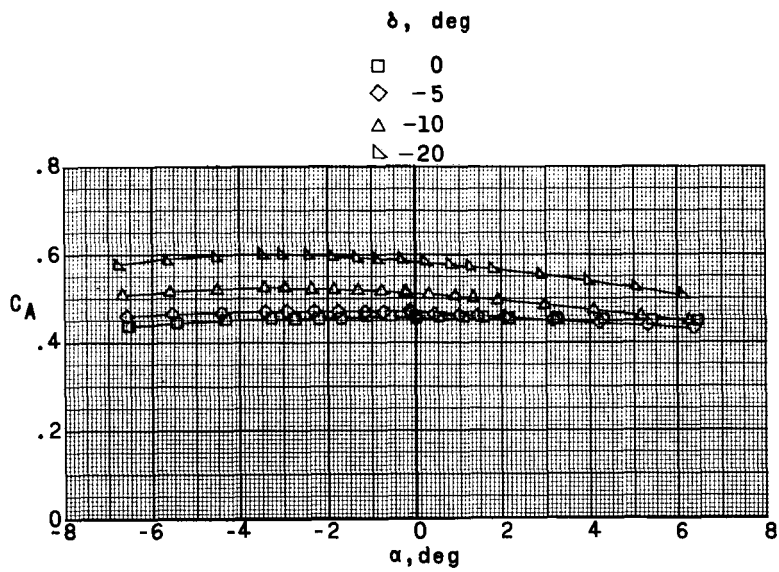
(a) M = 1.57. Concluded.

Figure 11.- Continued.
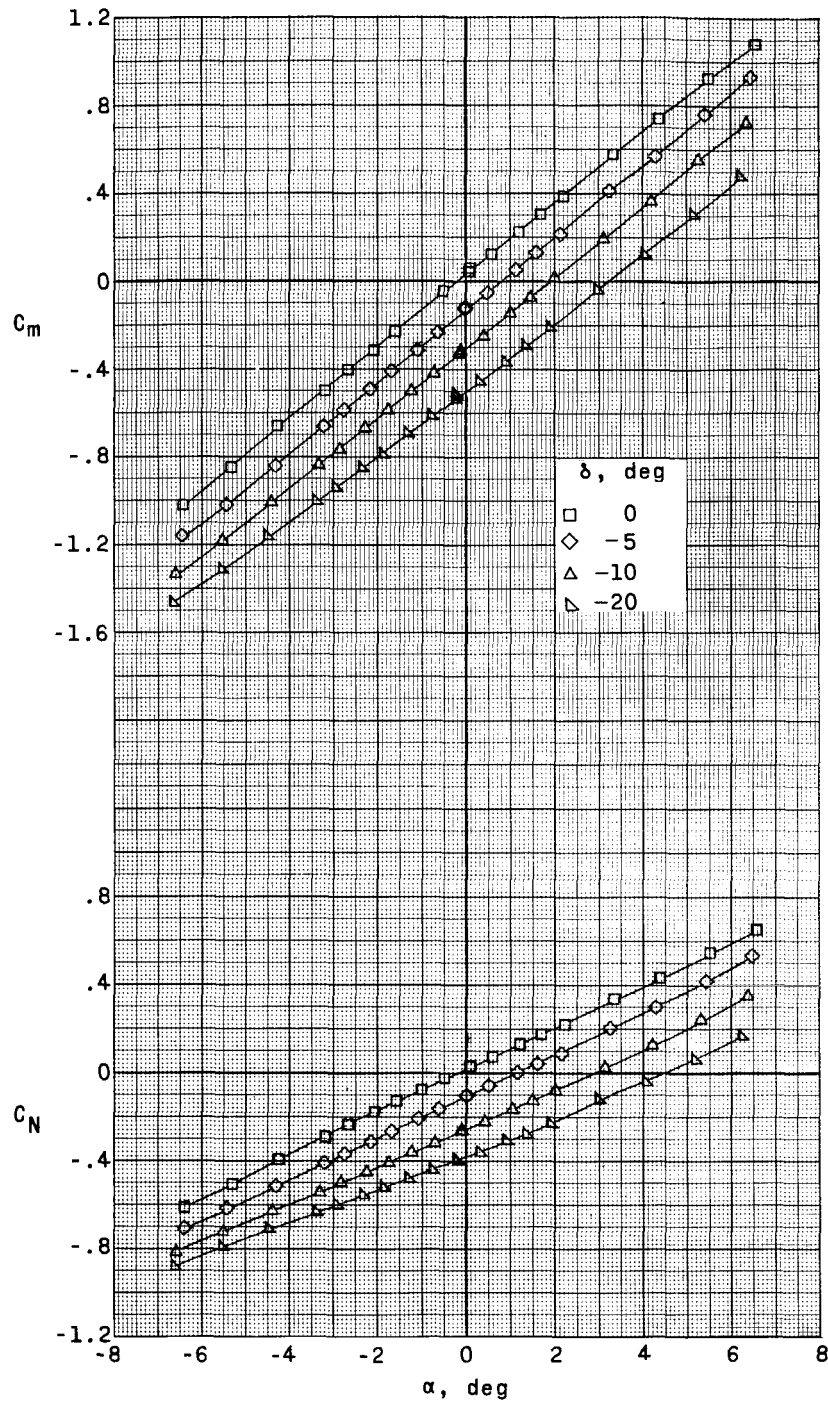
(b) M = 1.80.

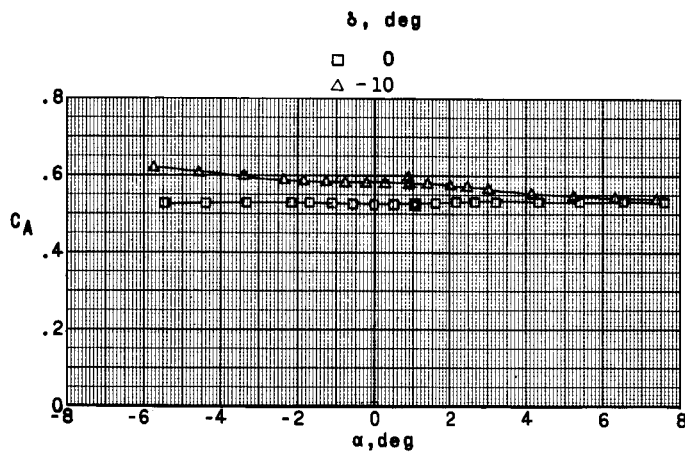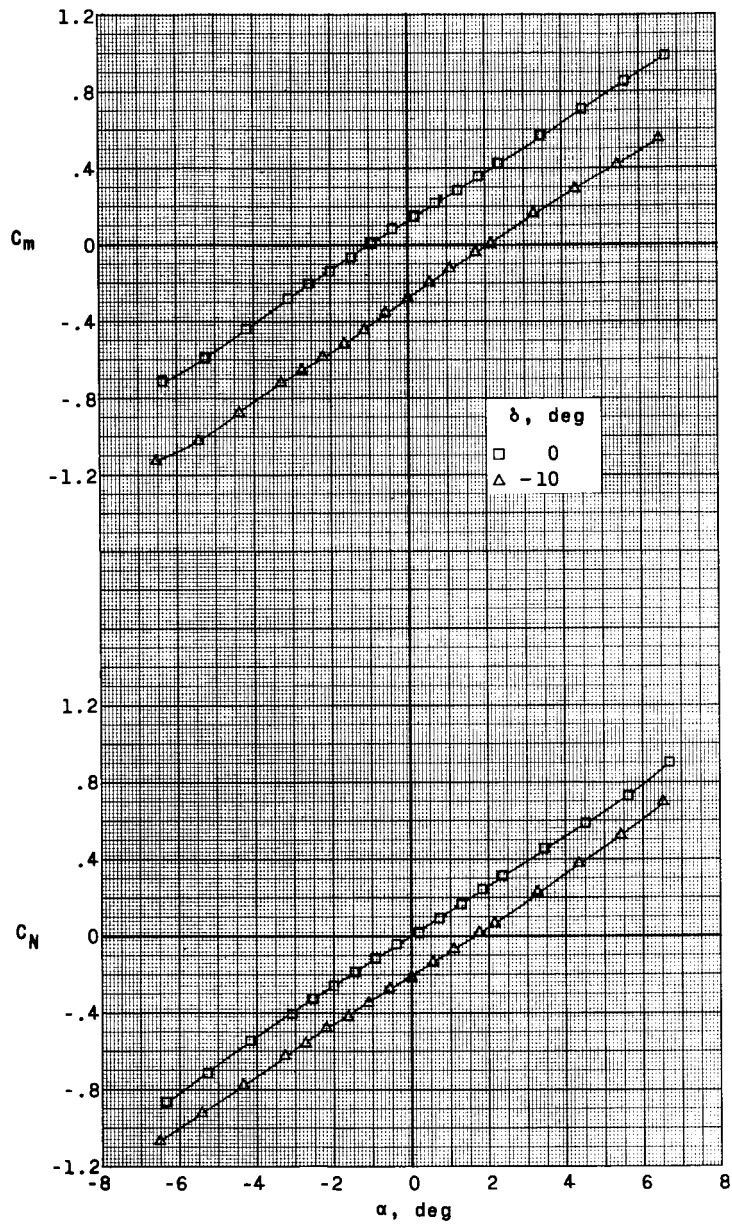Figure 11.- Continued.

δ, deg

□   0
◇ − 5
△ −10
◸ −20
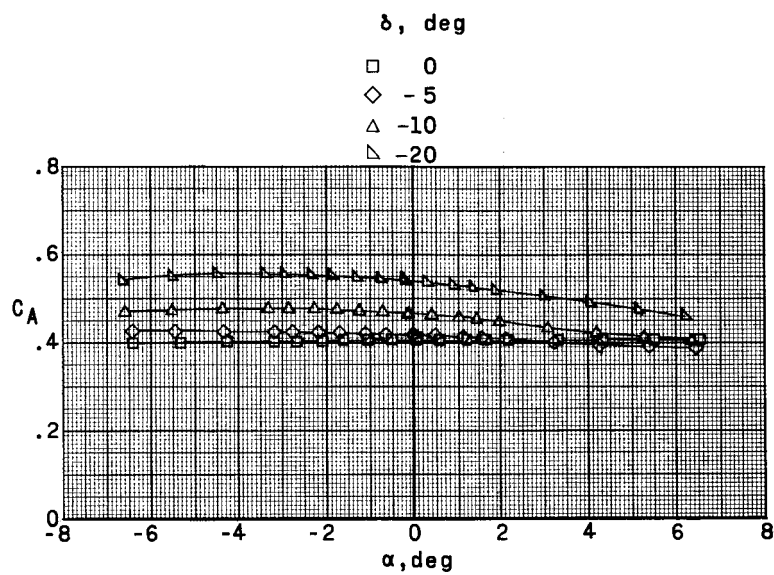
(b) M = 1.80. Concluded.

Figure 11.- Continued.
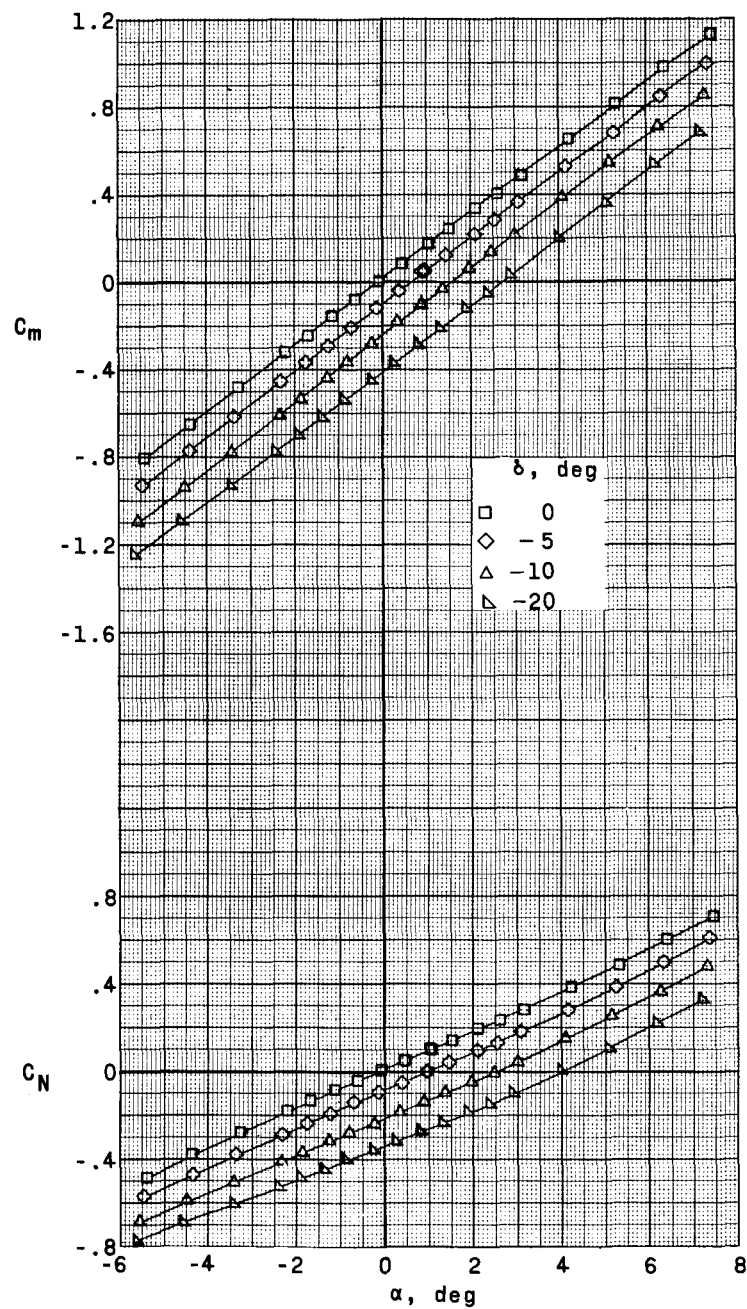
(c) M = 2.16.

Figure 11.- Continued.
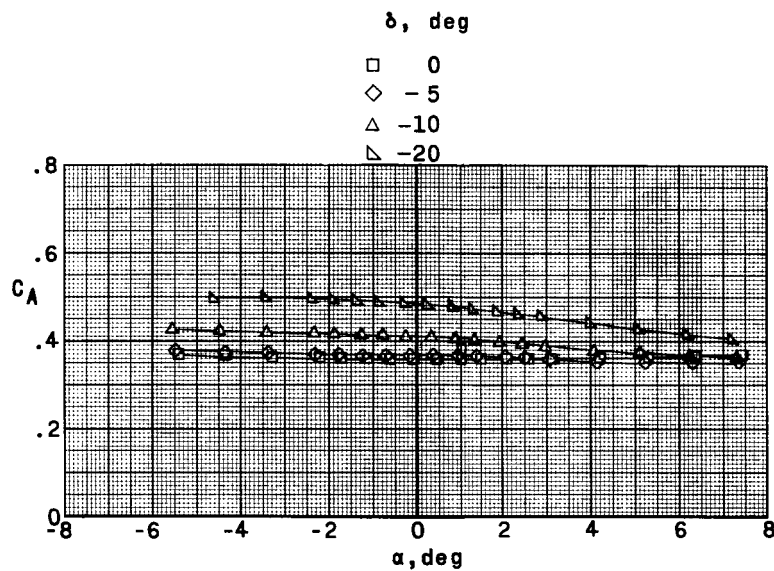
(c) M = 2.16. Concluded.

Figure 11.- Concluded.
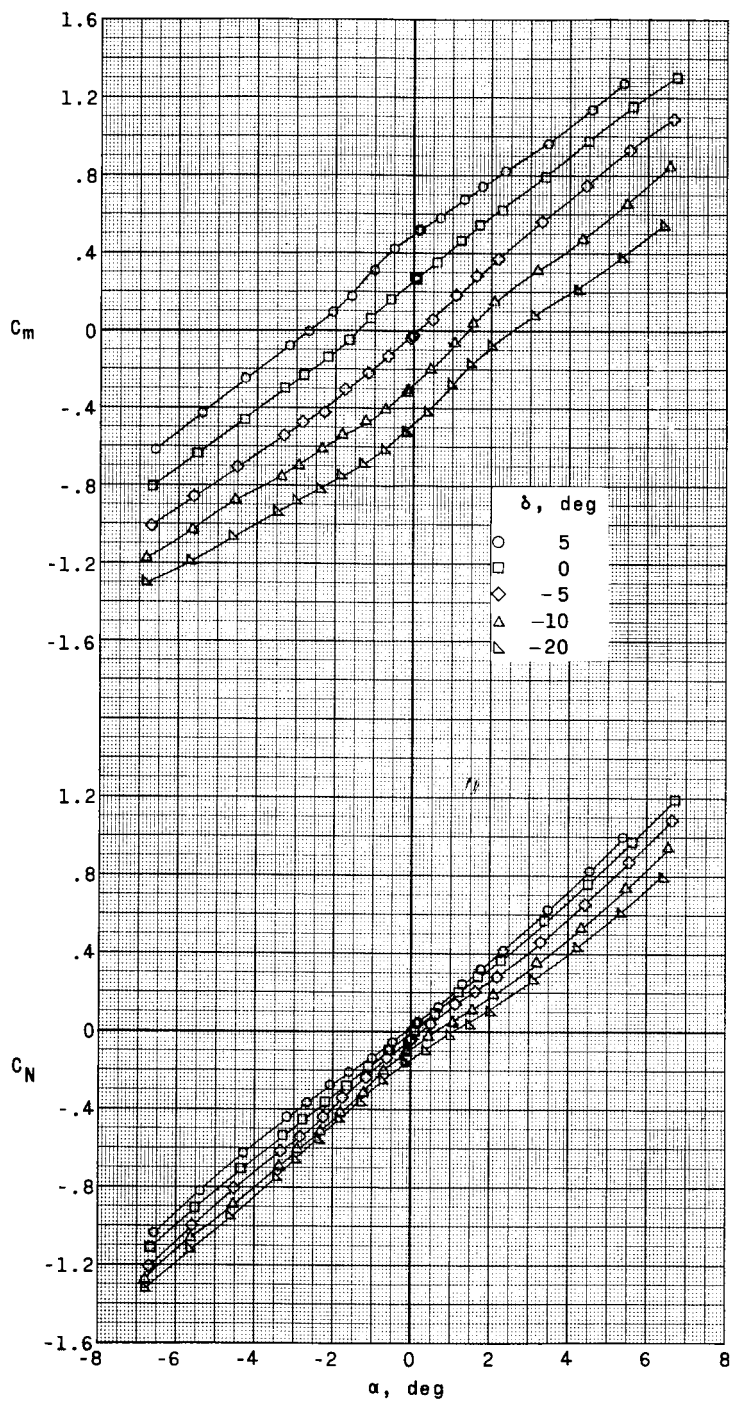
(a) M = 1.57.

Figure 12.- Effects of control deflection on the longitudinal aerodynamic characteristics of the Saturn-glider model with stabilizing fins G_2S_1VF.
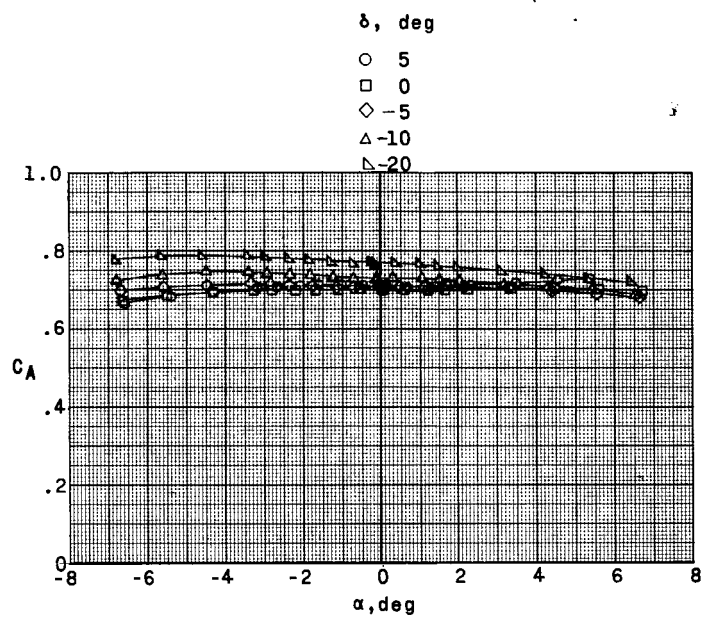
(a) M = 1.57. Concluded.

Figure 12.- Continued.
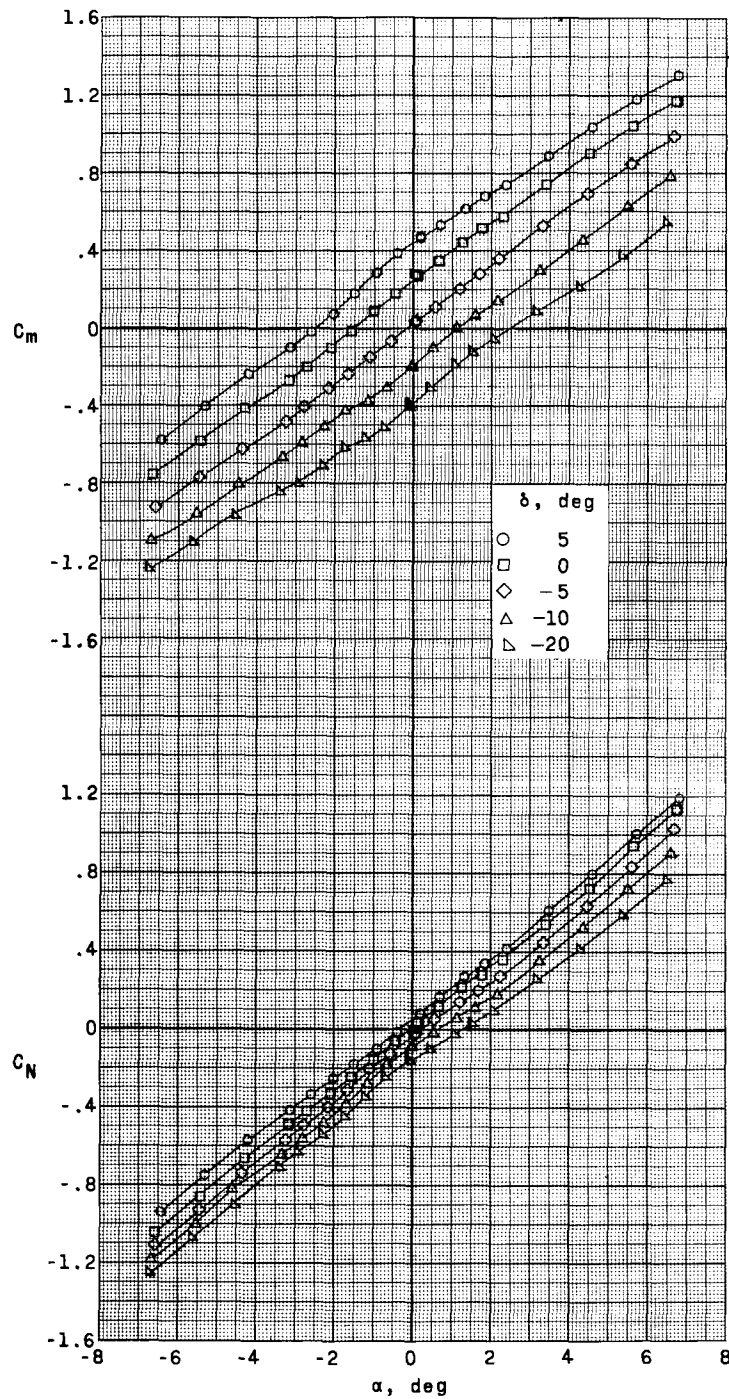
(b) M = 1.80.

Figure 12.- Continued.
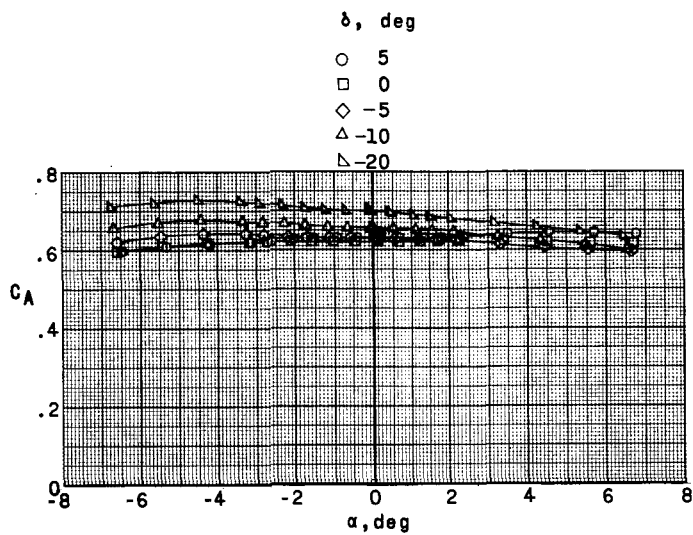
(b) M = 1.80. Concluded.

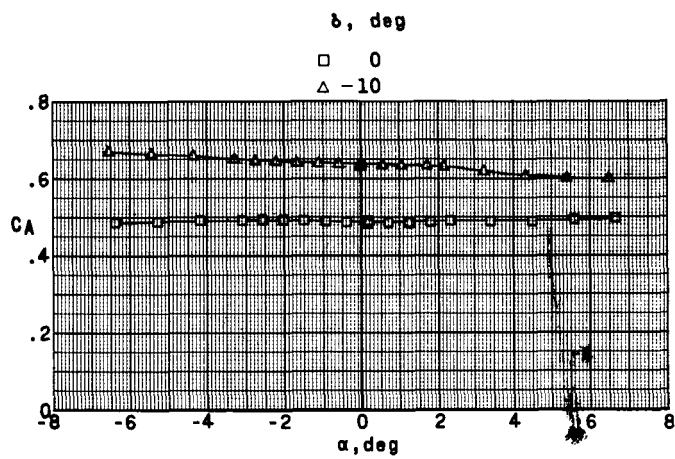Figure 12.- Continued.
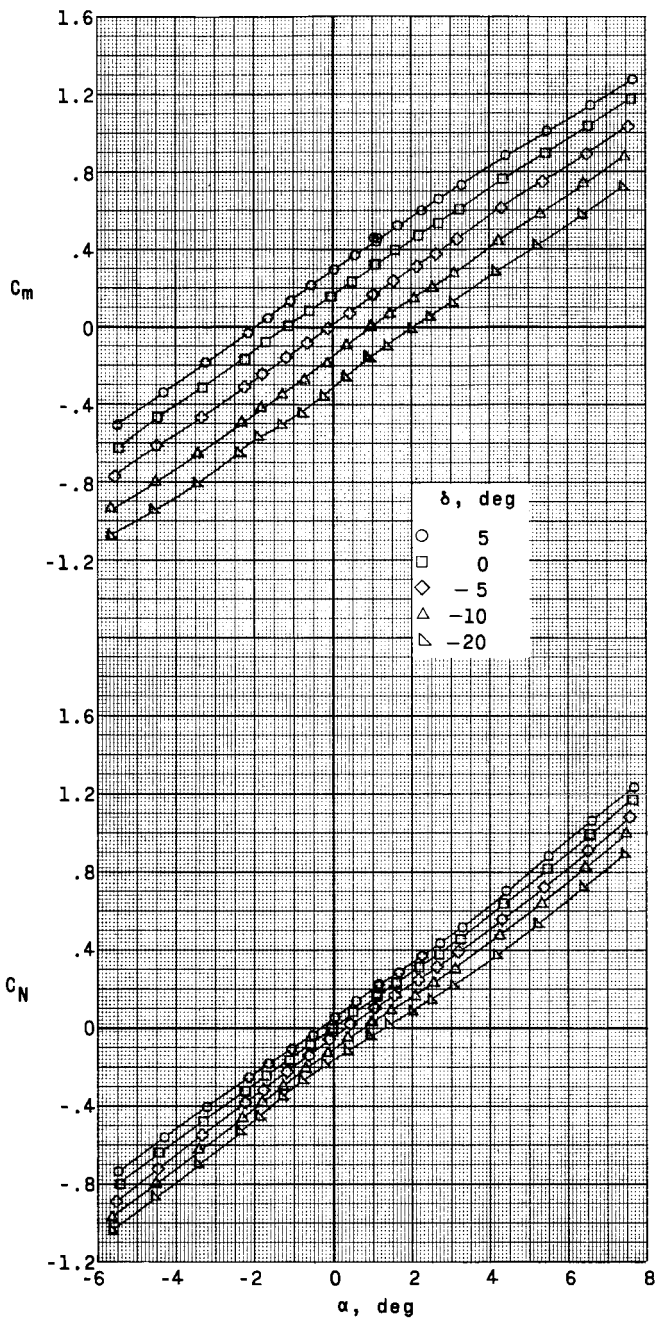
(c) M = 2.16.

Figure 12.- Continued.
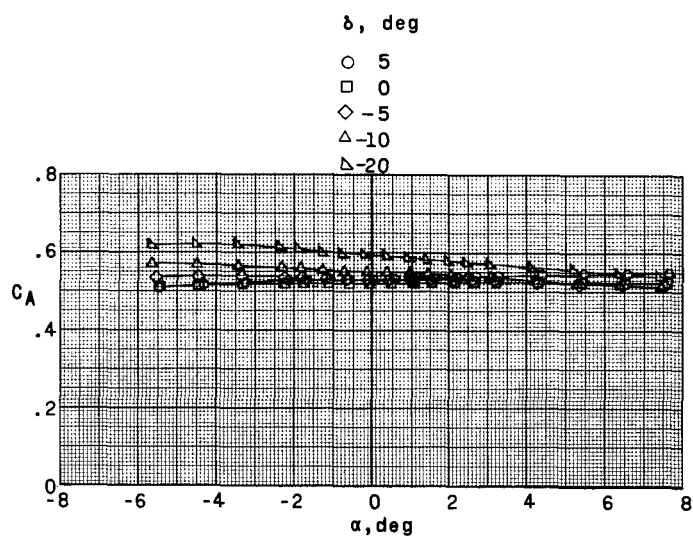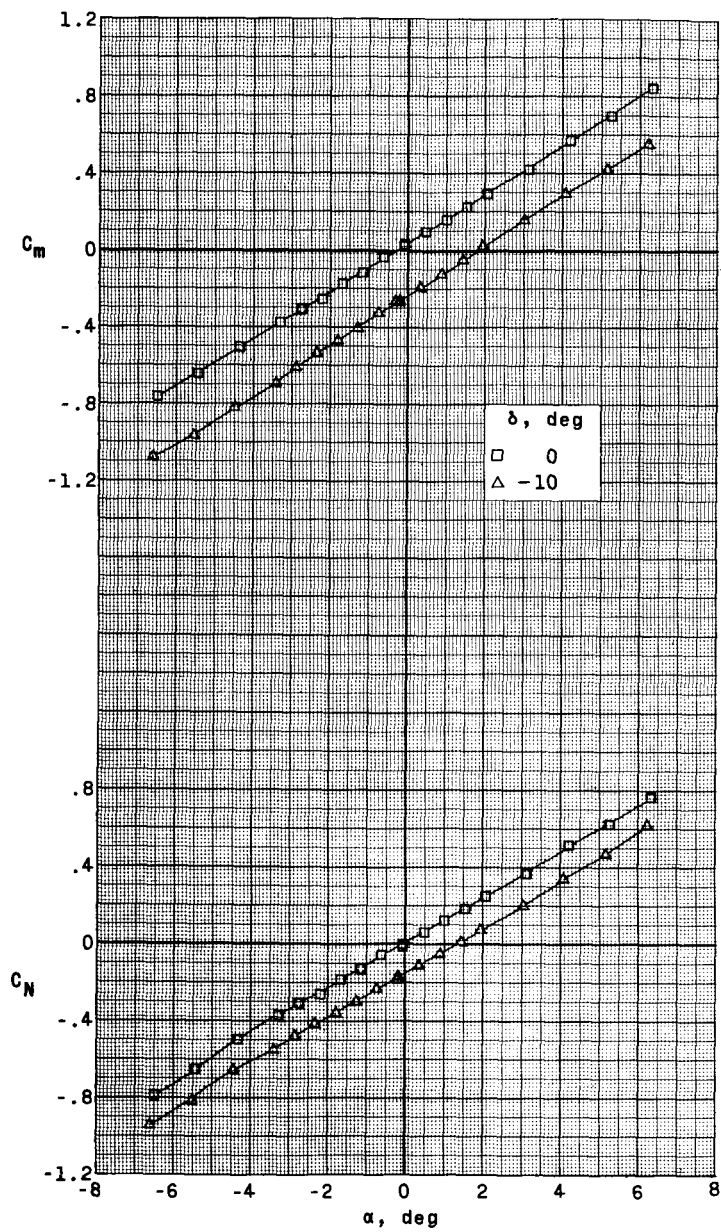
(c) M = 2.16. Concluded.

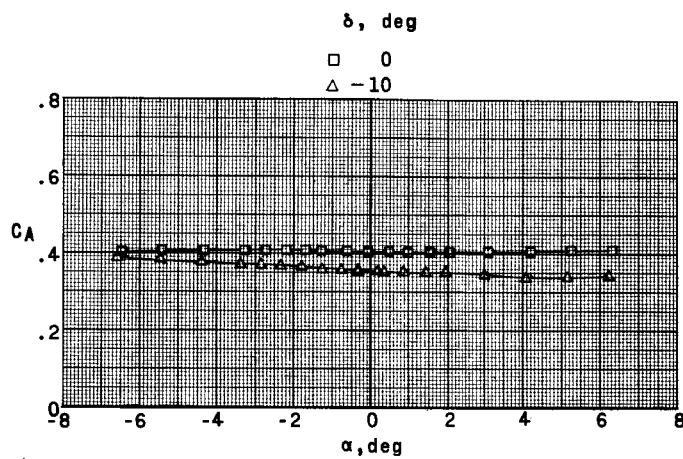Figure 12.- Continued.
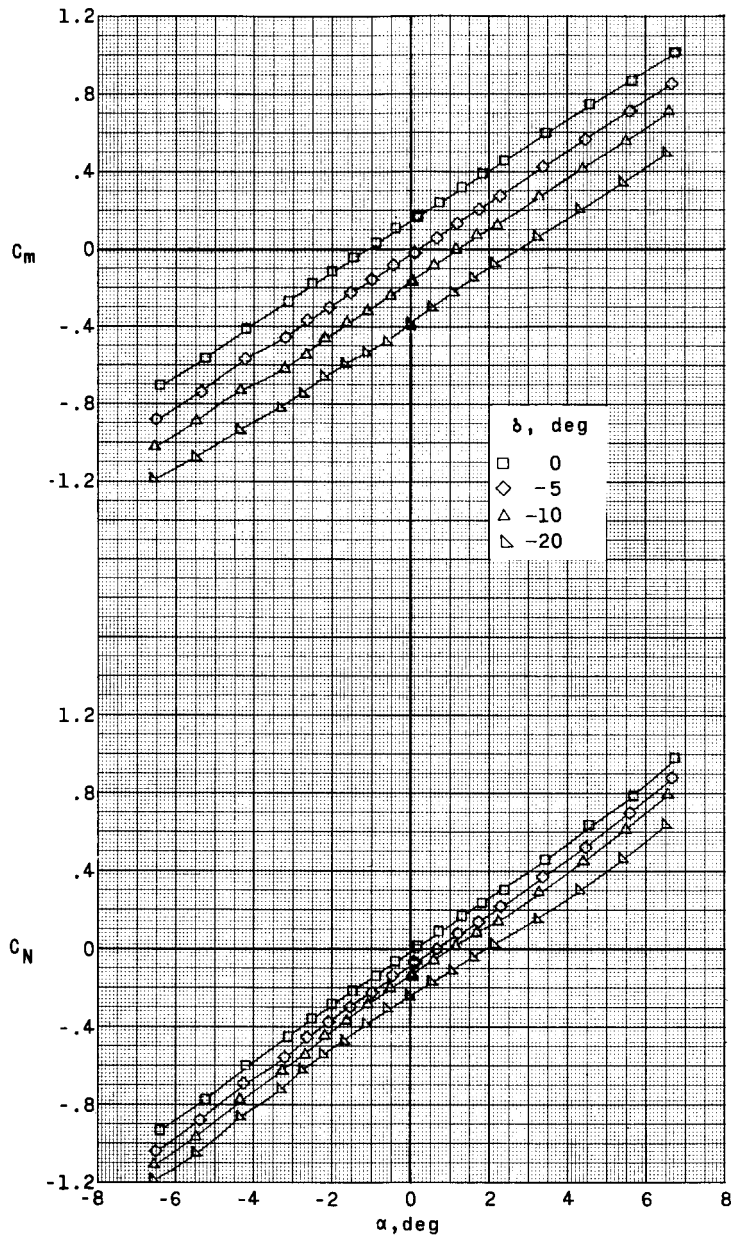
(d) M = 2.29.

Figure 12.- Continued.
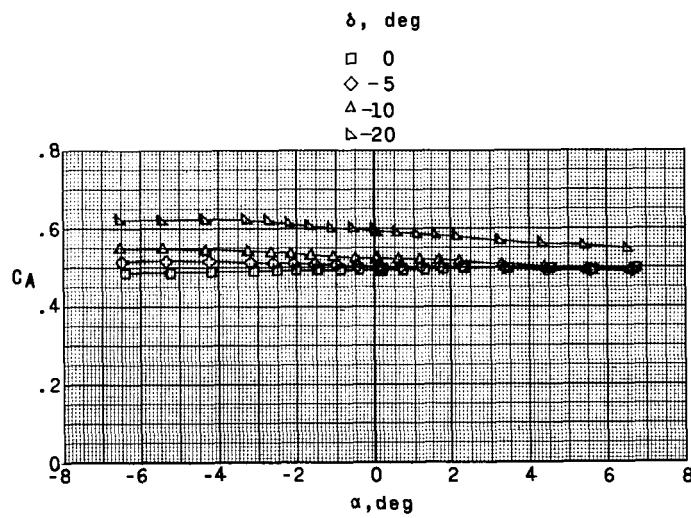
(d) M = 2.29.   Concluded.

Figure 12.- Continued.
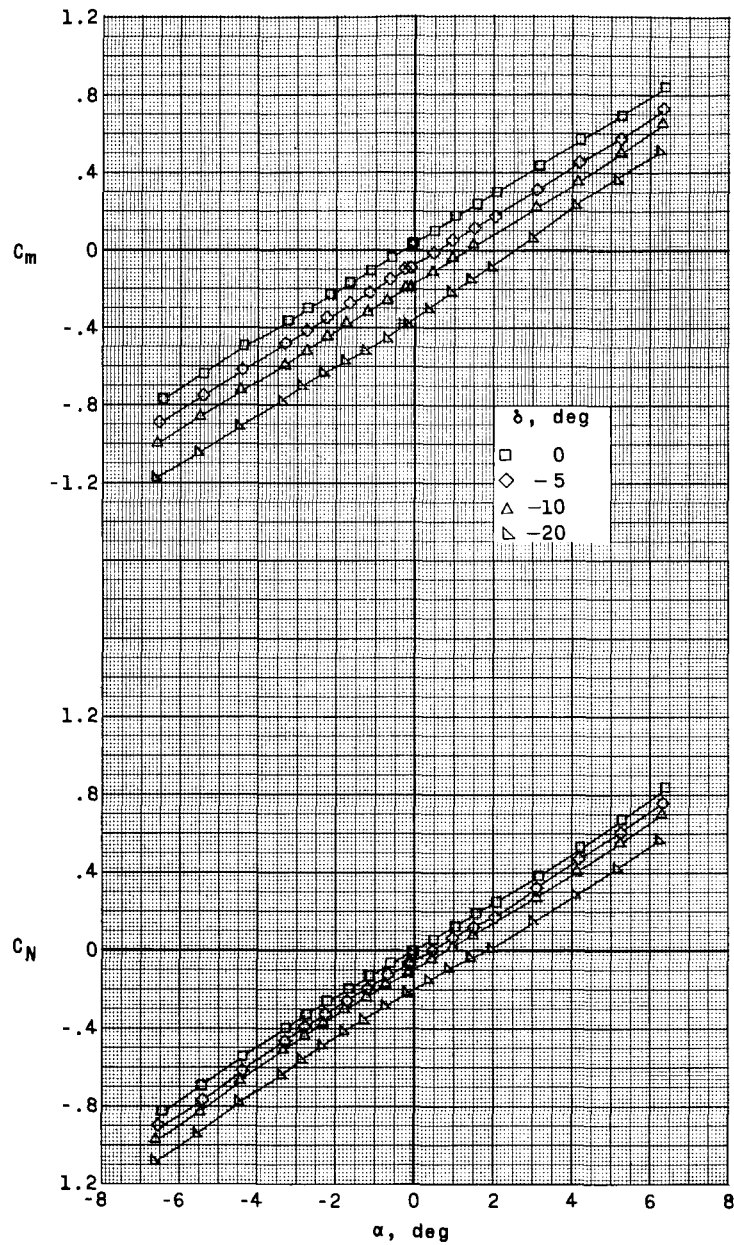
(e) M = 2.98.

Figure 12.- Continued.
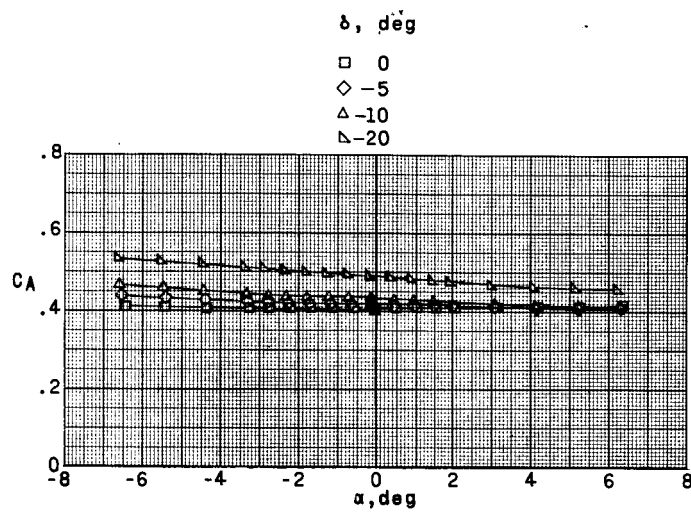
(e) M = 2.98. Concluded.

Figure 12.- Continued.
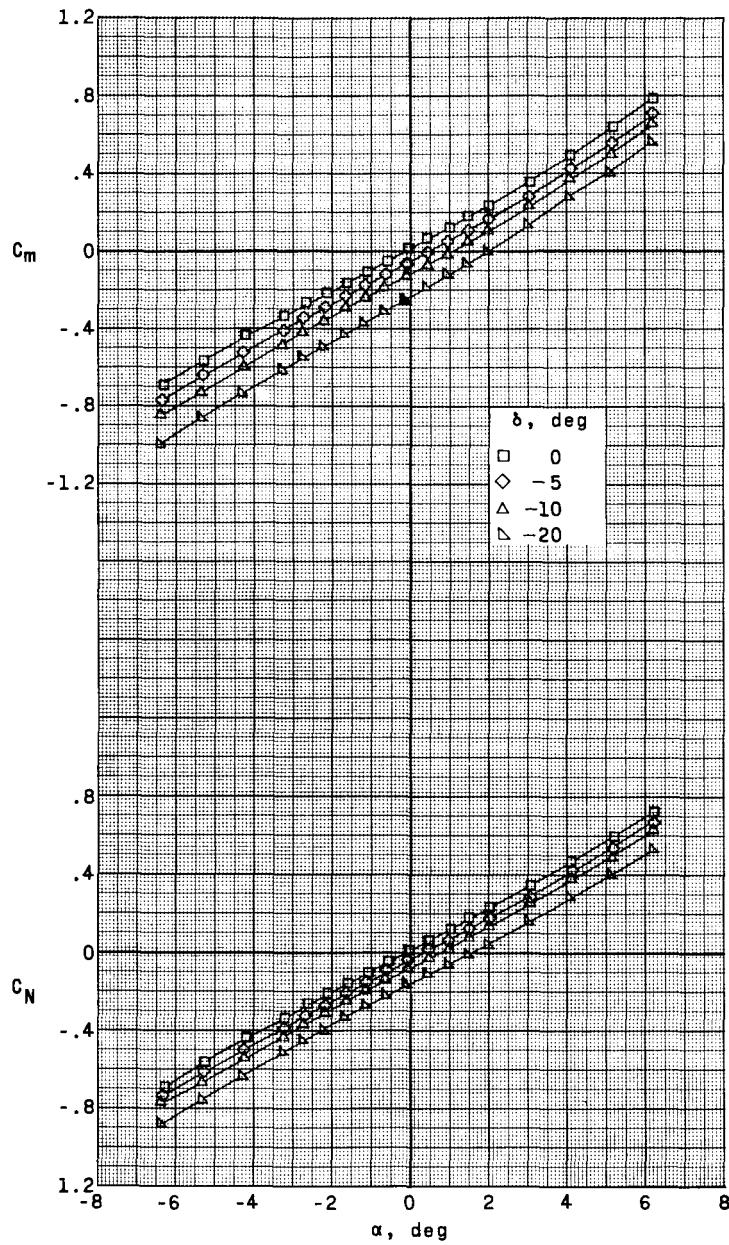
(f) M = 3.96.

Figure 12.- Continued.

δ, deg

□ 0
◇ -5
△ -10
◁ -20

C_A
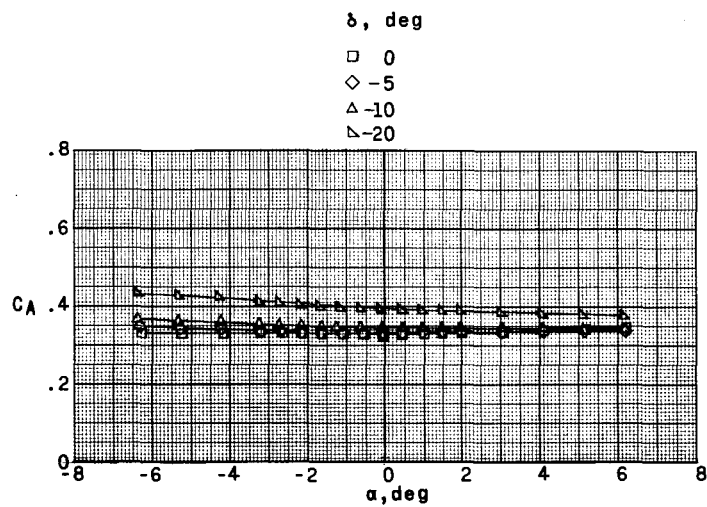
(f) M = 3.96. Concluded.

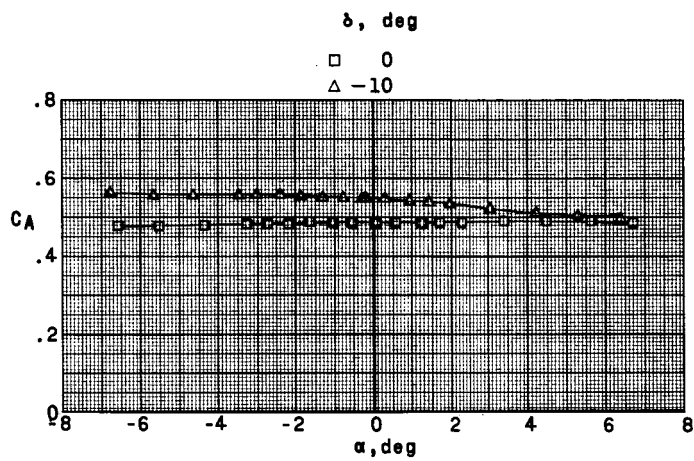Figure 12.- Continued.

(g) M = 4.65.

Figure 12.- Continued.
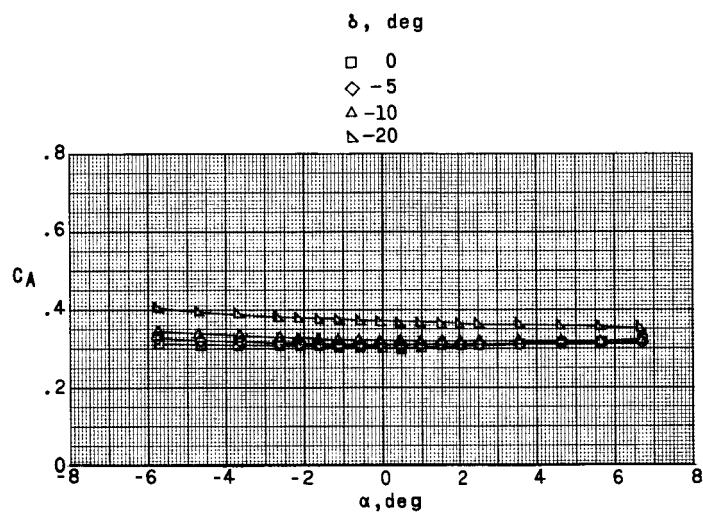
(g) M = 4.65. Concluded.

Figure 12.- Concluded.
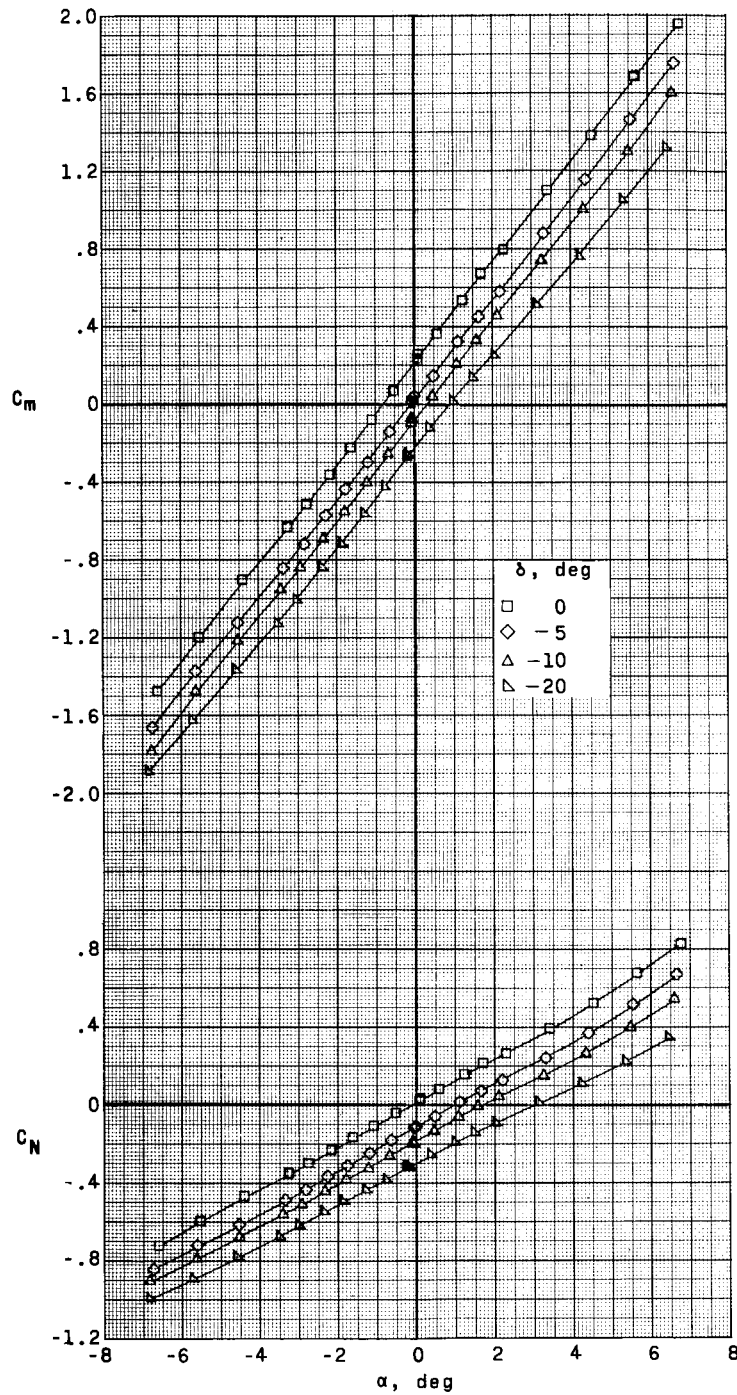
(a) M = 1.57.

Figure 13.- Effects of control deflection of the longitudinal aerodynamic characteristics of the Saturn-glider model without stabilizing fins G_2S_1V.
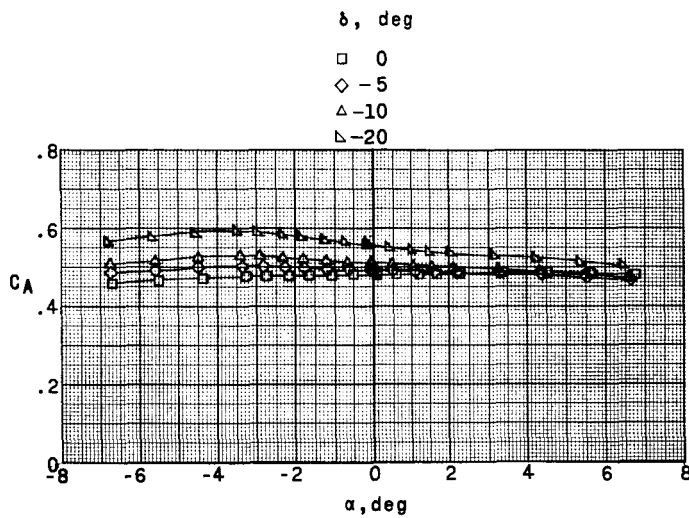
(a) M = 1.57. Concluded.

Figure 13.- Continued.
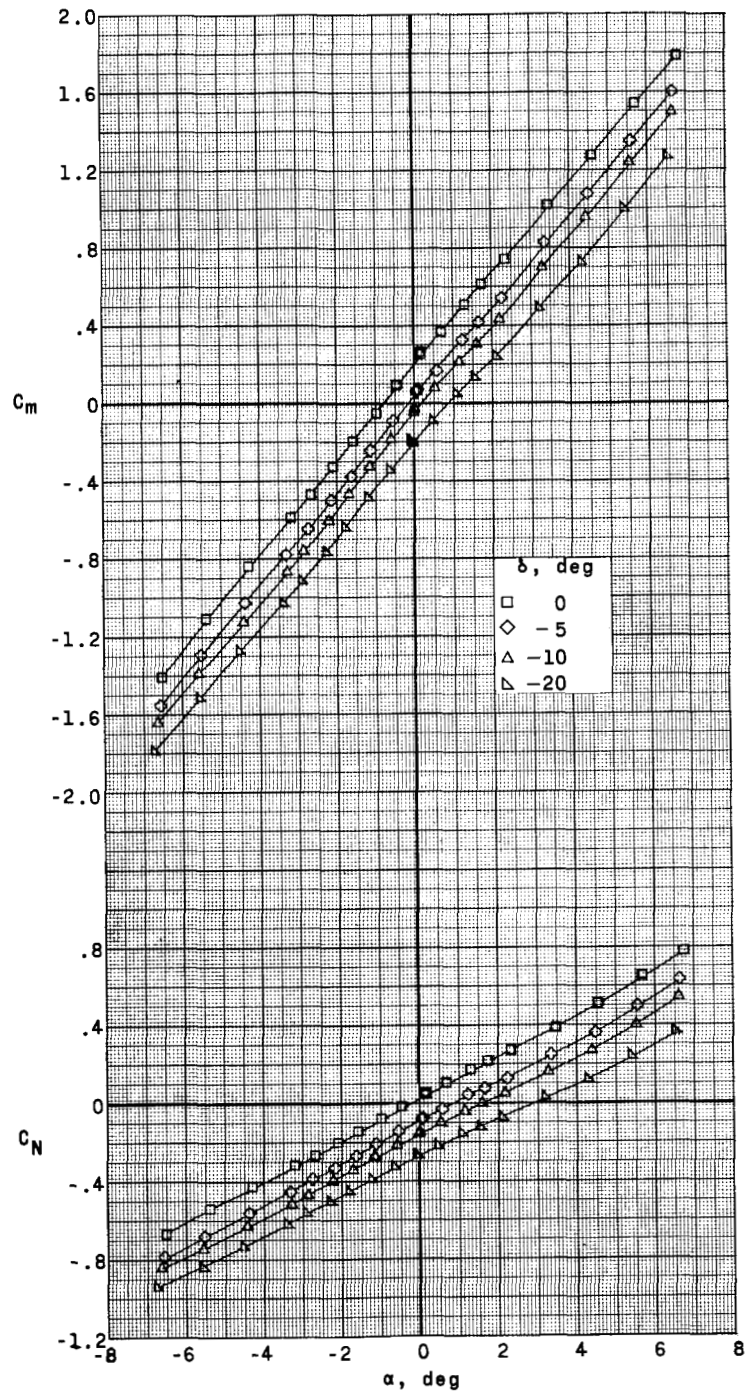
(b) M = 1.80.

Figure 13.- Continued.
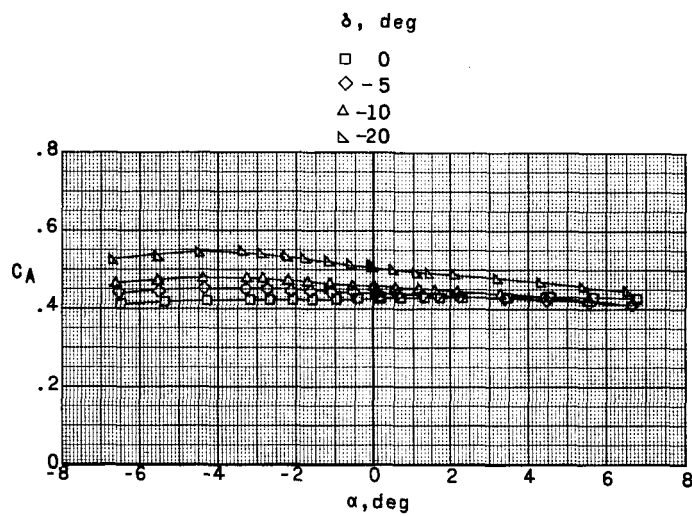
(b) M = 1.80. Concluded.

Figure 13.- Continued.
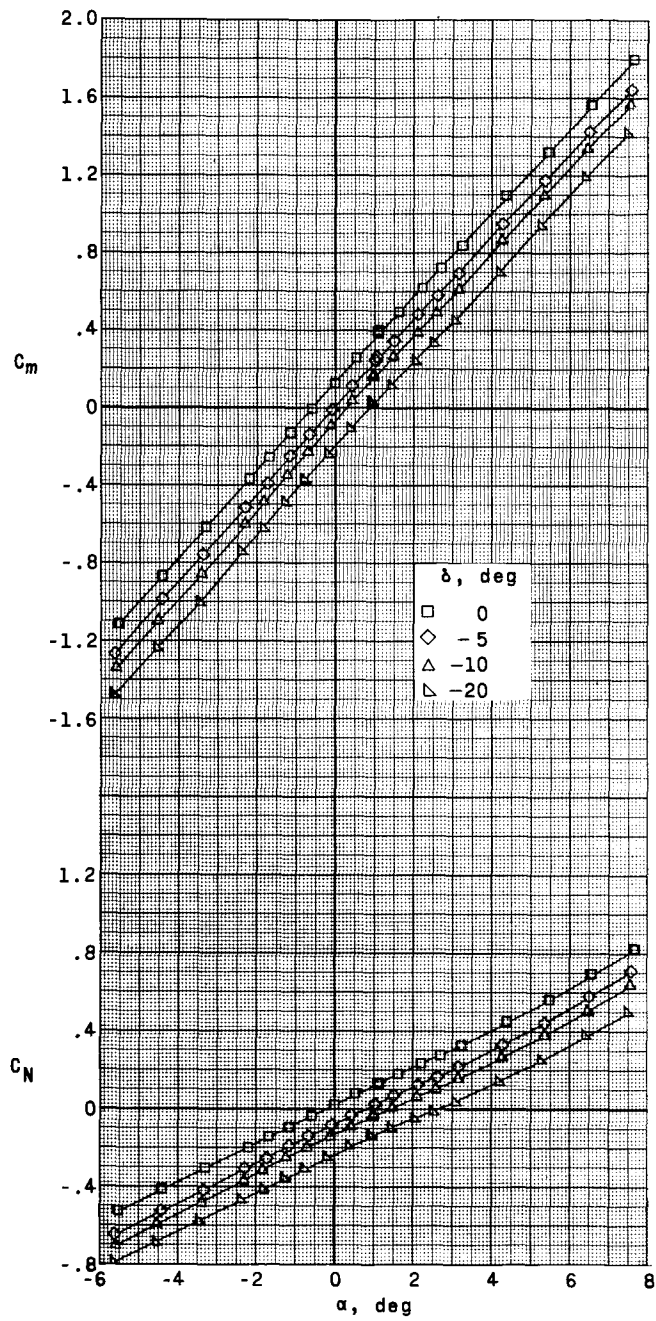
(c) M = 2.16.

Figure 13.- Continued.

δ, deg
□ 0
◇ -5
△ -10
◁ -20
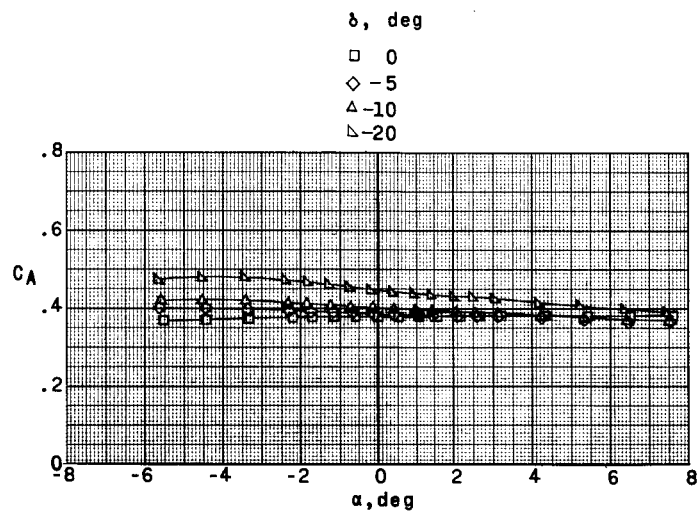
(c) M = 2.16. Concluded.

Figure 13.- Continued.
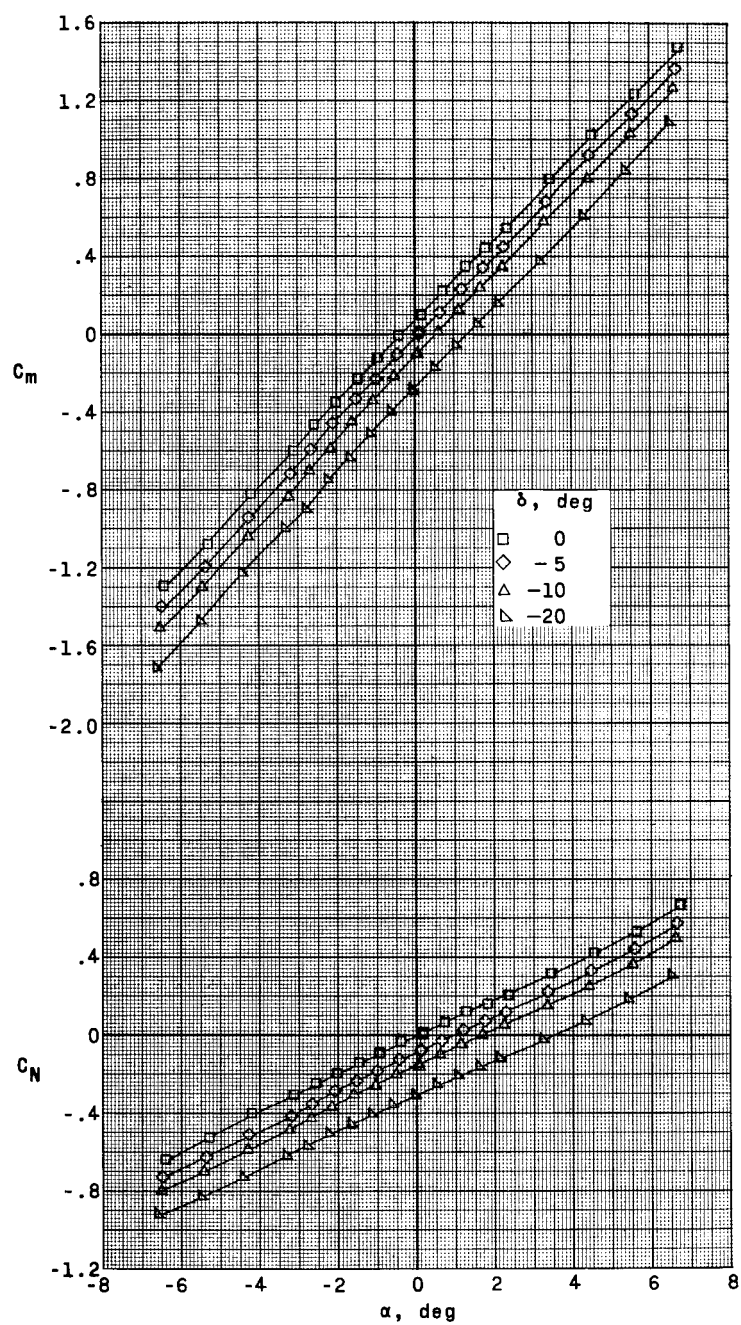
(d) M = 2.29.

Figure 13.- Continued.

δ, deg

□ 0
◇ −5
△ −10
◺ −20

C_A

α,deg
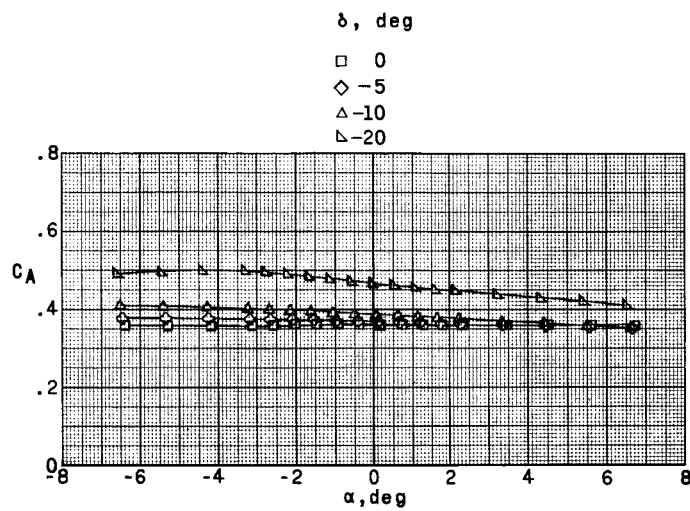
(d) M = 2.29. Concluded.

Figure 13.- Continued.
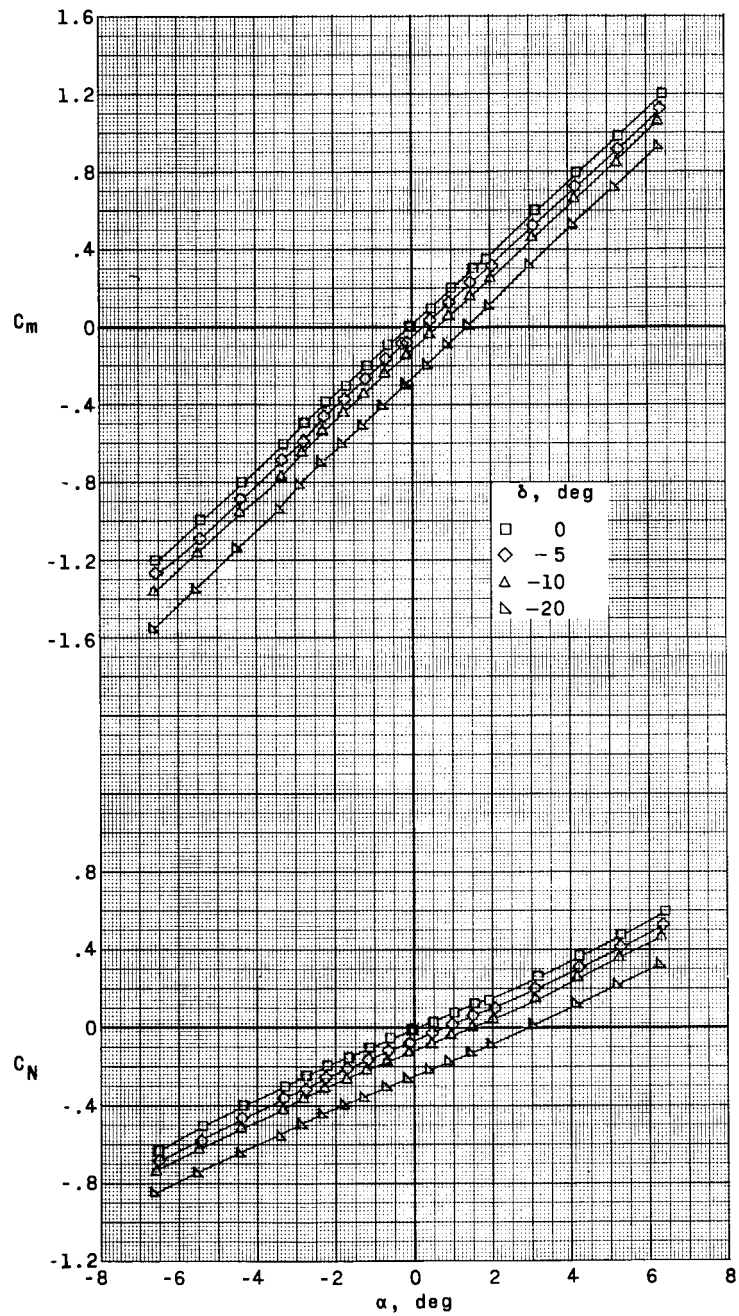
(e) M = 2.98.

Figure 13.- Continued.
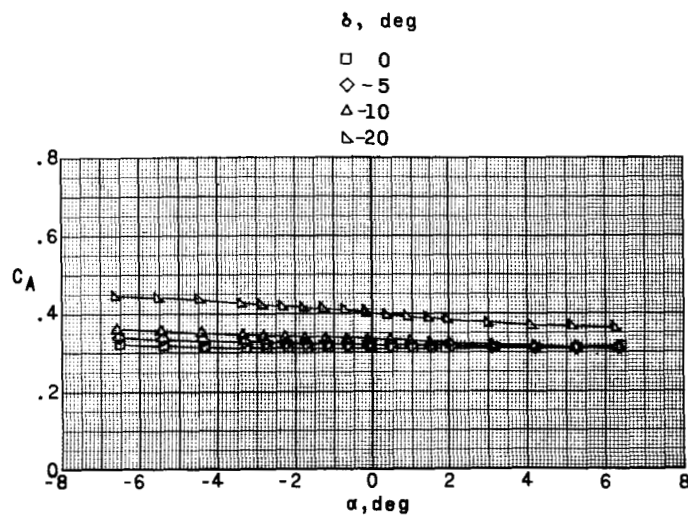
(e) M = 2.98. Concluded.

Figure 13.- Continued.
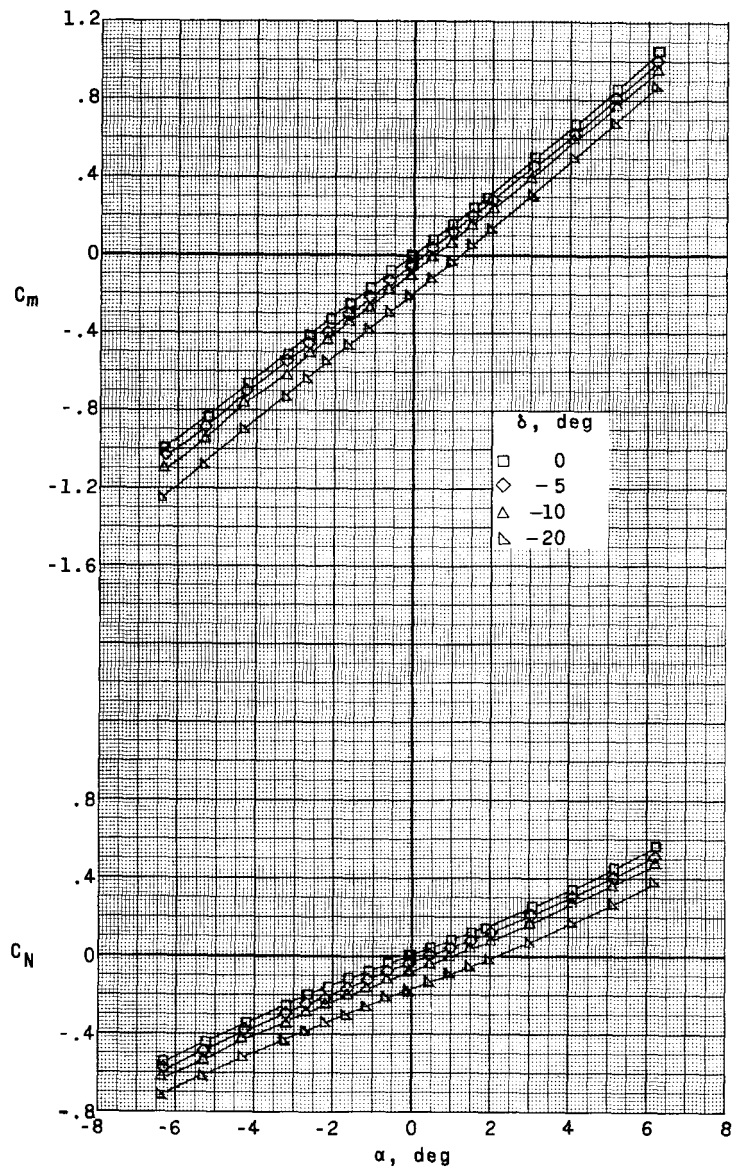
(f) M = 3.96.

Figure 13.- Continued.

δ, deg
□ 0
◇ -5
△ -10
◺ -20
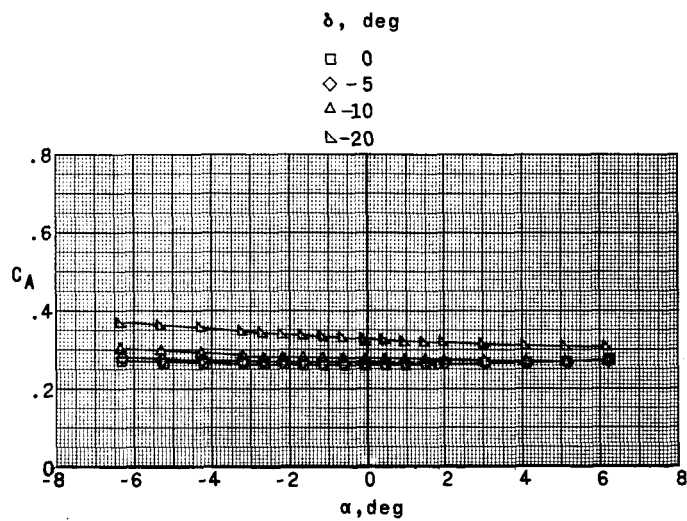
(f) M = 3.96. Concluded.

Figure 13.- Continued.

(g) M = 4.65.

Figure 13.- Continued.
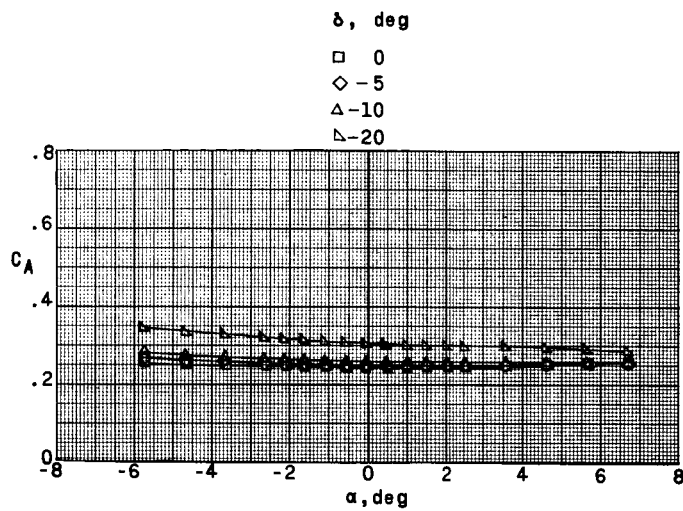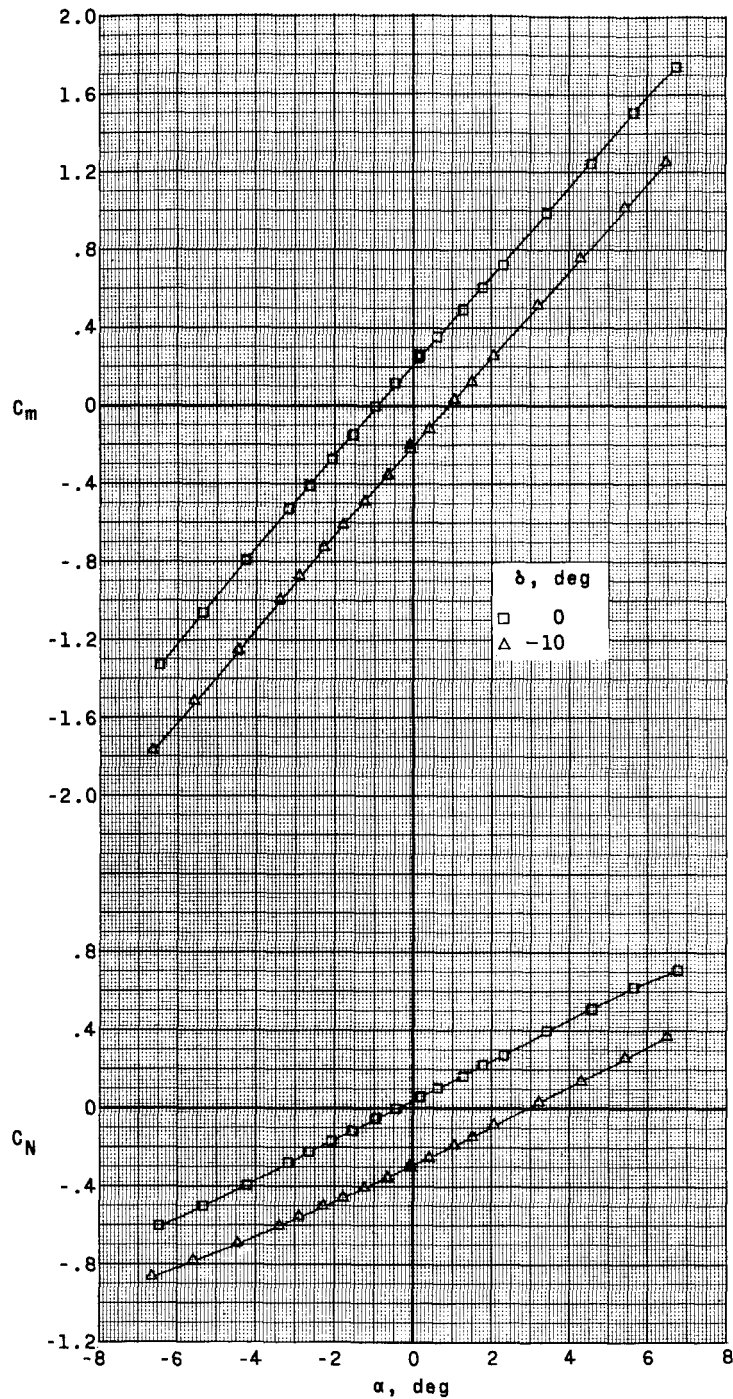
(g) M = 4.65. Concluded.

Figure 13.- Concluded.
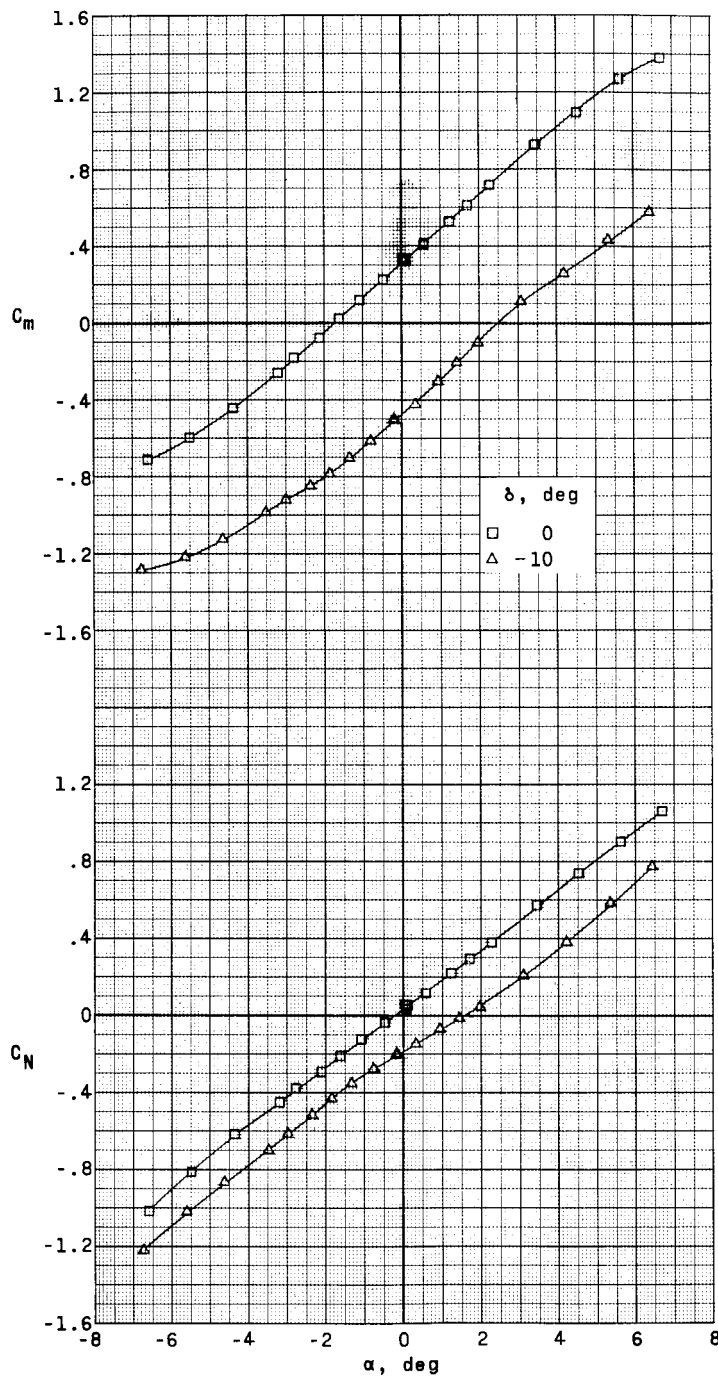
(a) M = 1.57.

Figure 14.- Effects of control deflection on the longitudinal aerodynamic characteristics of the Saturn-glider model with the control and stabilizing surfaces interdigitated with the glider wing $G_3S_1V_1F$.
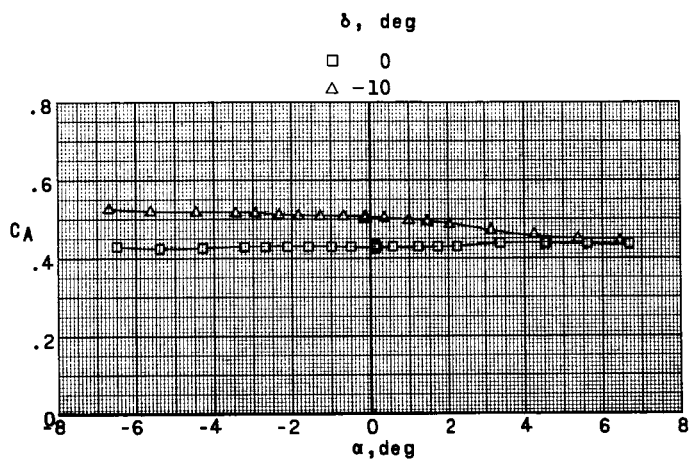
δ, deg

□ 0
△ −10

(a) M = 1.57. Concluded.

Figure 14.- Continued.

(b) M = 1.80.

Figure 14.- Continued.

δ, deg

□ 0

△ −10
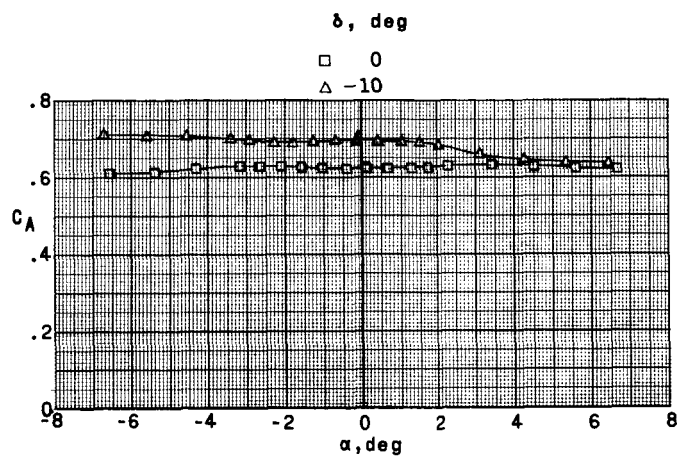
(b) M = 1.80. Concluded.

Figure 14.- Continued.
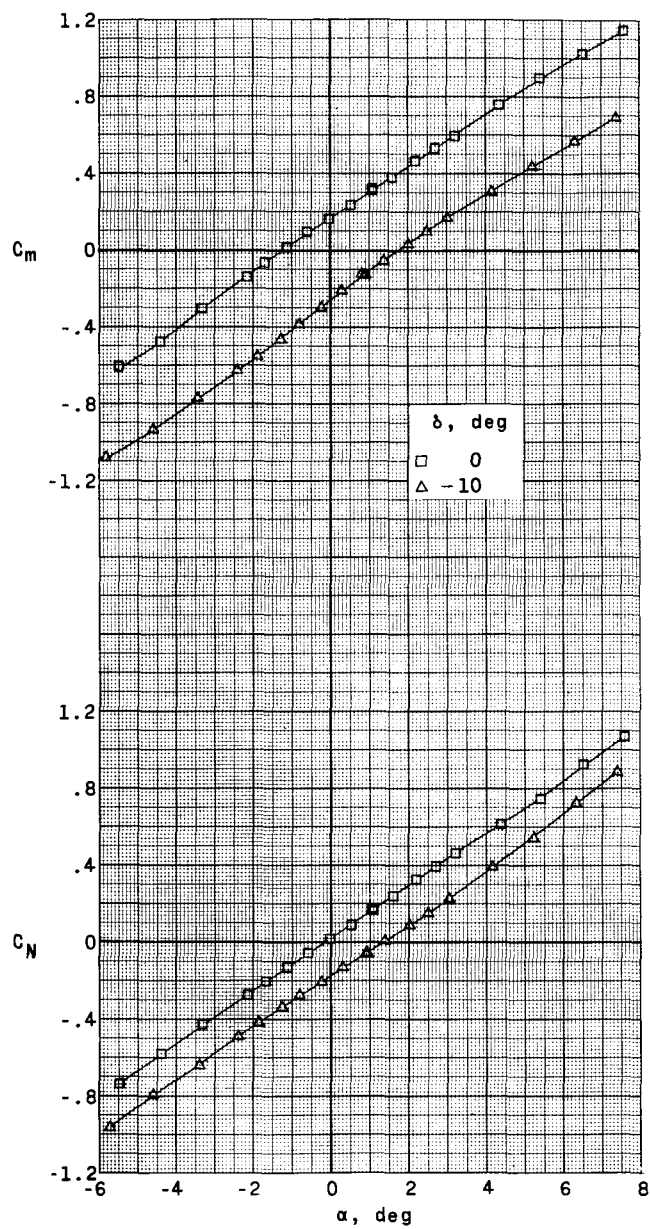
(c) M = 2.16.

Figure 14.- Continued.

(c) M = 2.16. Concluded.

Figure 14.- Continued.

(d) M = 2.29.

Figure 14.- Continued.

(d) M = 2.29. Concluded.

Figure 14.- Continued.

(e) M = 2.98.

Figure 14.- Continued.

(e) M = 2.98. Concluded.

Figure 14.- Continued.
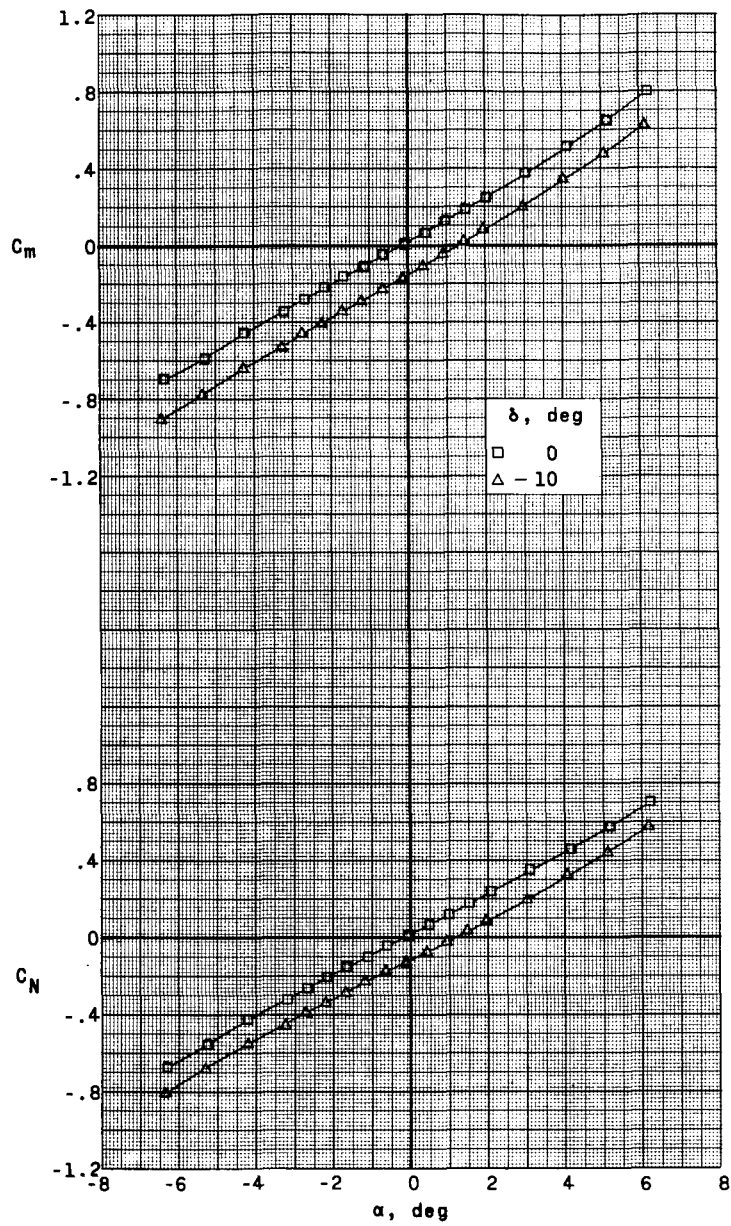
(f) M = 3.96.

Figure 14.- Continued.
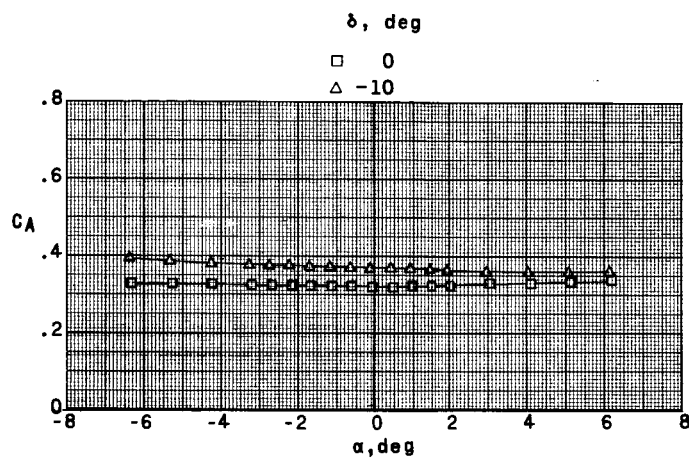
(f) M = 3.96. Concluded.

Figure 14.- Continued.
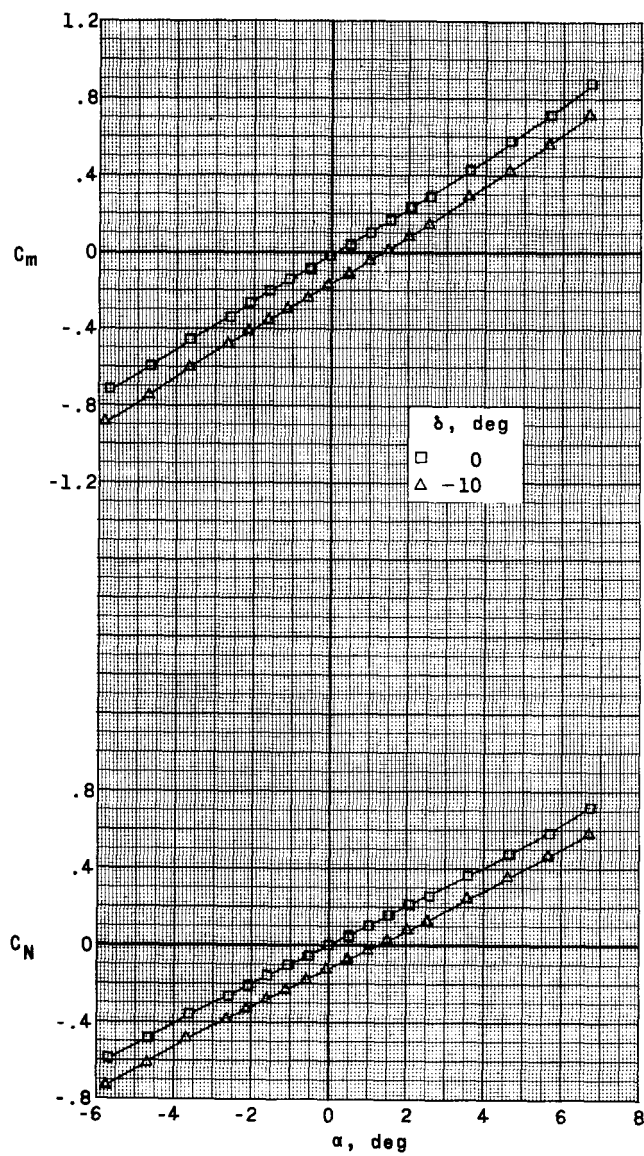
(g) M = 4.65.

Figure 14.- Continued.
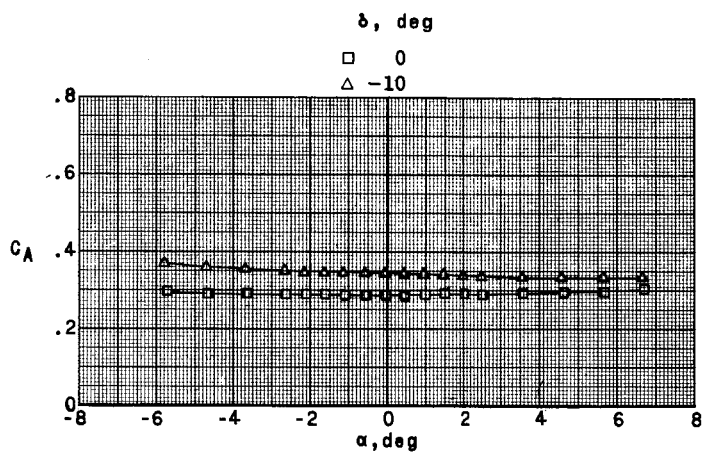
(g) M = 4.65. Concluded.

Figure 14.- Concluded.
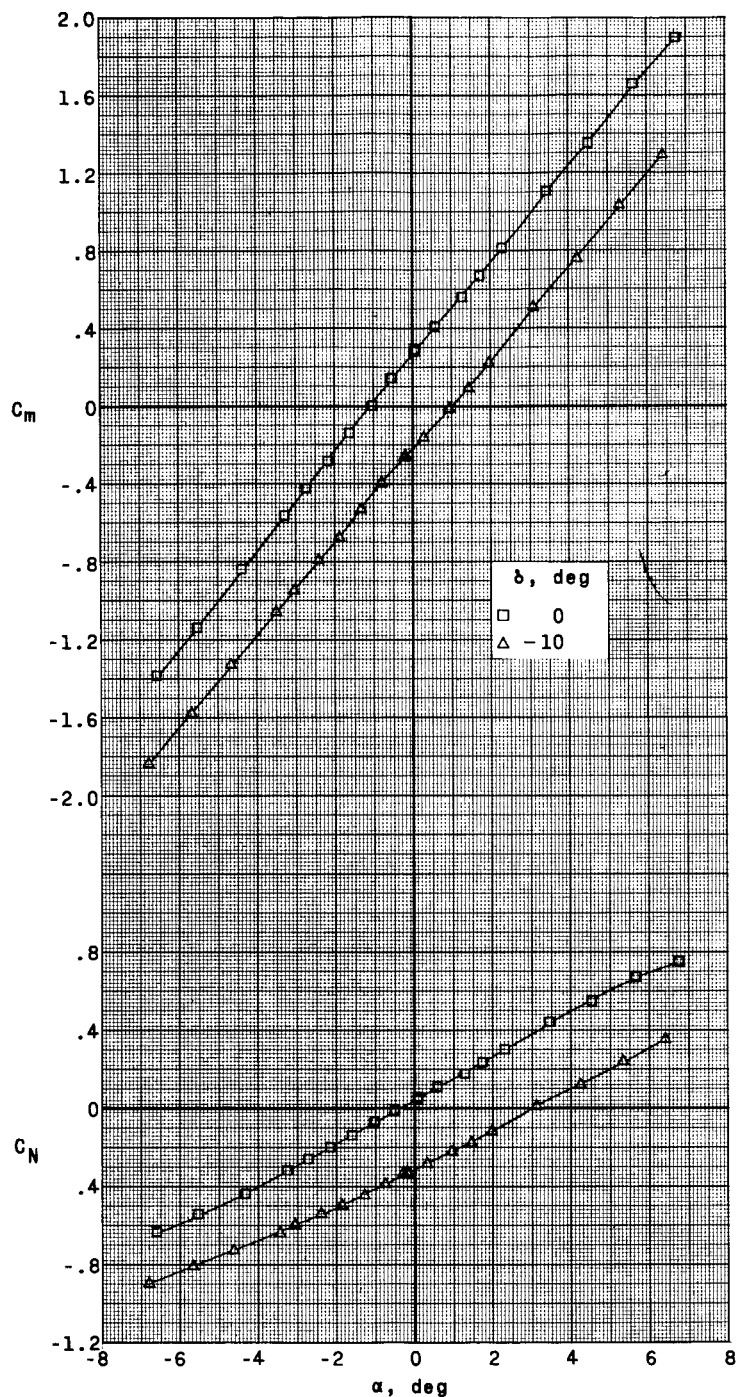
(a) M = 1.57.

Figure 15.- Effects of control deflection on the longitudinal aerodynamic characteristics of the Saturn-glider model with the control surfaces interdigitated with the glider wing $G_3S_1V_1$.

(a) M = 1.57. Concluded.

Figure 15.- Continued.

(b) M = 1.80.

Figure 15.- Continued.

(b) M = 1.80. Concluded.

Figure 15.- Continued.
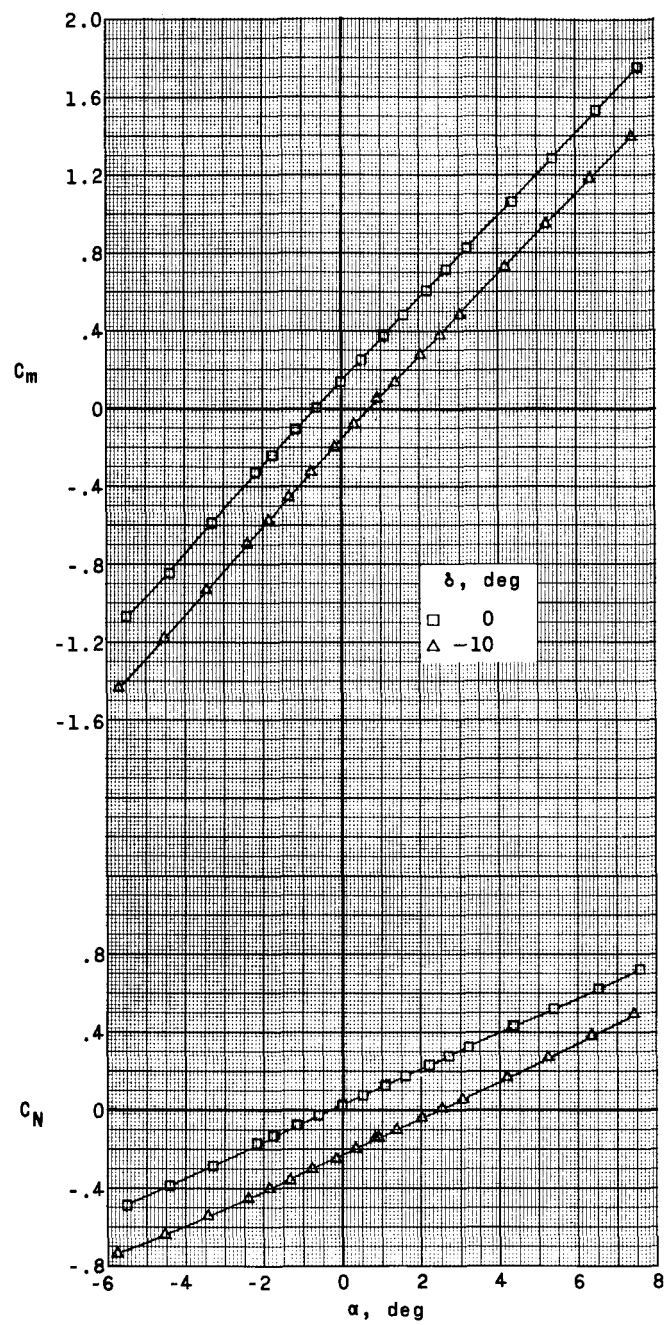
(c) M = 2.16.

Figure 15.- Continued.
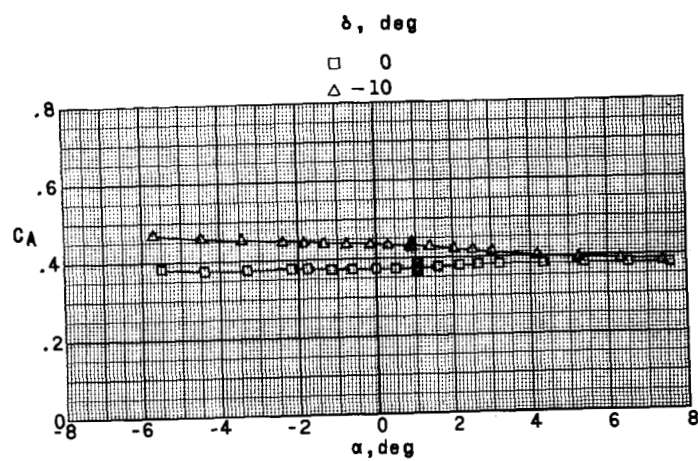
(c) M = 2.16. Concluded.

Figure 15.- Concluded.
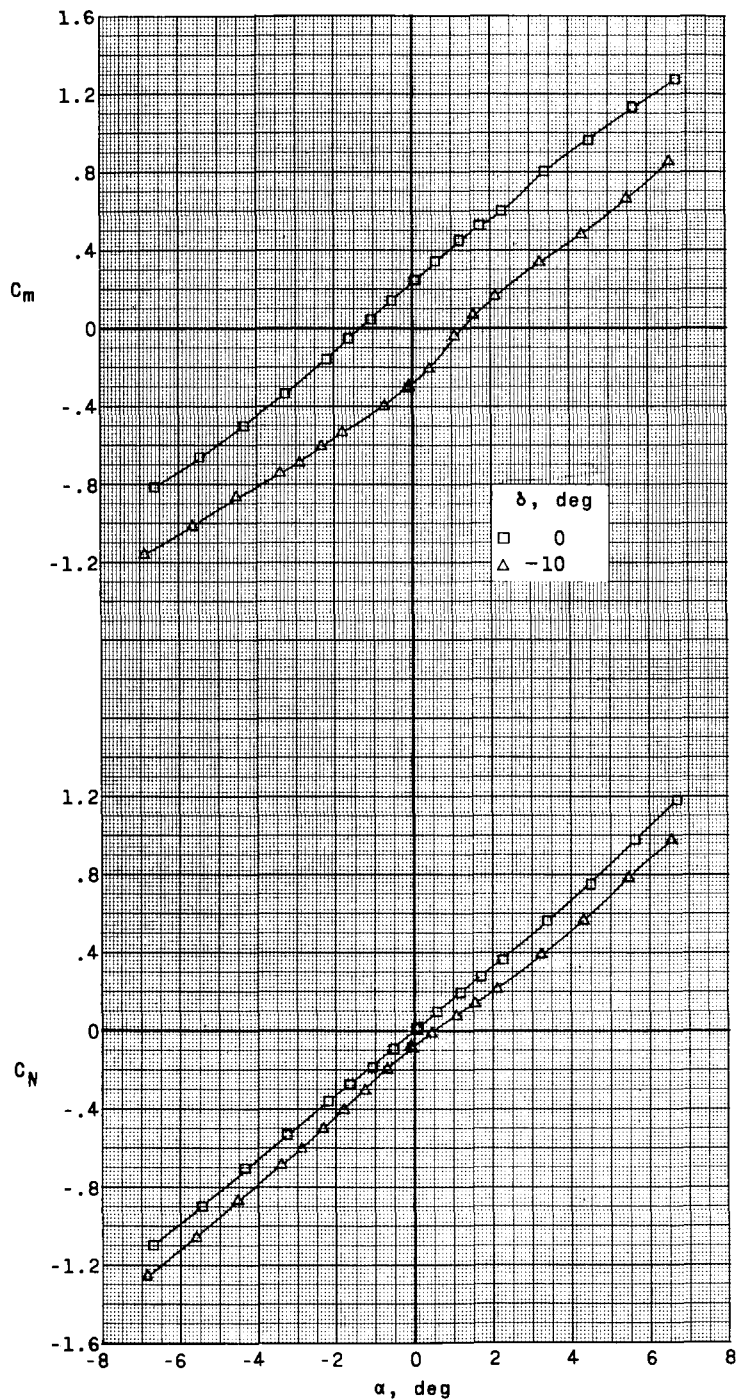
(a) M = 1.57.

Figure 16.- Effects of control deflection on the longitudinal aerodynamic characteristics of the
Saturn-glider model with the glider at 2° incidence G₂SVF.

δ, deg
□ 0
△ −10
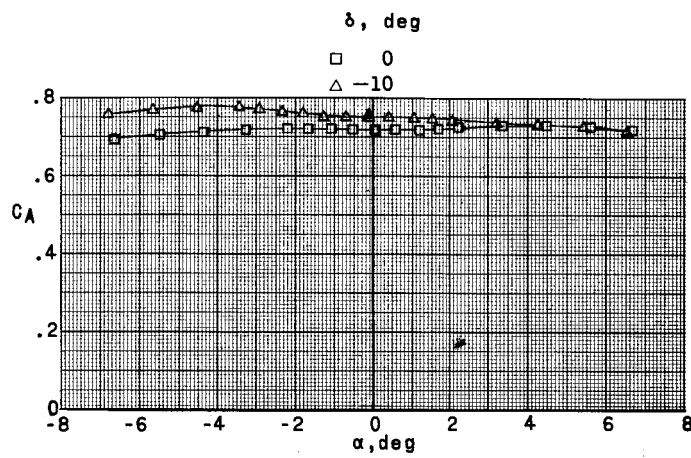
(a) M = 1.57. Concluded.

Figure 16.- Continued.
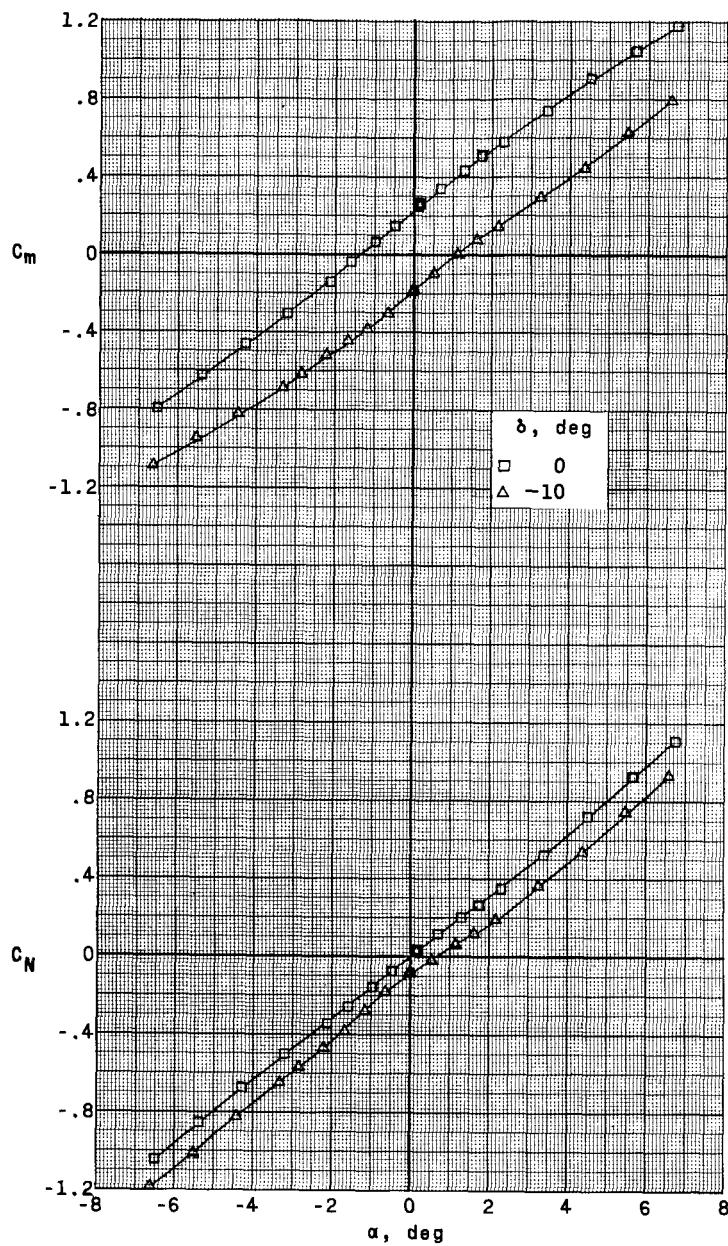
(b) M = 1.80.

Figure 16.- Continued.

δ, deg
□   0
△ −10
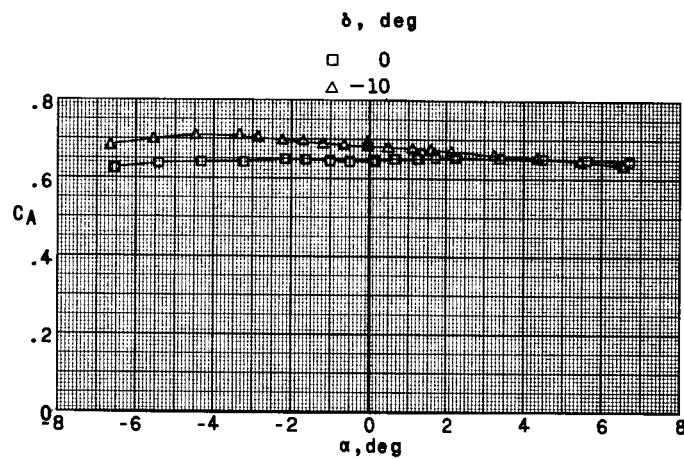
(b) M = 1.80. Concluded.

Figure 16.- Continued.
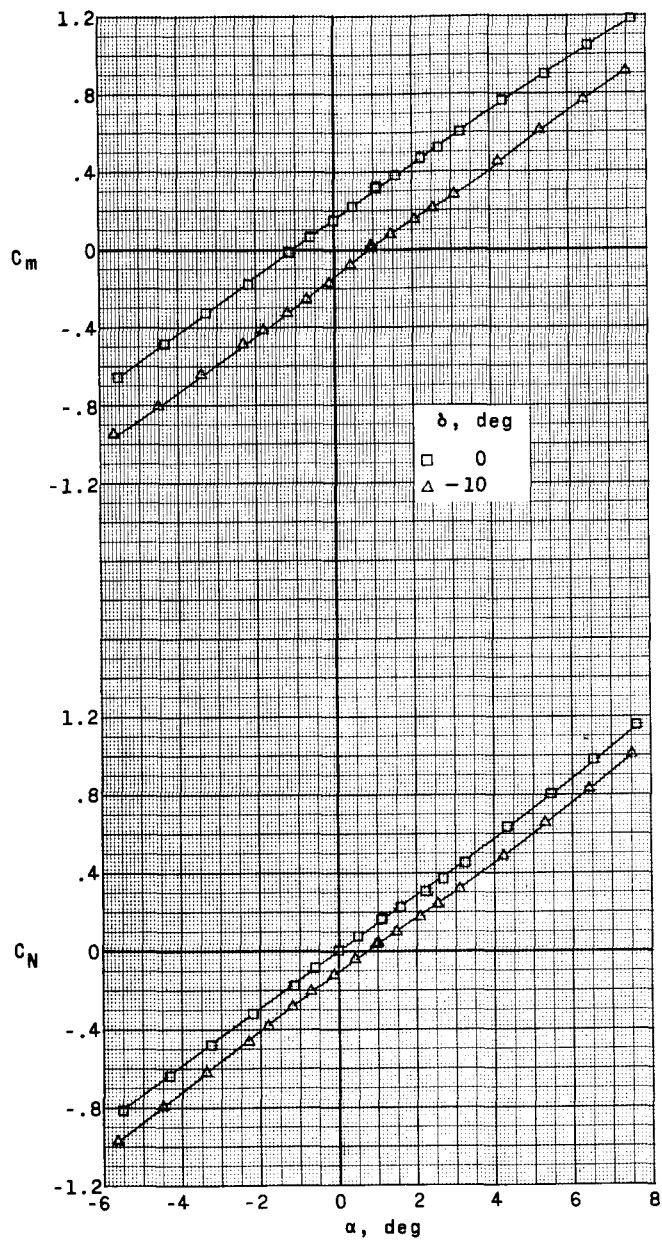
(c) M = 2.16.

Figure 16.- Continued.

δ, deg

□　0
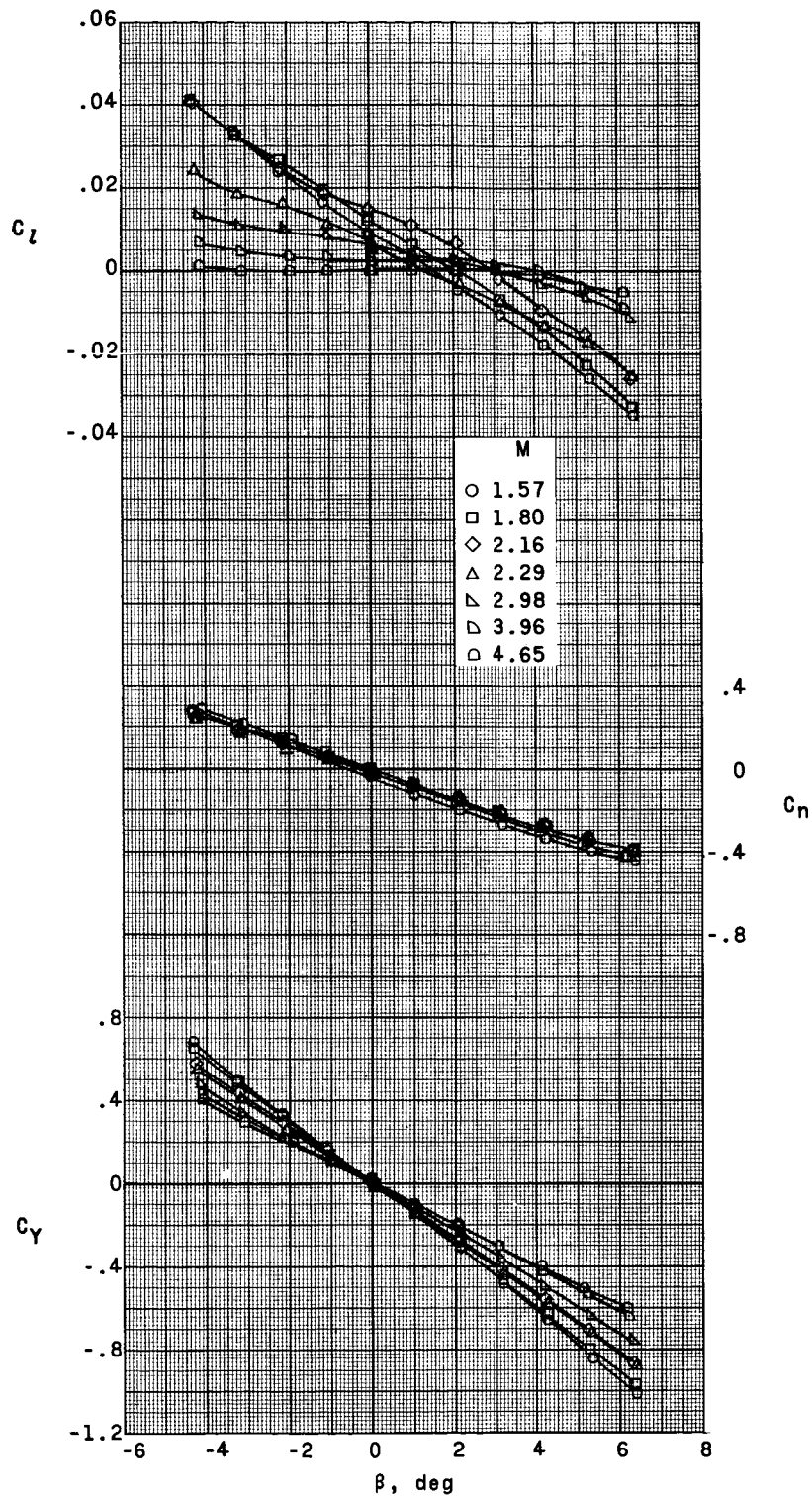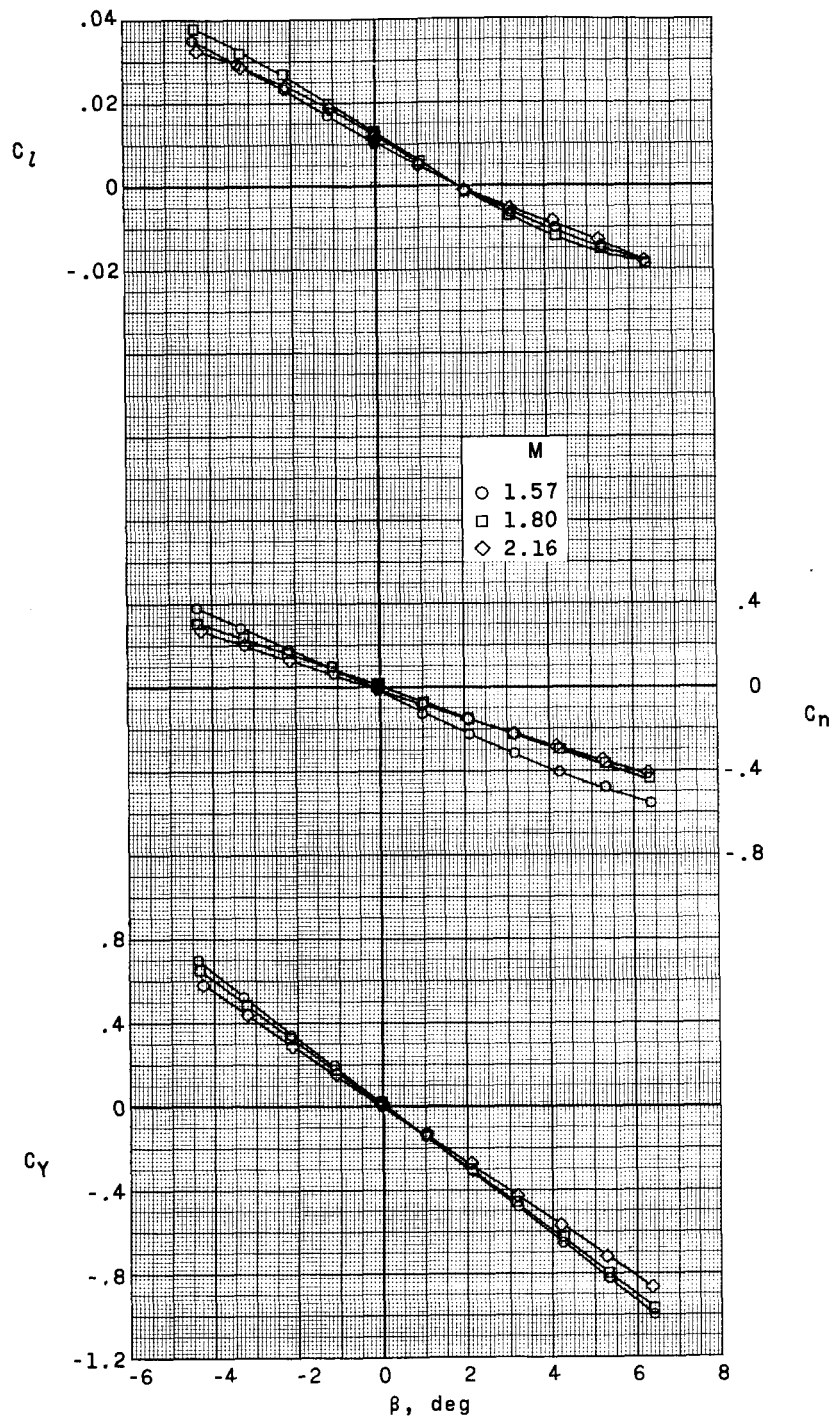△ − 10
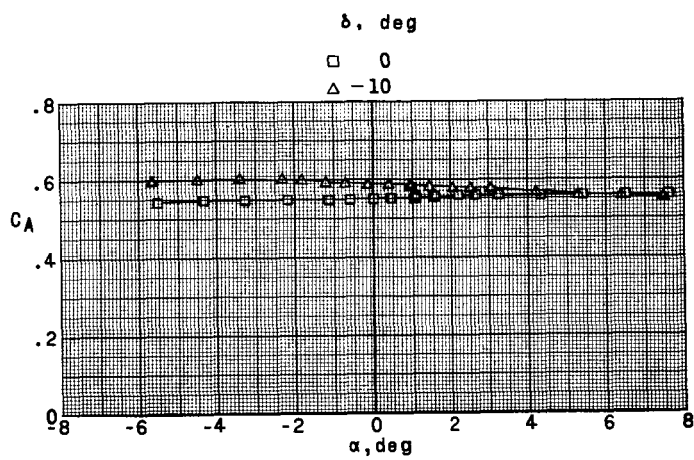
(c)　M = 2.16.　Concluded.

Figure 16.- Concluded.
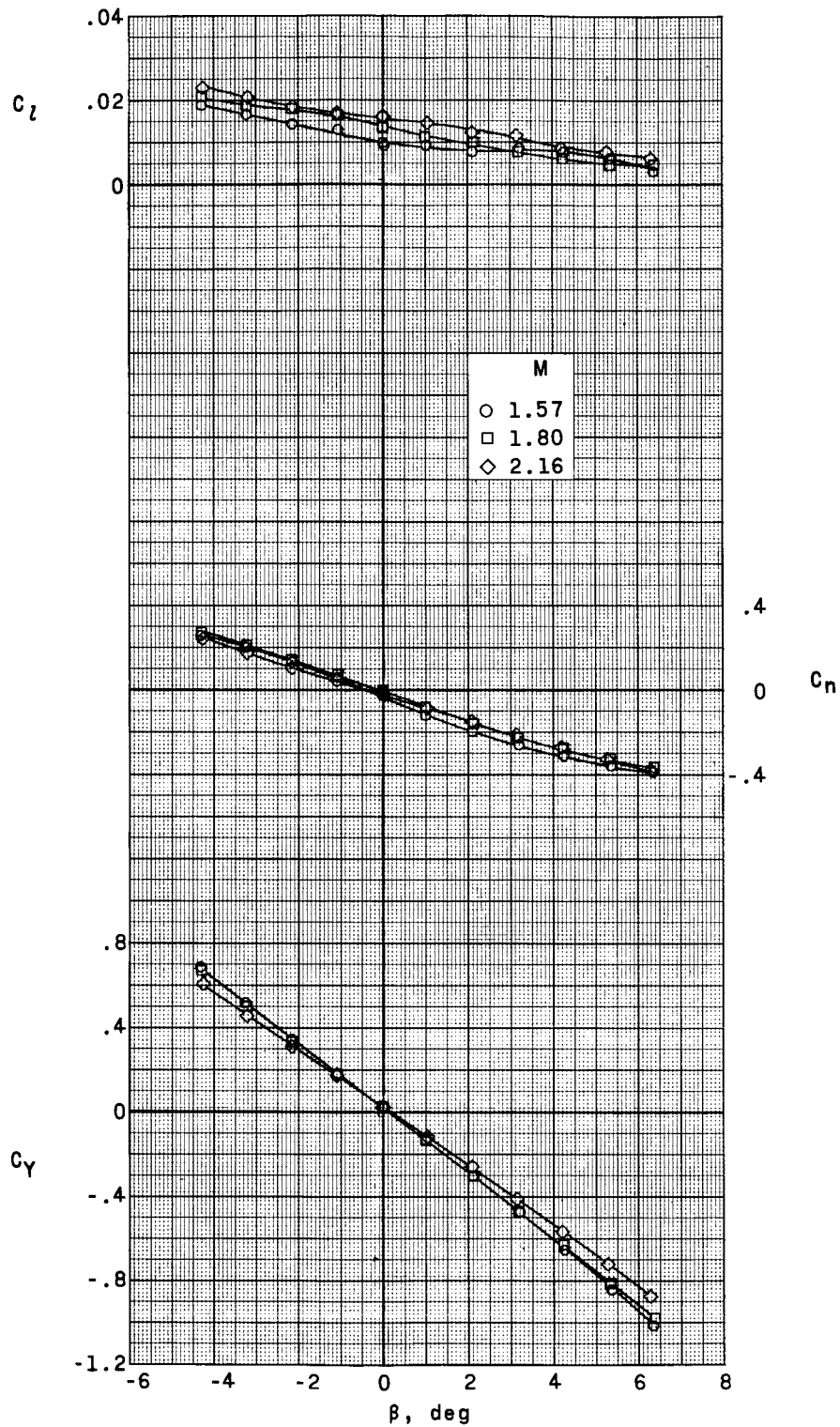
Figure 17.- Aerodynamic characteristics in sideslip for the Saturn-cone model CS_1VF. $\alpha \approx 0^o$.

(a) Model G_2S_1VF.

Figure 18.- Aerodynamic characteristics in sideslip for the Saturn-glider model. $\alpha \approx 0°$.

(b) Model $G_3S_1V_1F$.
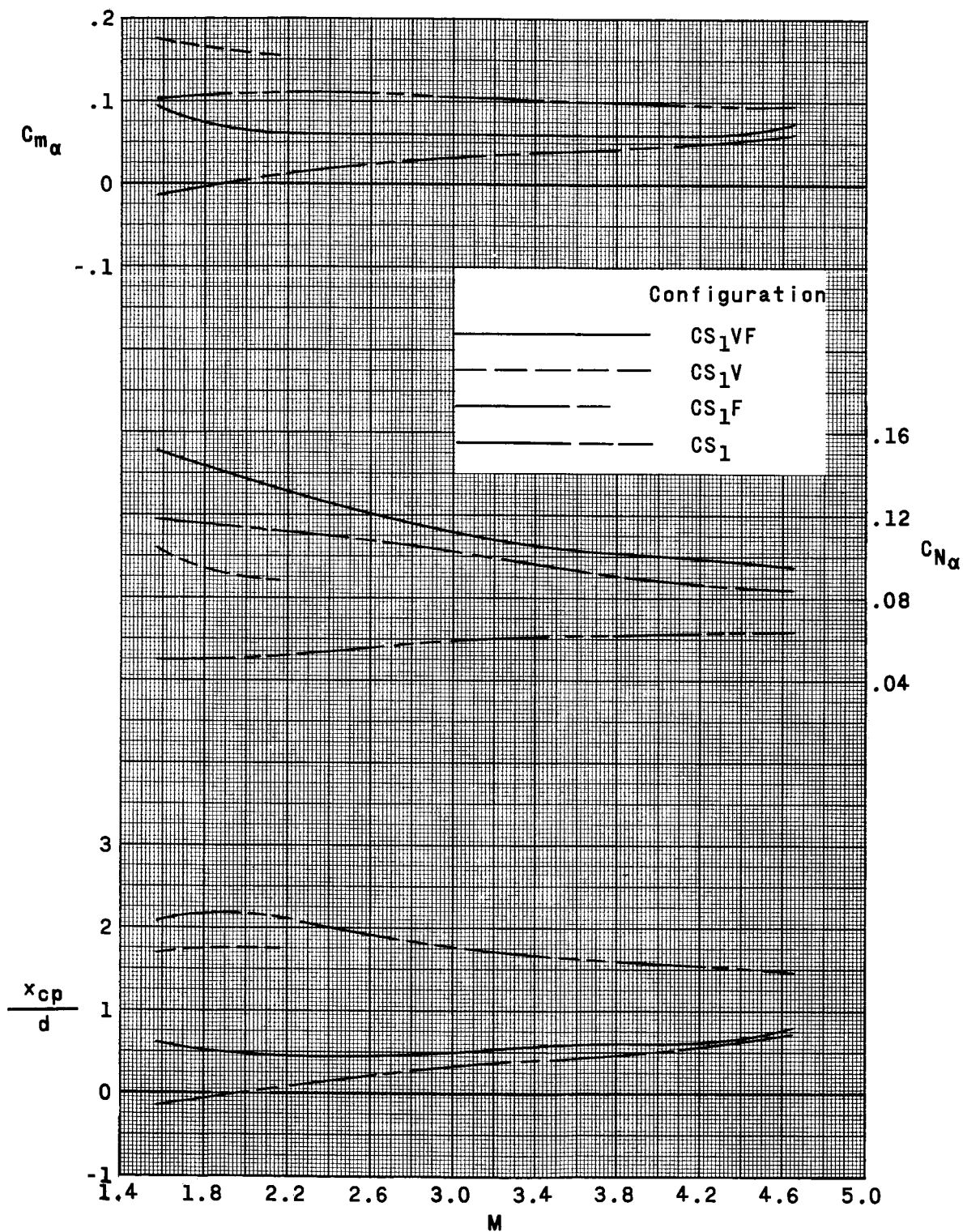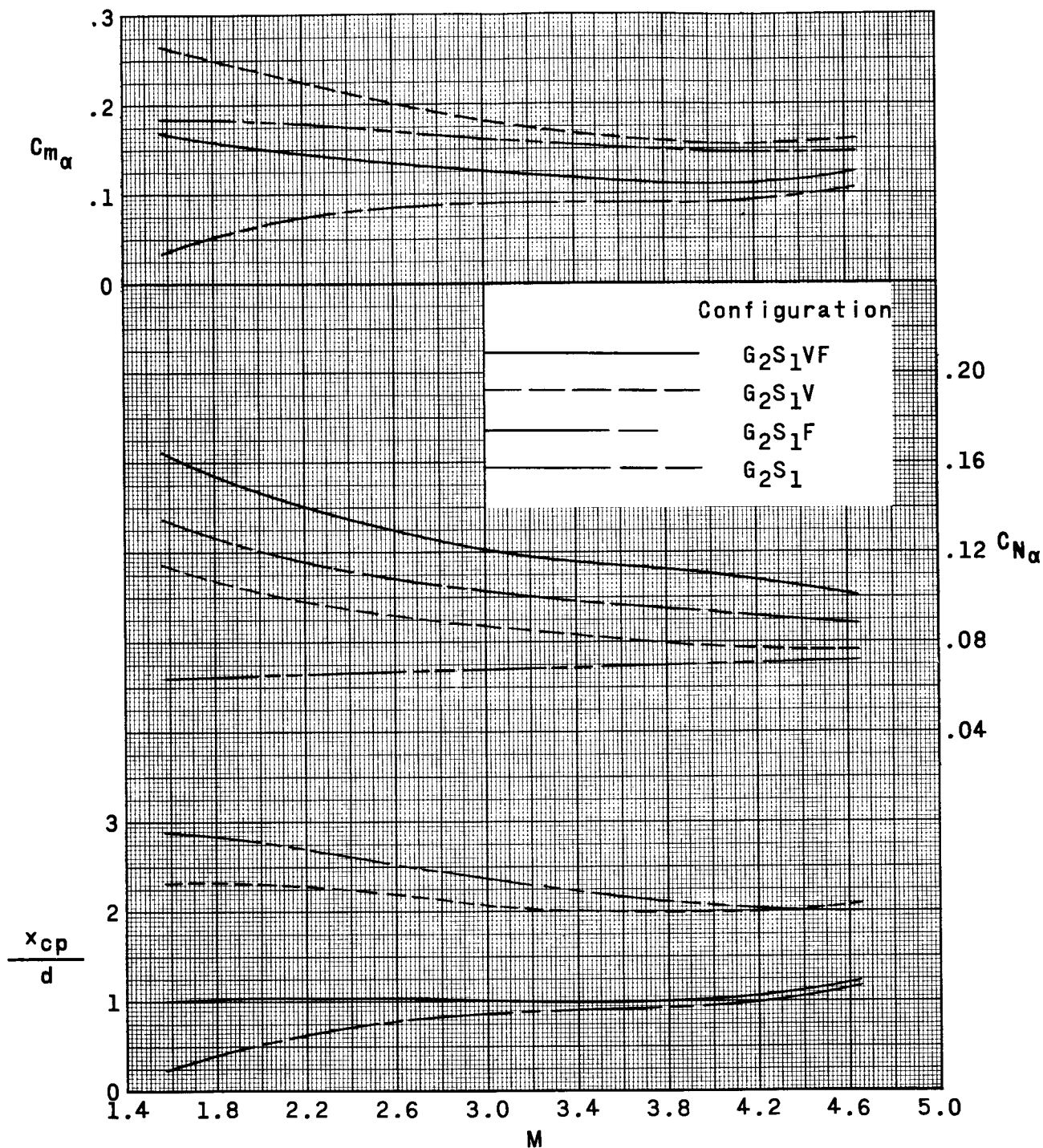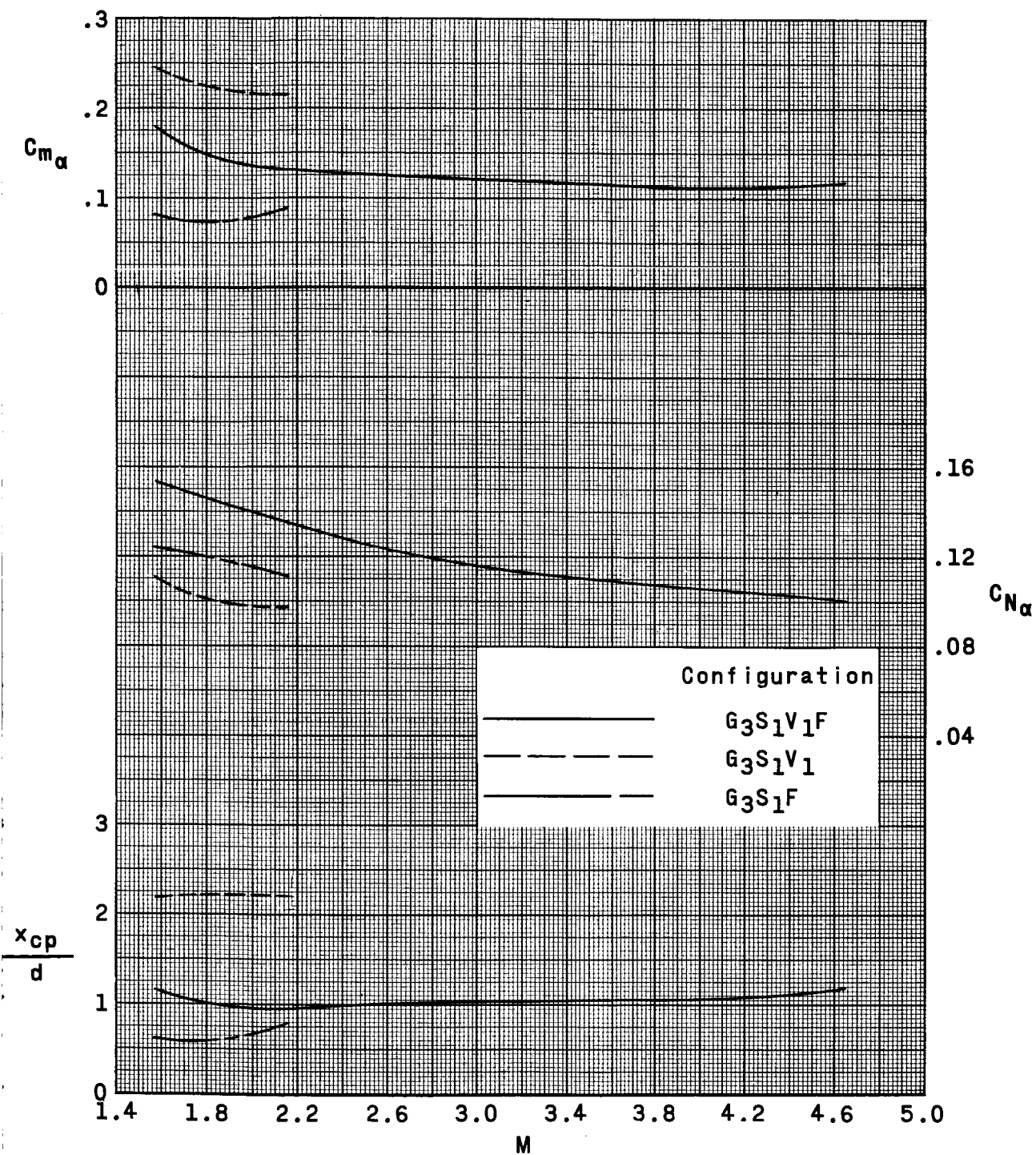
Figure 18.- Concluded.

Figure 19.- Summary of the longitudinal aerodynamic characteristics for the Saturn-cone model.
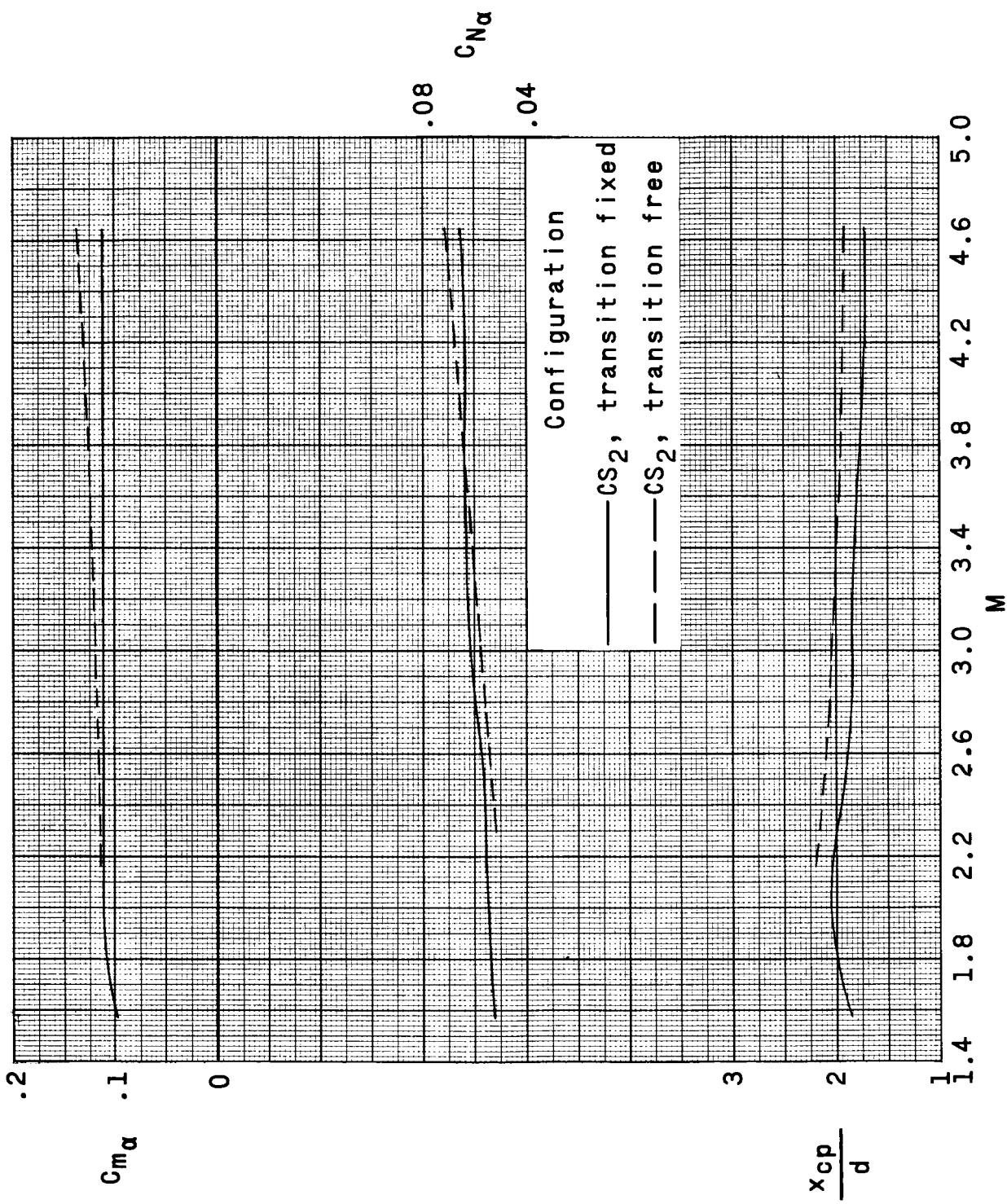
(a) Control surfaces in line with wing chord plane.

Figure 20.- Summary of the longitudinal aerodynamic characteristics for the Saturn-glider model.

(b) Control surfaces interdigitated with wing chord plane.

Figure 20.- Concluded.

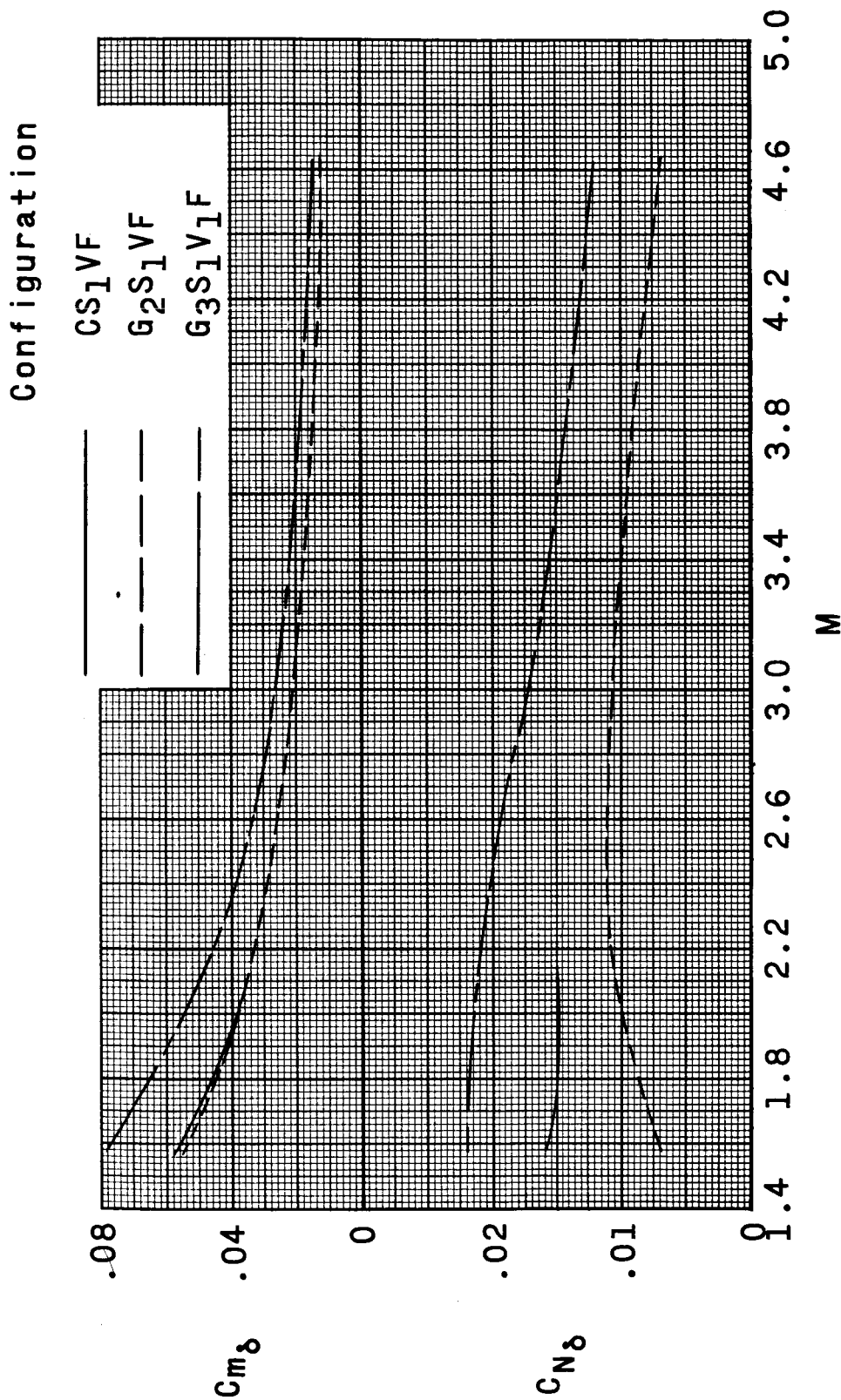Figure 8).- Summary of the longitudinal aerodynamic characteristics for the three-stage Saturn cone model

Figure 22.- Summary of the control characteristics of the Saturn-cone and Saturn-glider models in line and interdigitated.